COMPUTATIONAL SEISMOLOGY

Imaging Earth's interior with 3D wave simulations

Ebru Bozdağ
Colorado School of Mines

with contributions from:
Heiner Igel, Carene Larmat, Daniel Peter, Carl Tape, Jeroen Tromp

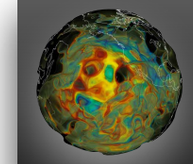

Seismology in a 3D planet

- **Forward problem**
  - **ray theoretical methods (Sanne)**
  - **quasi-analytic methods - normal modes (Jessica)**
  - **numerical methods**
- **Inverse problem (Ved)**
  - **gradient-based optimizations**
  - **seismic tomography with 3D wave simulations**
- **Current status in global imaging**
- **Challenges, future directions..**

Seismic modeling

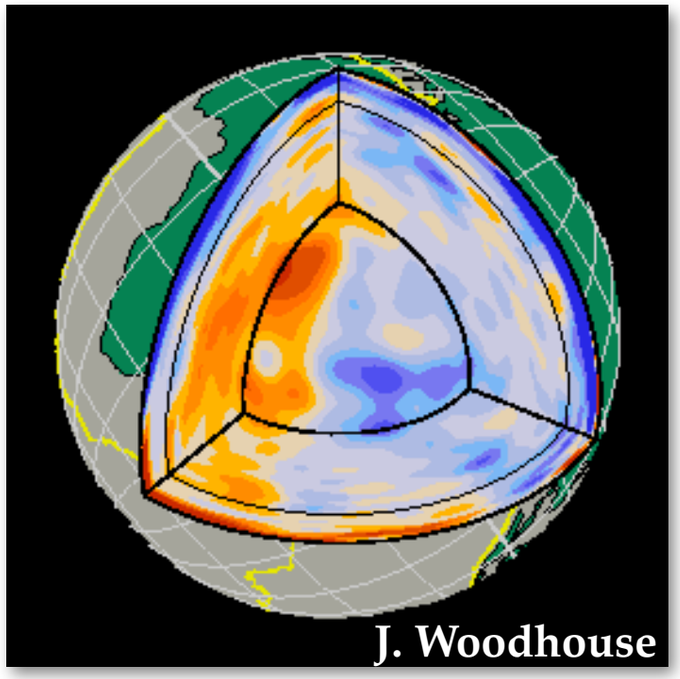

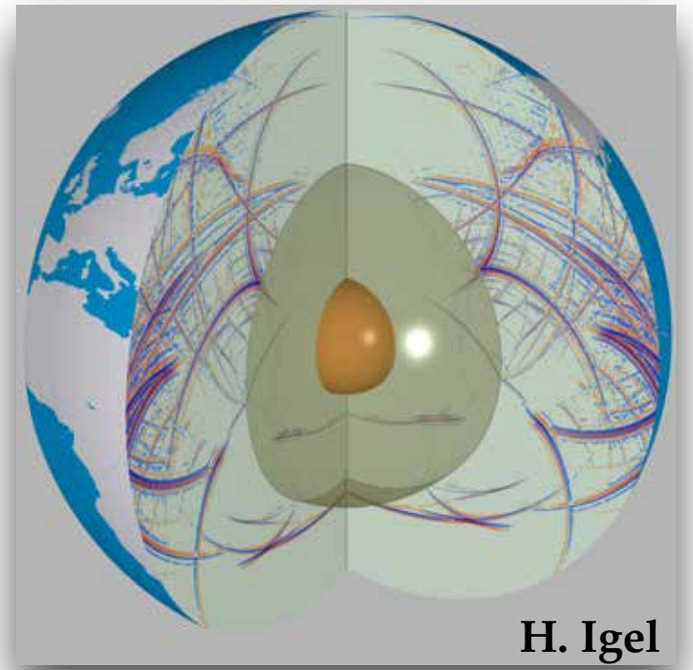

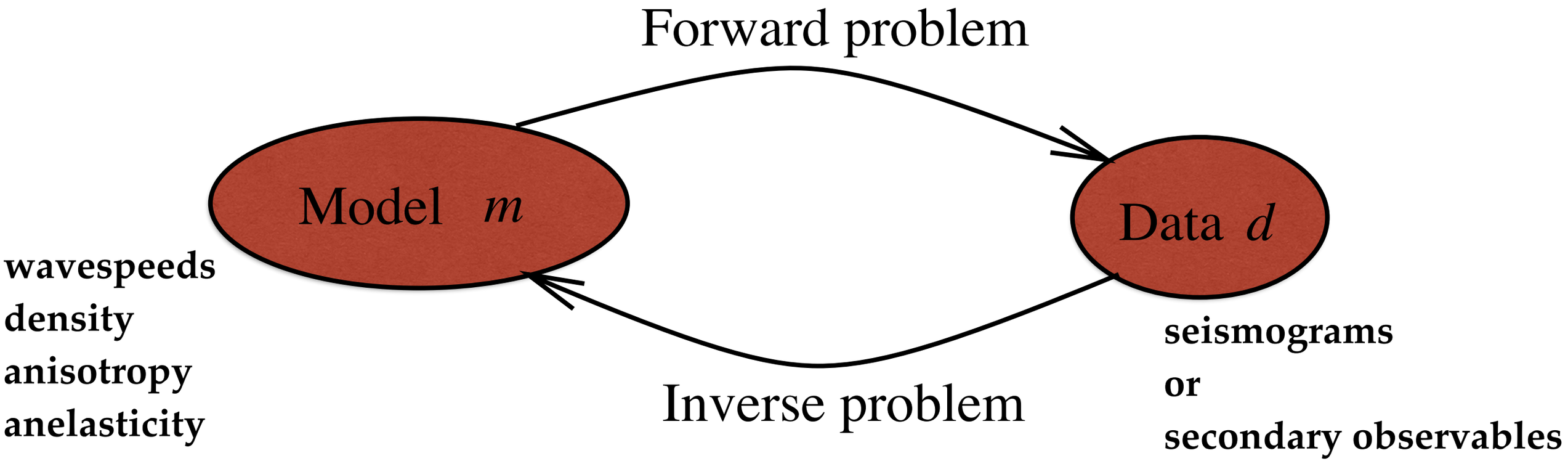

Seismic modeling

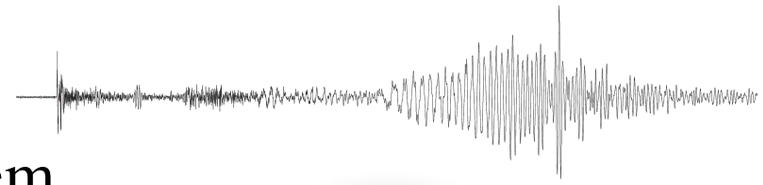

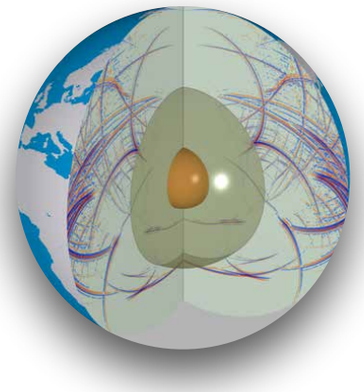

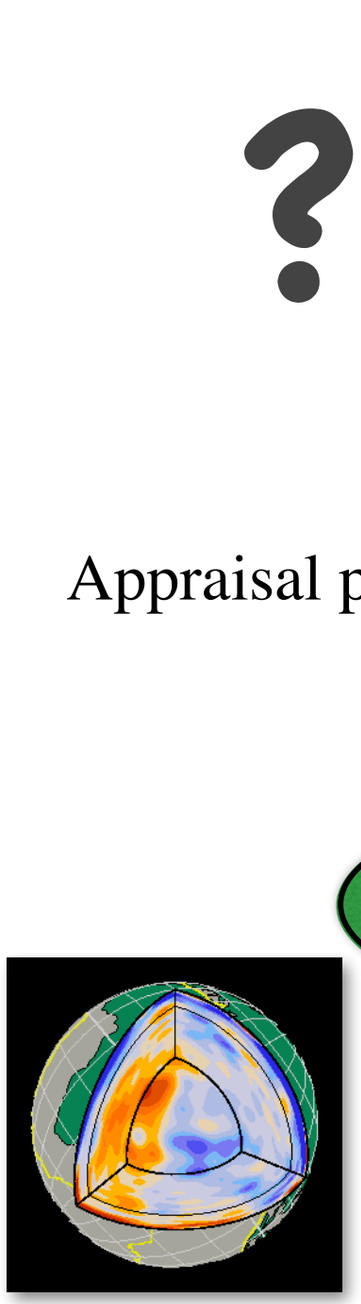

inversion = estimation problem + appraisal problem

Snieder & Trampert (2000)

Seismic period (frequency) band

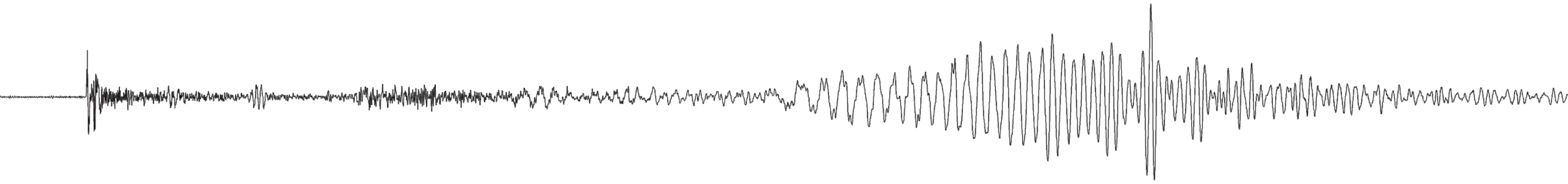

Figure 2.4-7: Seismic spectrum for various studies.

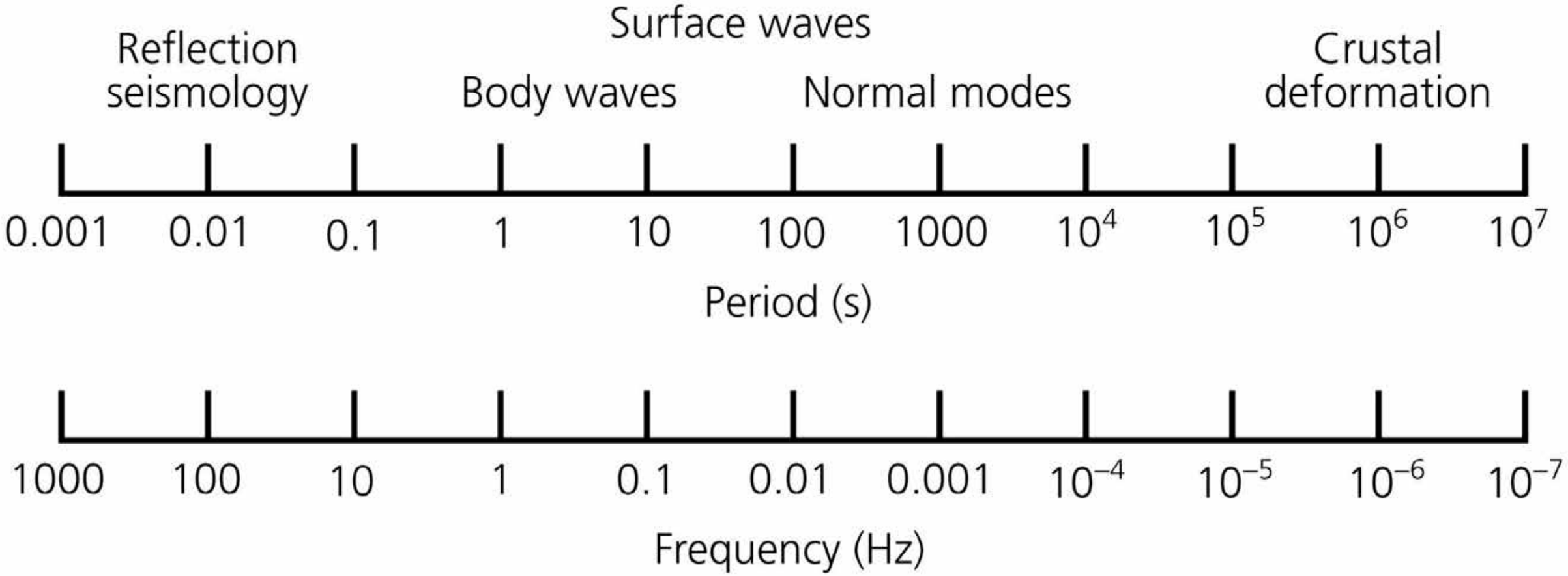

Stein & Wysession 2003

Ray theory vs. finite-frequency theory

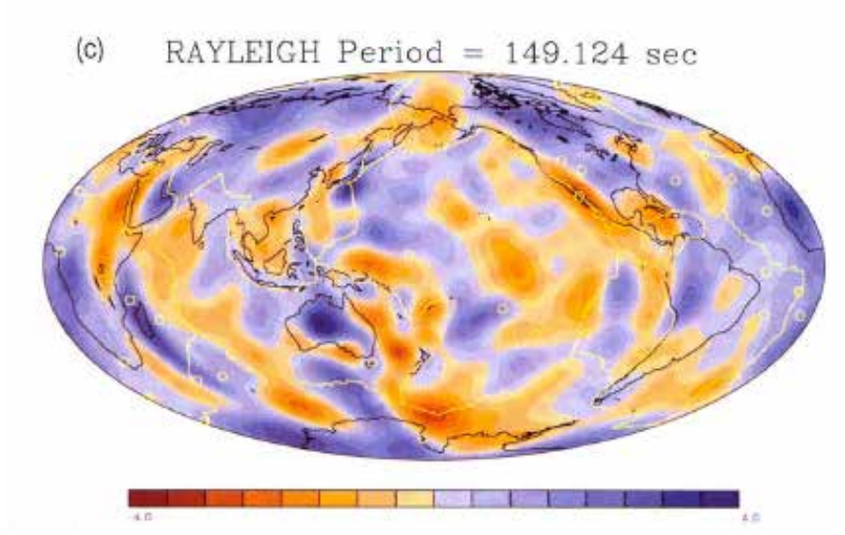

Trampert & Woodhouse, 1995, GJI

Ray theory is
a high-frequency approximation

Its validity depends on:

1) frequency of waves

2) propagation distance of waves

3) smoothness of heterogeneities

see e.g., Wang & Dahlen, 1995, GJI

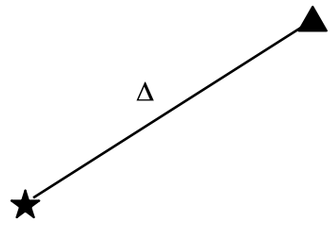

great circle approximation

$$\delta\phi = -\frac{\omega}{c_0}\int_0^{\Delta}\frac{\delta c}{c_0}(\theta,\varphi)\mathrm{d}\Delta$$

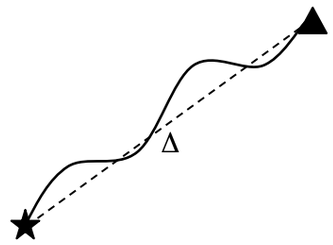

exact ray theory

$$\delta\phi = -\frac{\omega}{c_0}\int_{ray}\frac{\delta c}{c_0}(\theta,\varphi)\mathrm{d}s$$

finite frequency theory

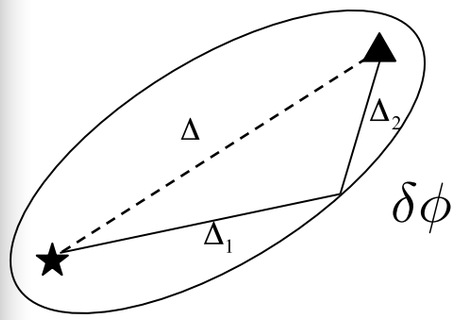

$$\delta\phi = -\frac{\omega}{c_0}\int\int_{sphere}K(\theta,\varphi)\frac{\delta c}{c_0}(\theta,\varphi)\mathrm{d}\theta\mathrm{d}\varphi$$

Ray theoretical phase and amplitude anomalies

$$\delta\psi = \int_{\text{ray}} \frac{\omega}{c(\theta,\phi)}\,ds - \frac{\omega a}{c_0}\Delta$$

$$= \frac{\omega a}{c_0}\int_0^{\Delta}\left[\frac{c_0}{c(\theta,\phi)}\left\{\frac{\nu(\phi)^2}{[1+\gamma^2(\phi)]^2}+\frac{1}{1+\gamma^2(\phi)}\right\}^{1/2}-1\right]d\phi$$

$$\ln A = \tfrac{1}{2}\,\text{cosec}\,\Delta\int_0^{\Delta}\sin(\Delta-\phi)\,c_0^{-1}\left[\sin\phi\,\partial_\theta^2-\cos\phi\,\partial_\phi\right]\delta c\,d\phi$$

Woodhouse & Wong, Geophys. J. R. Astr. SOC., 1986, 87, 753-773

Phase space of scattering

wavenumber

$$k = \frac{2\pi}{\lambda}$$

wavelength

$$c = \lambda \ f$$

a: **dominant wavelength of the heterogeneous medium**

L: **propagation distance**

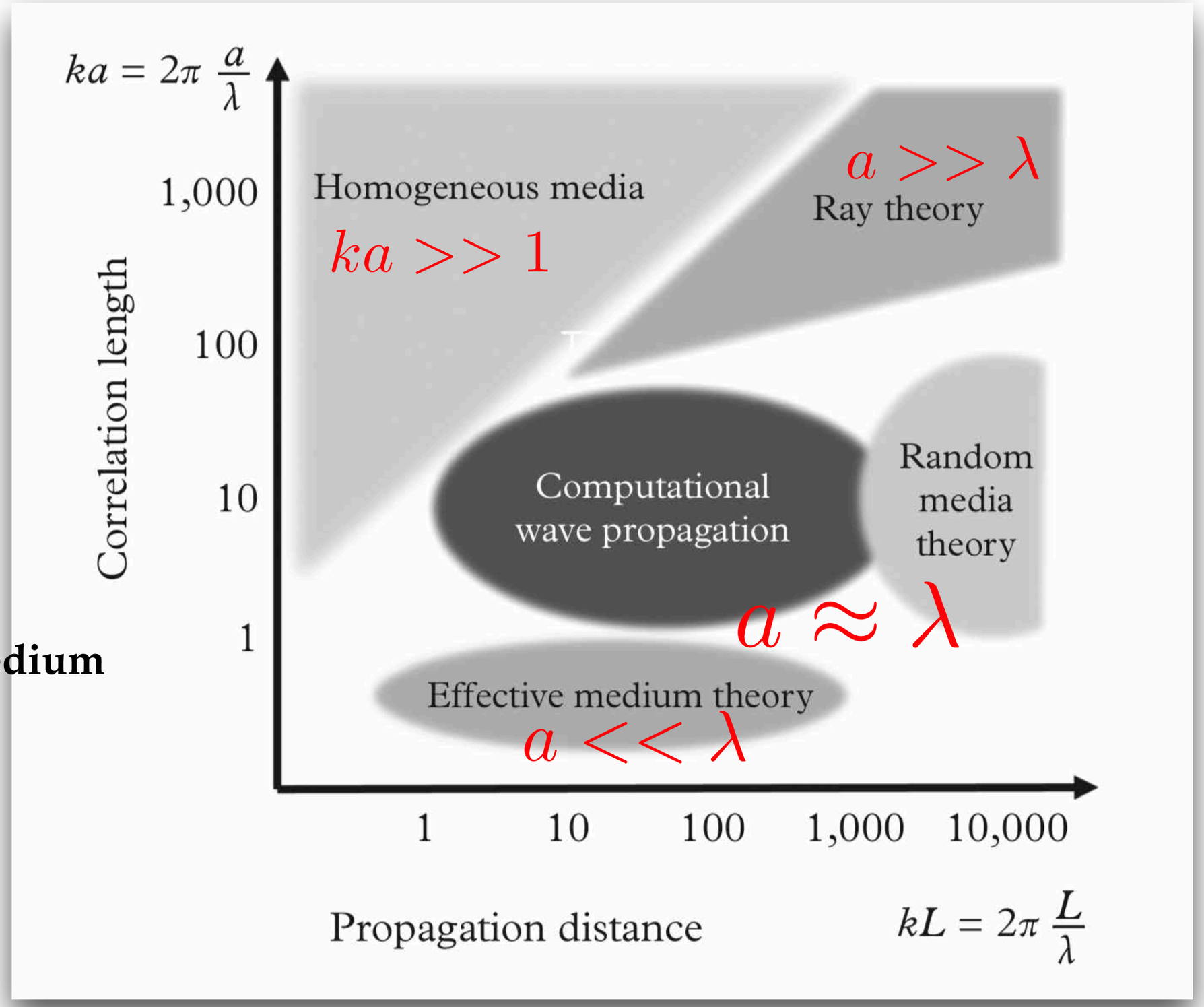

Heiner Igel, Computational Seismology, 2017 (after Aki & Richards 1980)

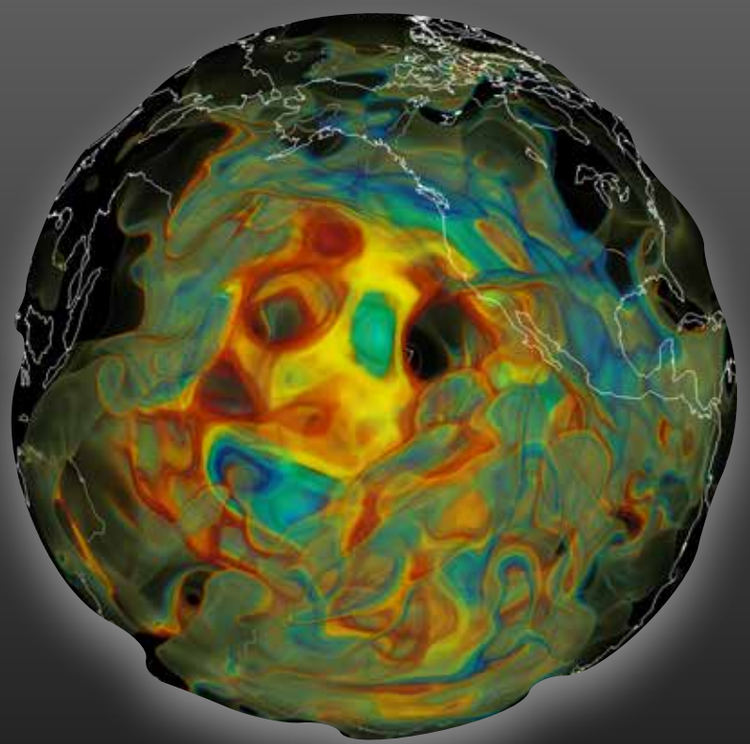

Numerical seismic wave simulations

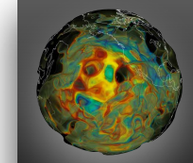

Computational Infrastructure for Geodynamics

- Short-Term Crustal Dynamics
- Long-Term Tectonics
- Mantle Convection
- Seismology
- Geodynamo
- Computational Science

SEISMOLOGY

SPECFEM3D GLOBE	SPECFEM3D_GLOBE simulates global and regional (continental-scale) seismic wave propagation.	D_CIG
SPECFEM3D Cartesian	SPECFEM3D Cartesian simulates acoustic (fluid), elastic (solid), coupled acoustic/elastic, poroelastic or seismic wave propagation in any type of conforming mesh of hexahedra (structured or not.) It can, for instance, model seismic waves propagating in sedimentary basins or any other regional geological model following earthquakes. It can also be used for non-destructive testing or for ocean acoustics.	D_CIG
BurnMan	BurnMan is an open source mineral physics toolbox written in Python to determine seismic velocities for the lower mantle. BurnMan calculates the isotropic thermoelastic moduli by solving the equations-of-state for a mixture of minerals defined by the user. The user may select from a list of minerals applicable to the lower mantle included or easily define one of their own.	D_CONTRIB
AxiSEM	AxiSEM is a parallel spectral-element method for 3D (an-)elastic, anisotropic and acoustic wave propagation in spherical domains. It requires axisymmetric background models and runs within a 2D computational domain, thereby reaching all desired highest observable frequencies (up to 2Hz) in global seismology. The Fortran2003 (OpenMP, MPI) code scales very well on supercomputers and is available under the GPL license. For more details see the website at www.axisem.info.	D_CONTRIB
SPECFEM3D GEOTECH	SPECFEM3D_GEOTECH is an open-source command-driven software for 3D slope stability analysis and simulation of 3D multistage excavation based on the spectral-element method.	D_CONTRIB
SW4	SW4 implements substantial capabilities for 3-D seismic modeling, with a free surface condition on the top boundary, absorbing super-grid conditions on the far-field boundaries, and an arbitrary number of point force and/or point moment tensor source terms. Each source time function can have one of many predefined analytical time dependencies, or interpolate a user defined discrete time series.	D_CONTRIB
SPECFEM2D	SPECFEM2D simulates forward and adjoint seismic wave propagation in two-dimensional acoustic, (an)elastic, poroelastic or coupled acoustic-(an)elastic-poroelastic media, with Convolution PML absorbing conditions.	D_CONTRIB
SEISMIC_CPML	SEISMIC_CPML is a set of eleven open-source Fortran90 programs to solve the two-dimensional or three-dimensional isotropic or anisotropic elastic, viscoelastic or poroelastic wave equation using a finite-difference method with Convolutional or Auxiliary Perfectly Matched Layer (C-PML or ADE-PML) conditions, developed by Dimitri Komatitsch and Roland Martin from CNRS, France. Contributions by other authors have recently been added.	S_CONTRIB
SPECFEM1D	SPECFEM1D simulates seismic wave propagation in a one-dimensional heterogeneous medium. It is a small code that allows users to learn how a spectral-element program is written.	S_CONTRIB
Flexwin	The FLEXWIN software package automates the time-window selection problem for seismologists. It operates on pairs of observed and synthetic single component seismograms, defining windows that cover as much of a given seismogram as possible, while avoiding portions of the waveform that are dominated by noise.	A
Mineos	Mineos computes synthetic seismograms in a spherically symmetric non-rotating Earth by summing normal modes.	A

COMPUTATIONAL INFRASTRUCTURE for GEODYNAMICS

https://geodynamics.org/cig/software/#seismo

Reference book suggestion

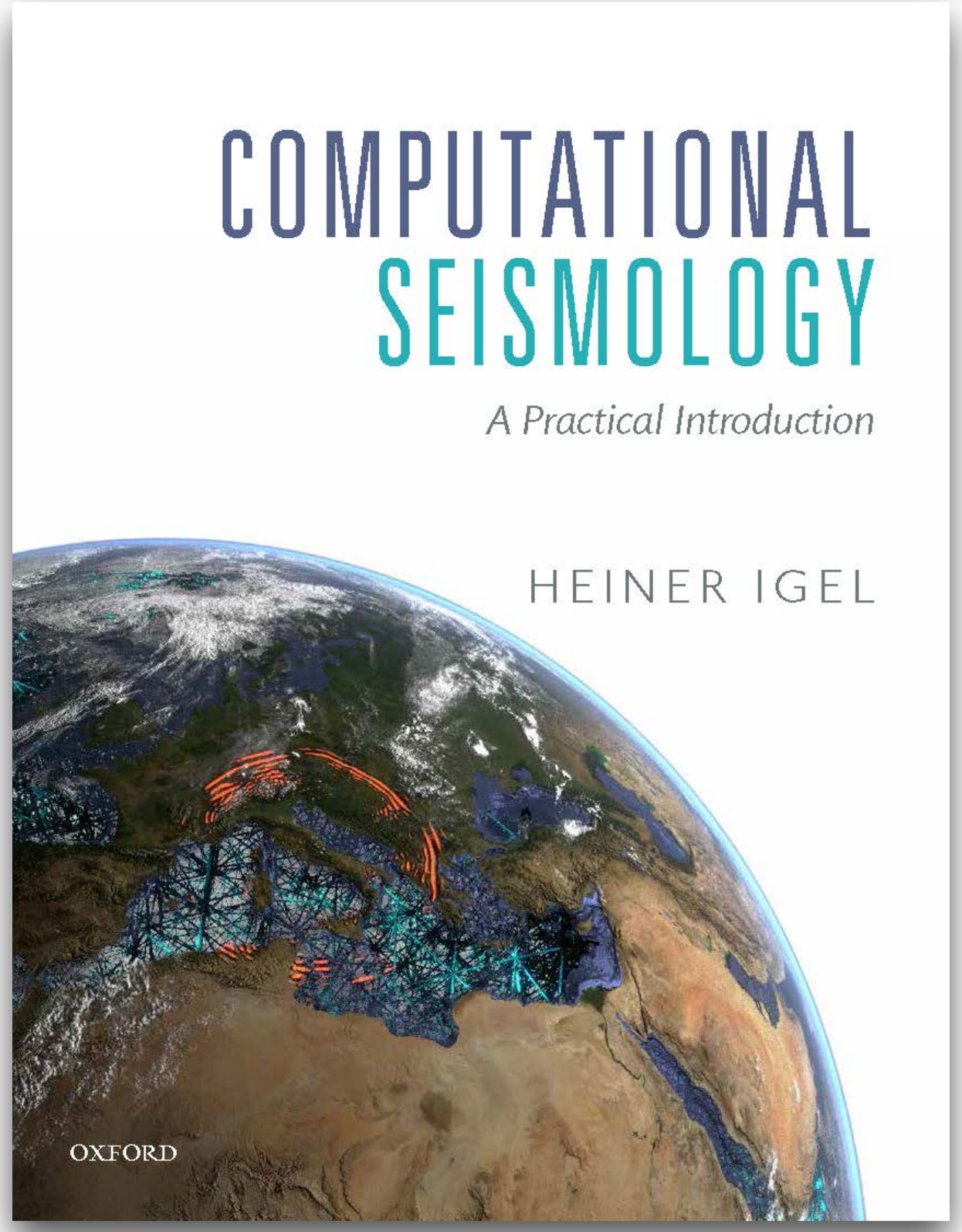

Jyupiter notebooks

http://krischer.github.io/seismo_live/

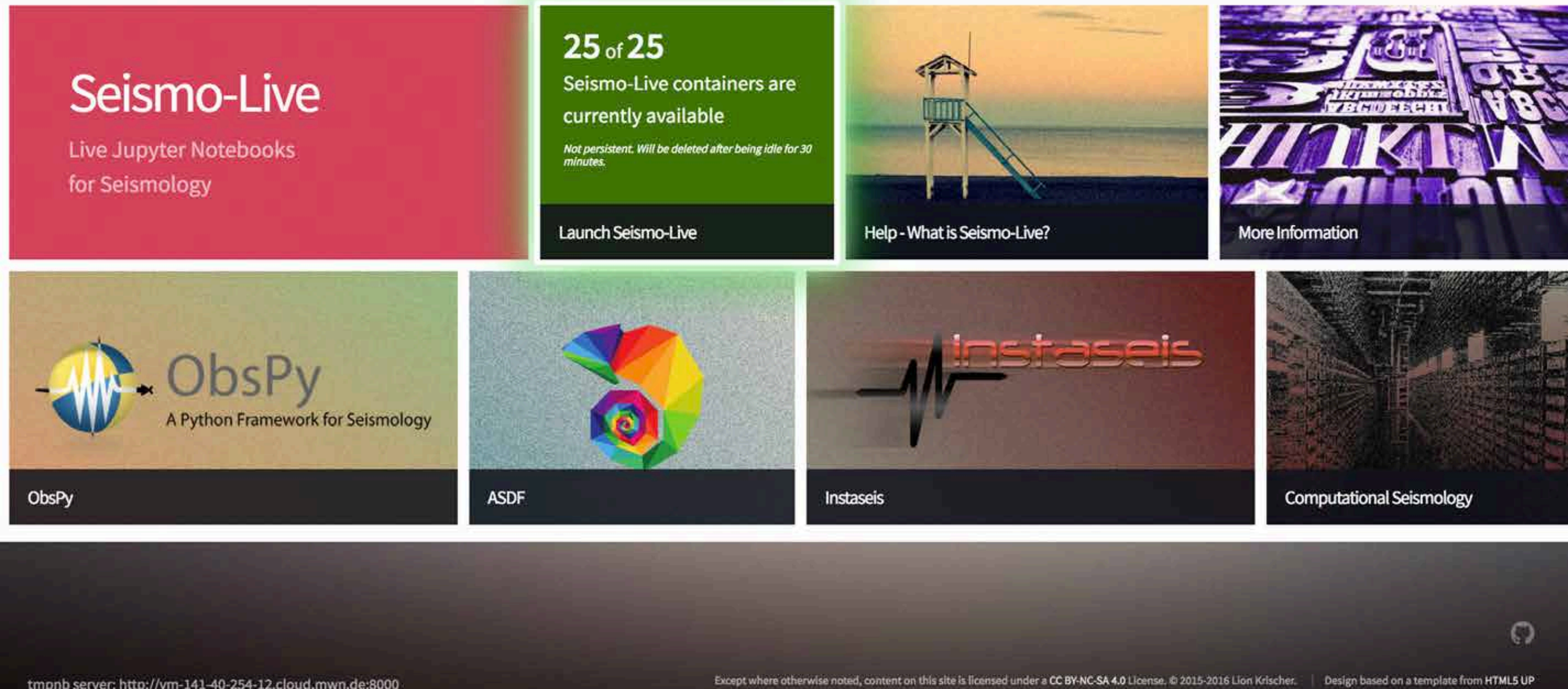

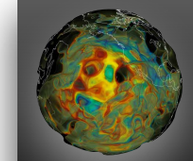

Numerical wave simulations

- Forward problem in seismology
- Numerical methods
  - **Finite difference**
  - Pseudo-spectral
  - Finite elements
  - **Spectral elements**
- How to use a black box?

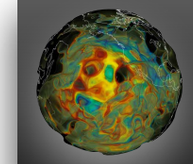

Forward problem in seismology

Equation of motion:

$$\rho \partial_t^2 \mathbf{s} - \nabla \cdot \mathbf{T} = \mathbf{f}$$

Earthquake source:

$$\mathbf{f} = \mathbf{M} \cdot \nabla \delta(\mathbf{x} - \mathbf{x_s}) S(t)$$

Hook's law:

$$\mathbf{T} = \mathbf{c} : \epsilon$$

Boundary conditions:

$$\hat{\mathbf{n}} \cdot \mathbf{T} = 0$$

Initial conditions:

$$\mathbf{s}(\mathbf{x}, 0) = 0 \qquad \partial_t \mathbf{s}(\mathbf{x}, 0) = 0$$

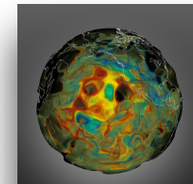

Finite-difference method

Equation of motion:

$$\rho\partial_t^2\mathbf{s} - \nabla\cdot\mathbf{T} = \mathbf{f}$$

density — displacement — stress tensor — source term

Strong form:

$$\partial_t\mathbf{v} = \rho^{-1}(\nabla\cdot\mathbf{T} + \mathbf{f}) \qquad \partial_t\mathbf{T} = \mathbf{c} : \nabla\mathbf{v}$$

$$\mathbf{v} = \partial_t\mathbf{s}$$

1D wave equation in a homogeneous medium

$$\partial_t^2 s(x,t) = \alpha^2\ \partial_x^2 s(x,t)$$

P-wave speed **S-wave speed**

$$\alpha = \sqrt{\frac{\lambda+2\mu}{\rho}} \qquad \left(\beta = \sqrt{\frac{\mu}{\rho}}\right)$$

$$c = \lambda + 2\mu \qquad (c = \mu)$$

Velocity-stress formulation

$$\partial_t v(x,t) = \rho^{-1}\ \partial_x T(x,t)$$

$$\partial_t T(x,t) = c\ \partial_x v(x,t)$$

where

$$v(x,t) = \partial_t s(x,t)$$

$$T(x,t) = c\ \partial_x s(x,t)$$

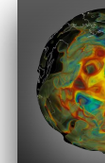

Discretized Earth

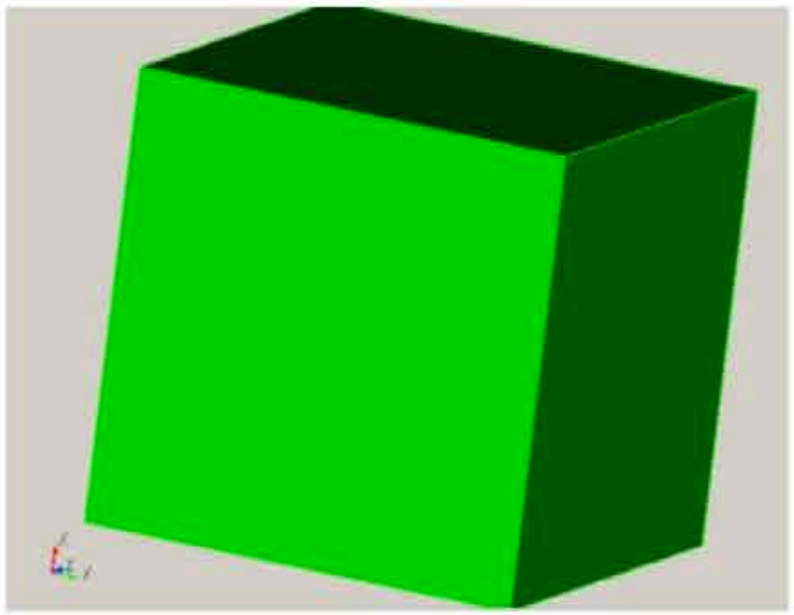

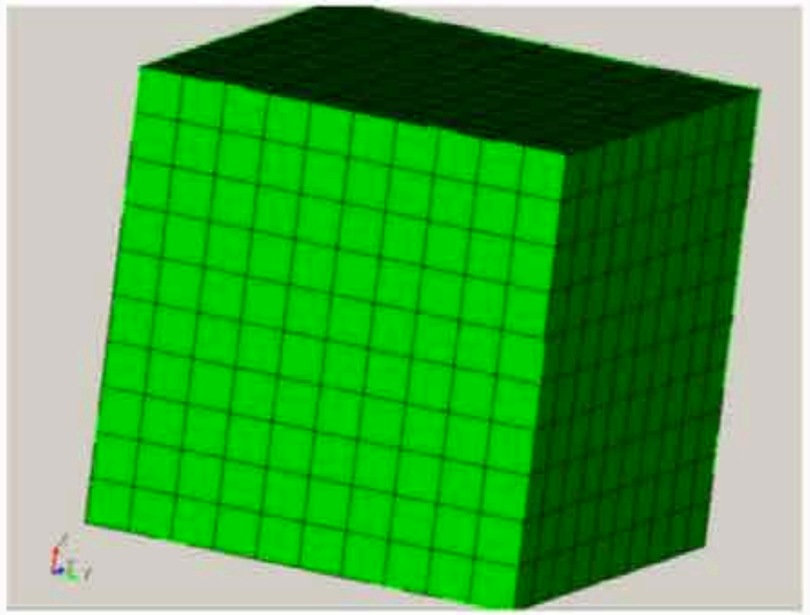

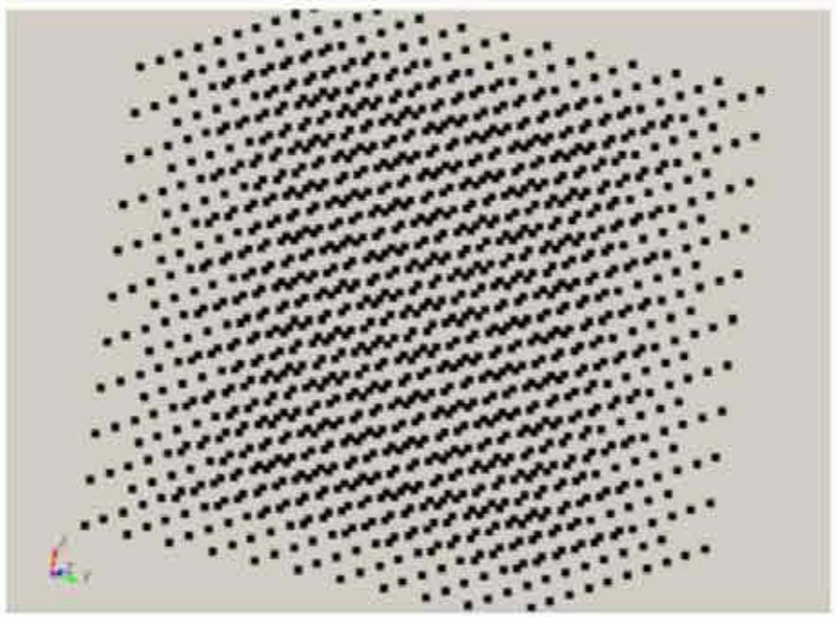

Discretise in both space & time!

Carene Larmat

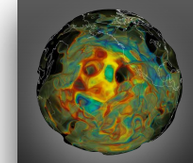

Finite difference & Taylor series

Accuracy of numerical simulations

Taylor series

$$f(x+dx) = f(x) + f'(x)dx + \frac{1}{2!}f''(x)dx^2 + \frac{1}{3!}f'''(x)dx^3 + ...$$

$$f(x-dx) = f(x) - f'(x)dx + \frac{1}{2!}f''(x)dx^2 - \frac{1}{3!}f'''(x)dx^3 + ...$$

Finite difference & Taylor series

$$\partial_t v(x,t) = \rho^{-1}\ \partial_x T(x,t) \qquad \partial_t T(x,t) = c\ \partial_x v(x,t)$$

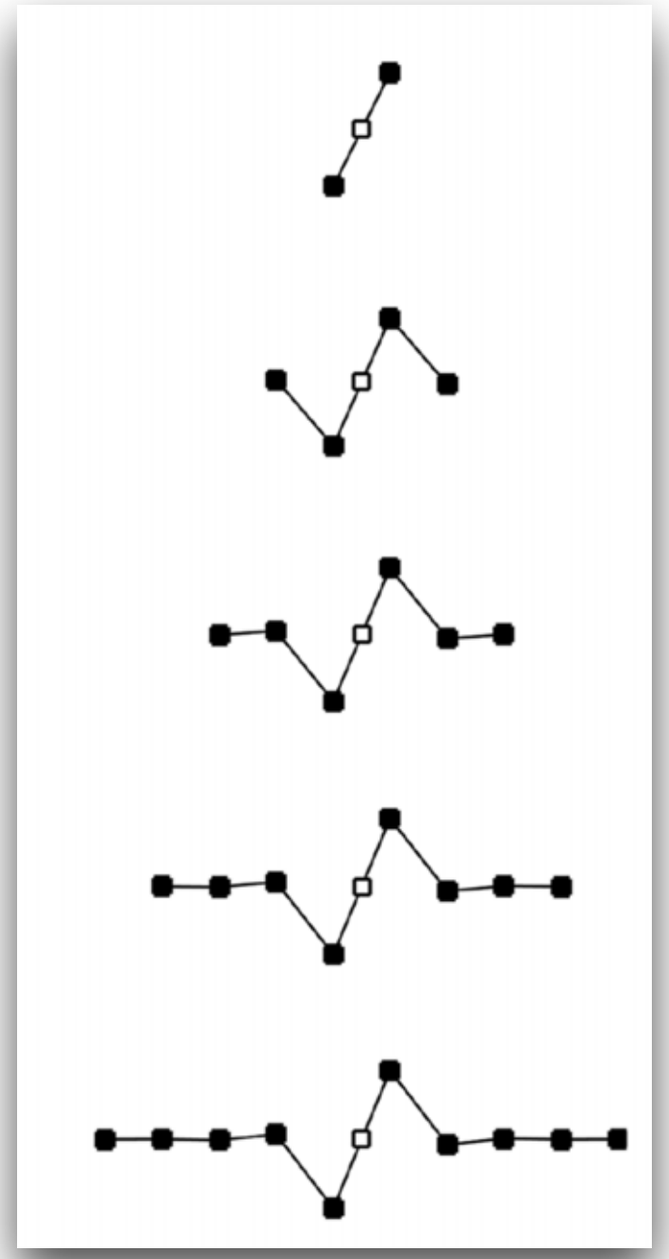

Heiner Igel

$$\frac{f(x+dx)-f(x)}{dx} = f'(x) + O(dx)$$

Forward difference

$$\frac{f(x)-f(x-dx)}{dx} = f'(x) + O(dx)$$

Backward difference

$$\frac{f(x+dx)-f(x-dx)}{2dx} = f'(x) + O(dx^2)$$

Central difference

Stability

Von Neumann Analysis of stability:

$$\frac{p_j^{n+1} - 2p_j^n + p_j^{n-1}}{dt^2} = c_j^2 \left[\frac{p_{j+1}^n - 2p_j^n + p_{j-1}^n}{dx^2}\right]$$

$$with \qquad p_j^n = e^{i(kjdx - \omega ndt)}$$

$$\rightarrow \quad \sin\left(\omega \frac{dt}{2}\right) = c\frac{dt}{dx} sin\left(k\frac{dx}{2}\right)$$

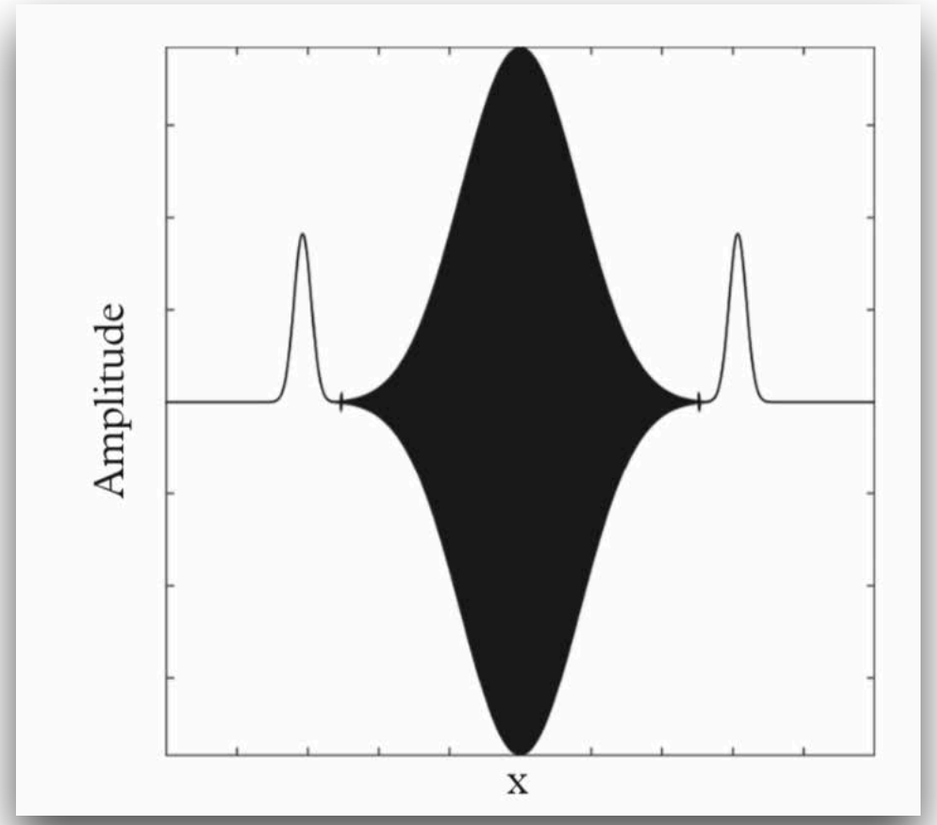

Courant–Friedrichs–Lewy

(CFL) criterion

$$\epsilon = c\frac{dt}{dx} \leq 1$$

sampling rate in time

sampling rate in space

wavespeed

$$\epsilon > 1$$

Wave dispersion

Stein & Wysession 2003

Figure 2.8-4: Example of Love wave group velocity dispersion through bandpass filtering.

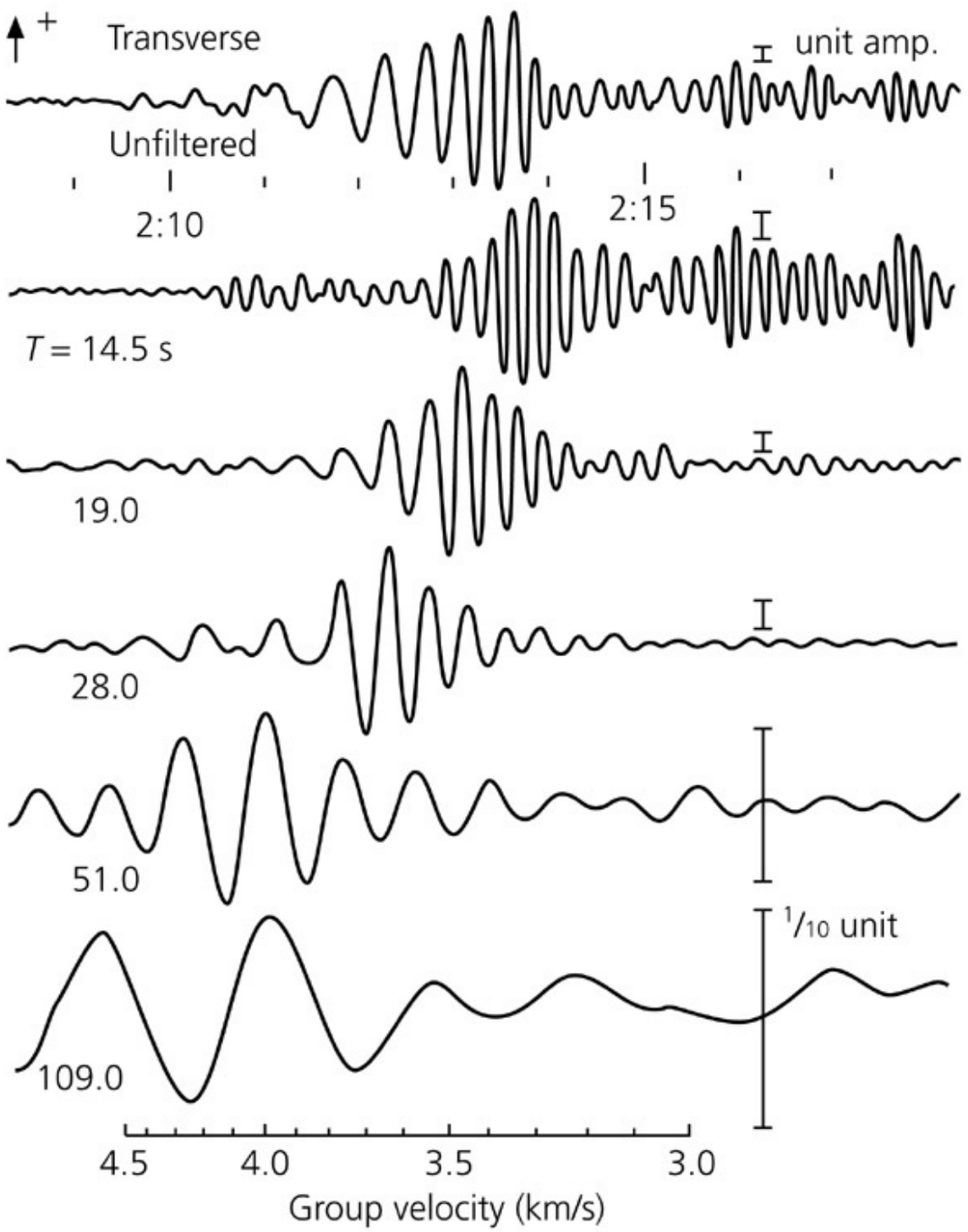

Figure 2.8-2: Fundamental mode Love wave group and phase velocities.

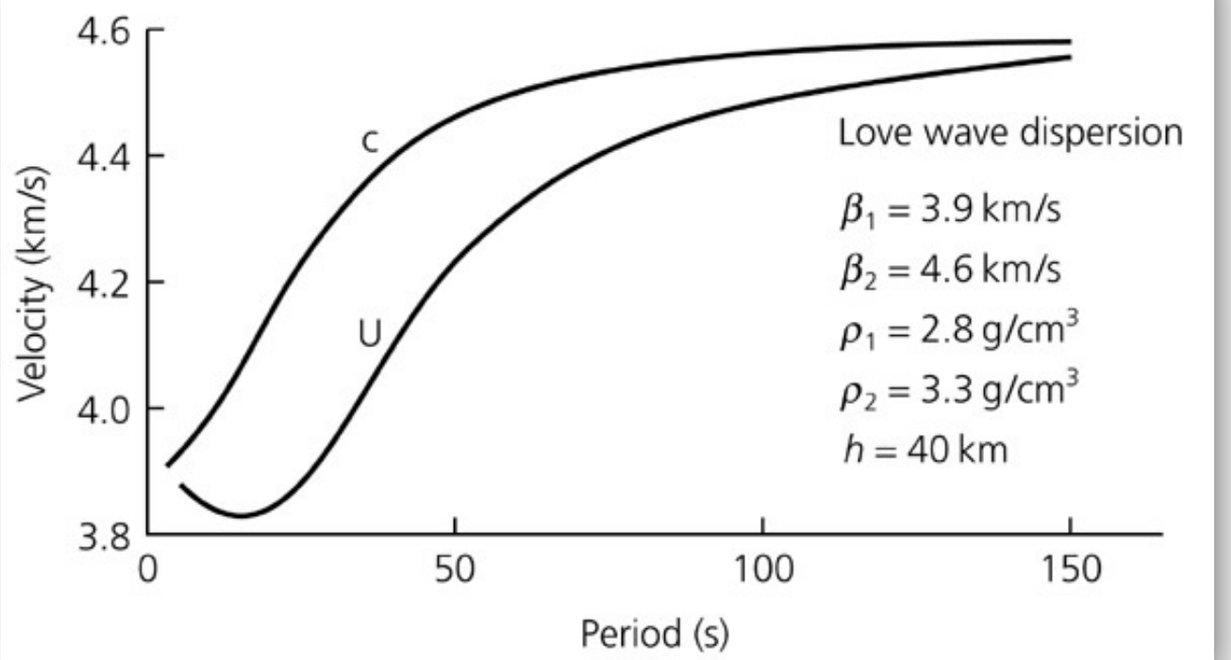

$$c(f) = \lambda(f)\ f \qquad c(f) = \frac{\Delta}{t}$$

Numerical dispersion

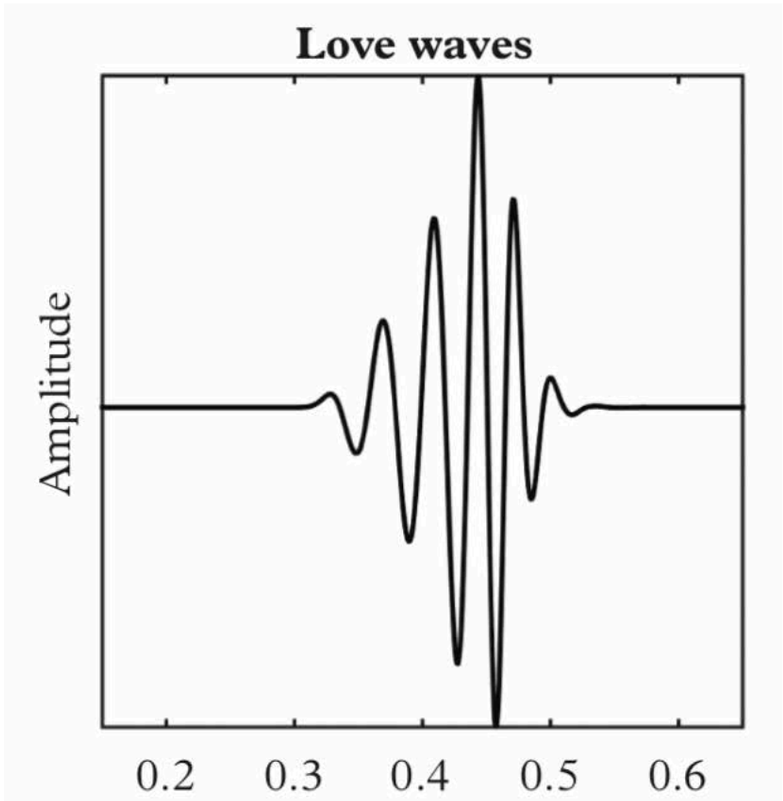

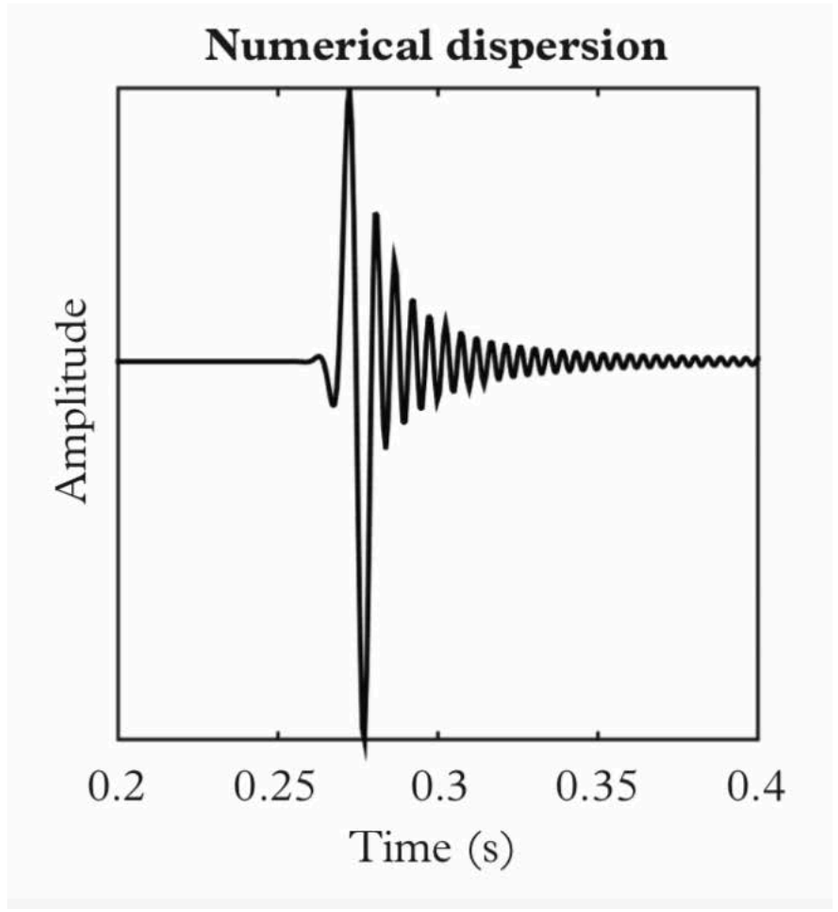

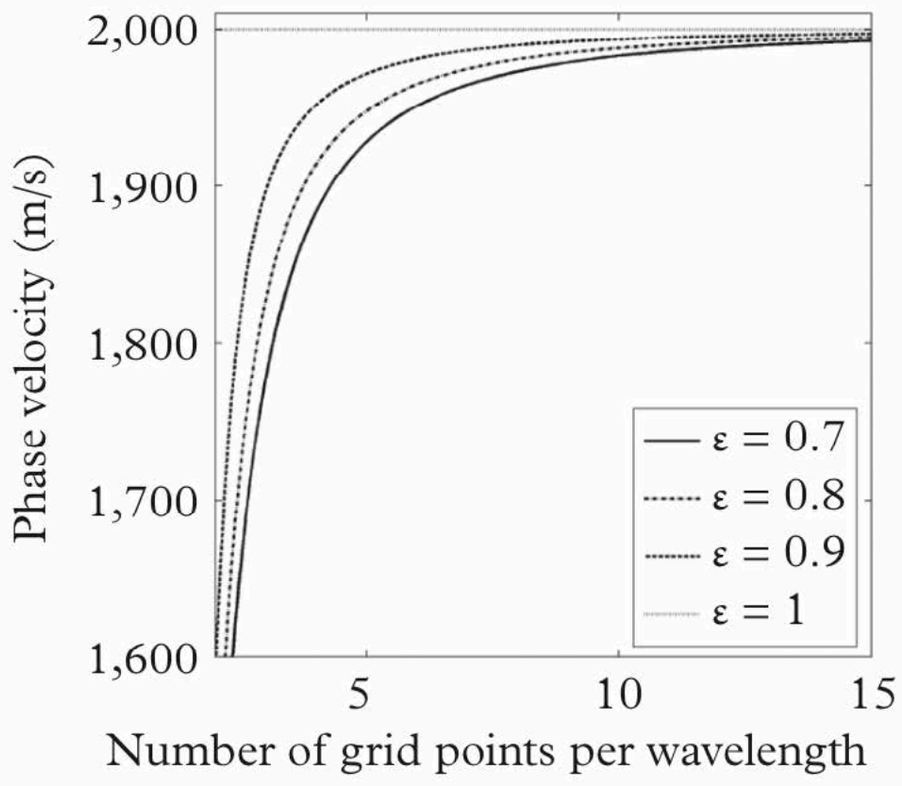

velocity depends on wavenumber!

$$\omega = \frac{2}{dt} \sin^{-1}\left[c\frac{dt}{dx} \sin k\frac{dx}{2} \right]$$

$$c(k) = \frac{\omega}{k} = \frac{2}{kdt} \sin^{-1}\left[c\frac{dt}{dx} \sin k\frac{dx}{2} \right]$$

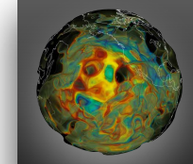

Weak methods (integral form)

Equation of motion:

$$\rho\partial_t^2\mathbf{s} - \nabla\cdot\mathbf{T} = \mathbf{f}$$

Strong form:

$$\partial_t\mathbf{v} = \rho^{-1}(\nabla\cdot\mathbf{T} + \mathbf{f}) \qquad \partial_t\mathbf{T} = \mathbf{c} : \nabla\mathbf{v}$$

$$\mathbf{v} = \partial_t\mathbf{s}$$

Weak form:

$$\int_\Omega \rho\mathbf{w}\cdot\partial_t^2\mathbf{s}\mathrm{d}^3\mathbf{x} = \int_\Omega \nabla\mathbf{w} : \mathbf{T}\mathrm{d}^3\mathbf{x} + \mathbf{M} : \nabla\mathbf{w}(\mathbf{x}_s)S(t)$$

Finite-fault rapture:

$$\mathbf{M} : \nabla\mathbf{w}(\mathbf{x_s})S(t) \rightarrow \int_{S_s} \mathbf{m}(\mathbf{x_s}, t) : \nabla\mathbf{w}(\mathbf{x_s})\mathbf{d^2x_s}$$

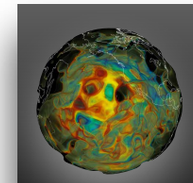

Weak methods (integral form)

Equation of motion:

$$\rho\partial_t^2\mathbf{s} - \nabla\cdot\mathbf{T} = \mathbf{f}$$

Str

- implicitly accounts for free-surface boundary condition
- fluid-solid coupling terms may be explicitly added
- source term explicitly integrated
- valid for any test vector

We

(t)

Finite-fault rapture:

$$\mathbf{M} : \nabla\mathbf{w}(\mathbf{x_s})S(t) \rightarrow \int_{S_s} \mathbf{m}(\mathbf{x_s}, t) : \nabla\mathbf{w}(\mathbf{x_s})\mathbf{d^2x_s}$$

Spectral-element method

- hexahedral elements
- Gauss-Lobatto-Legendre quadrature
- finite elements with high-degree polynomial interpolation: accuracy of pseudo-spectral element methods with the flexibility of finite-element methods
- diagonal mass matrix makes parallel implementation very efficient
- mesh honours major discontinuities
- explicit time-marching scheme

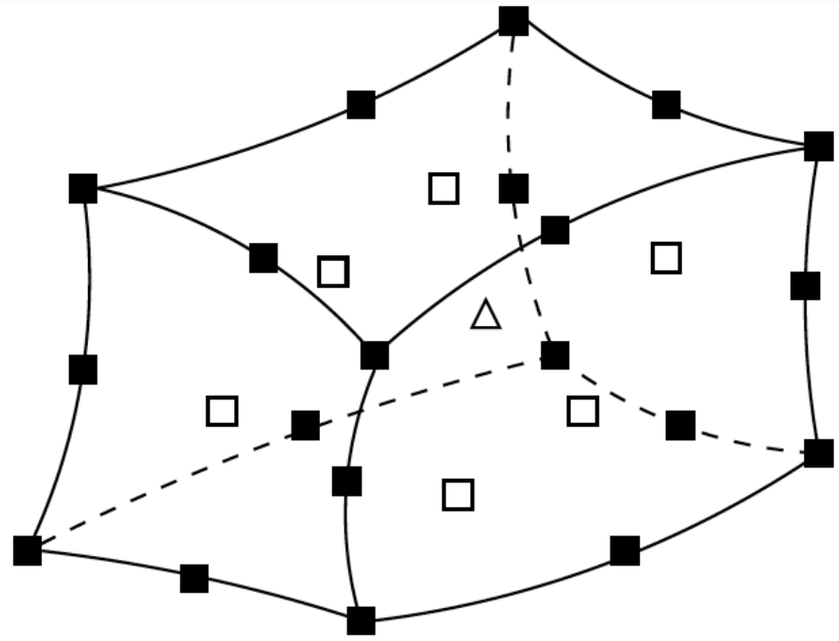

5 Degree 4 Lagrange polynomials

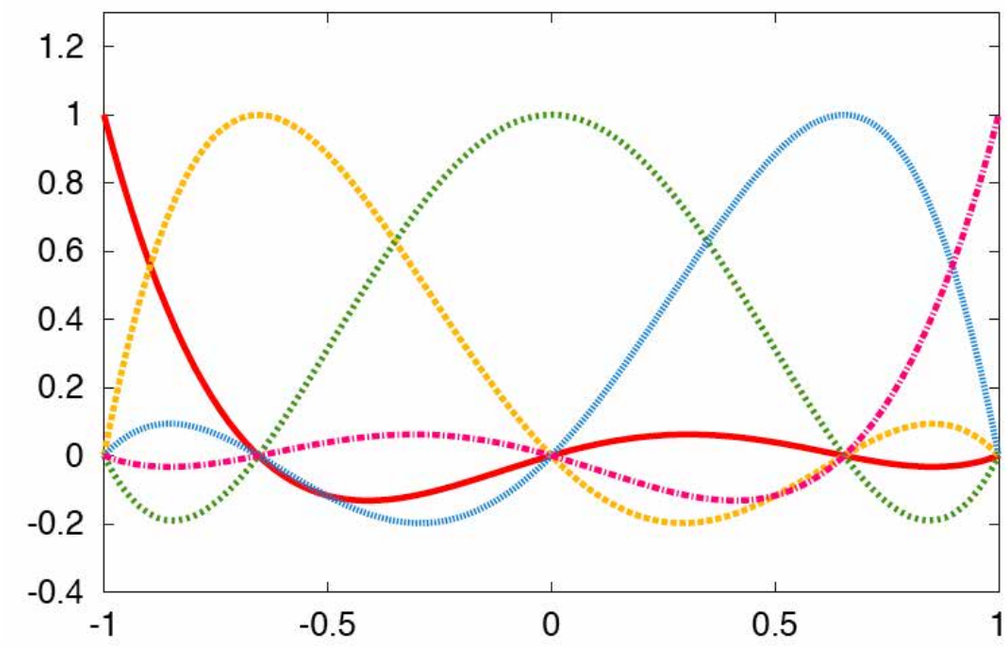

Spectral-element method

- **hexahedral elements**

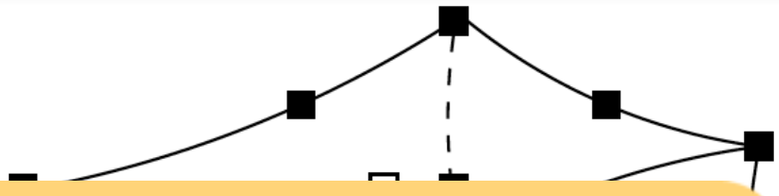

- Capdeville, Y., Chaljub, E., Vilotte, J.P. & Montagner, J.P., 2003. Coupling the spectral element method with a modal solution for elastic wave prop- agation in global earth models, *Geophys. J. Int.*, 152, 34–67.
- Chaljub, E. & Valette, B., 2004. Spectral element modelling of three- dimensional wave propagation in a self-gravitating Earth with an arbi- trarily stratified outer core, *Geophys. J. Int.*, 158, 131–141.
- Komatitsch, D. & Tromp, J., 2002a. Spectral-element simulations of global seismic wave propagation – I. Validation, *Geophys. J. Int.*, 149(2), 390–412.
- Peter, D. *et al.*, 2011. Forward and adjoint simulations of seismic wave propagation on fully unstructured hexahedral meshes, *Geophys. J. Int.*, **186**(2), 721–739.
- Nissen-Meyer, T., van Driel, M., Stähler, S. C., Hosseini, K., Hempel, S., Auer, L., Colombi, A., and Fournier, A., 2014. AxiSEM: broadband 3-D seismic wavefields in axisymmetric media, Solid Earth, 5, 425-445, doi:10.5194/se-5-425-2014, 2014.

- **mesh honours major discontinuities**

- **explicit time-marching scheme**

ials

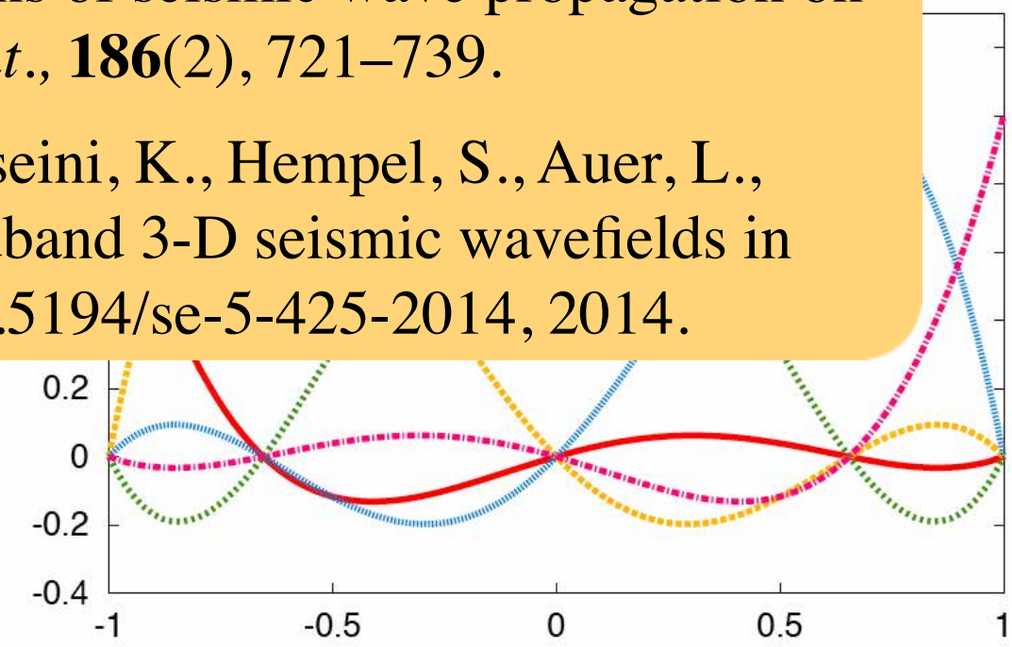

Coffee cup simulation by Daniel

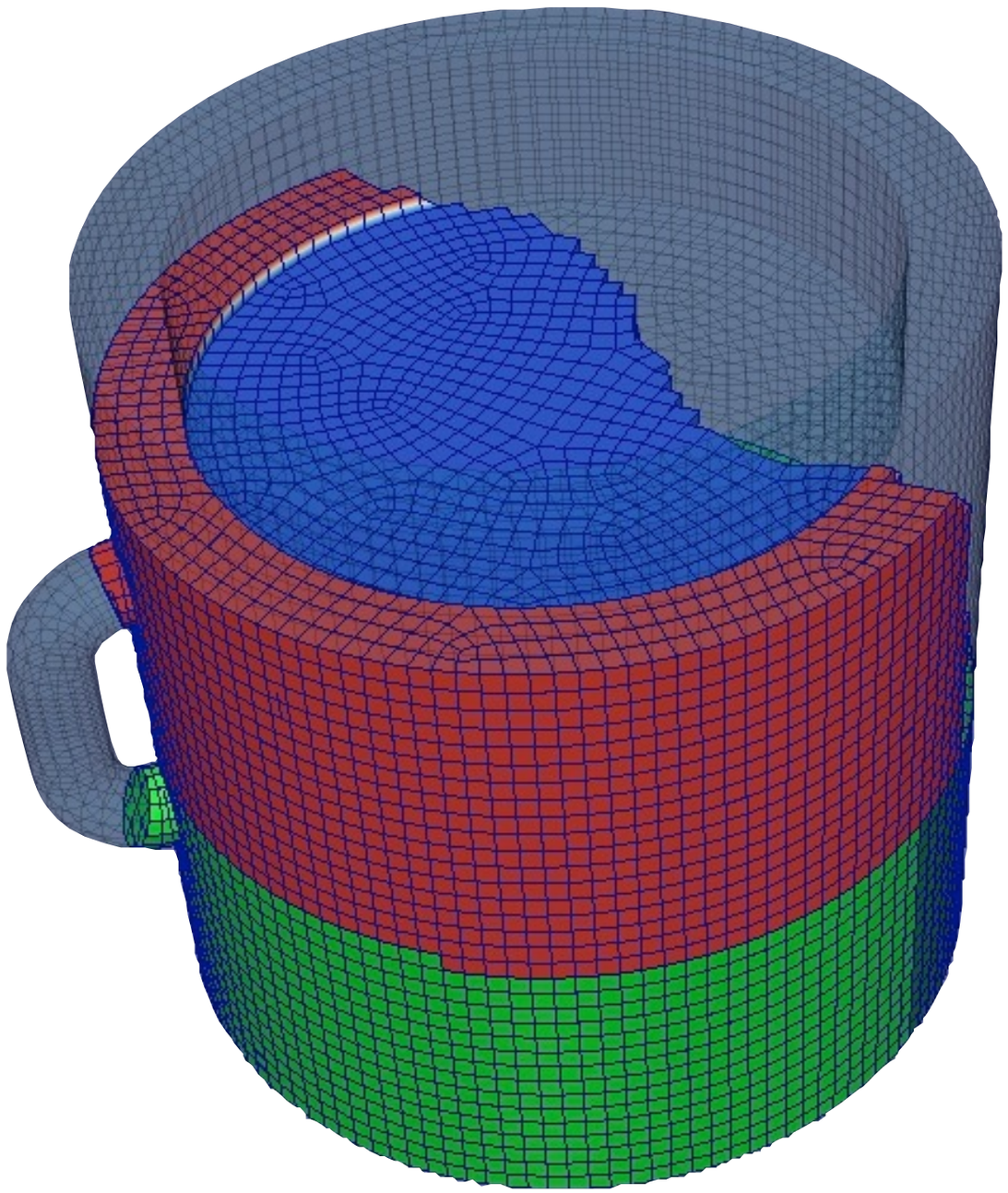

Daniel Peter

Finite-source effects

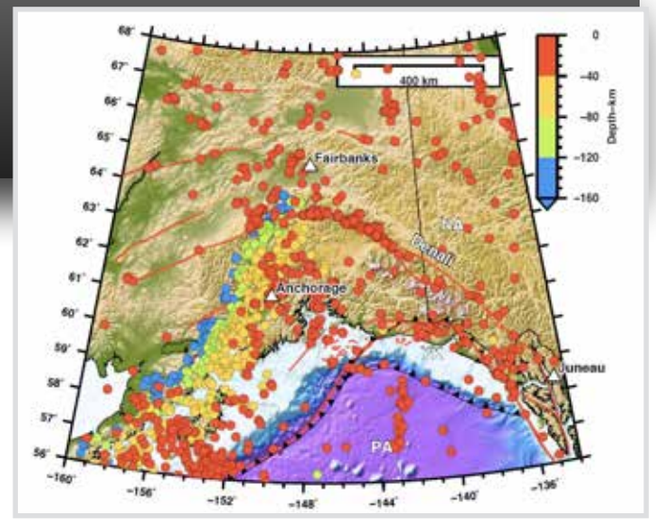

1964 Alaska Earthquake

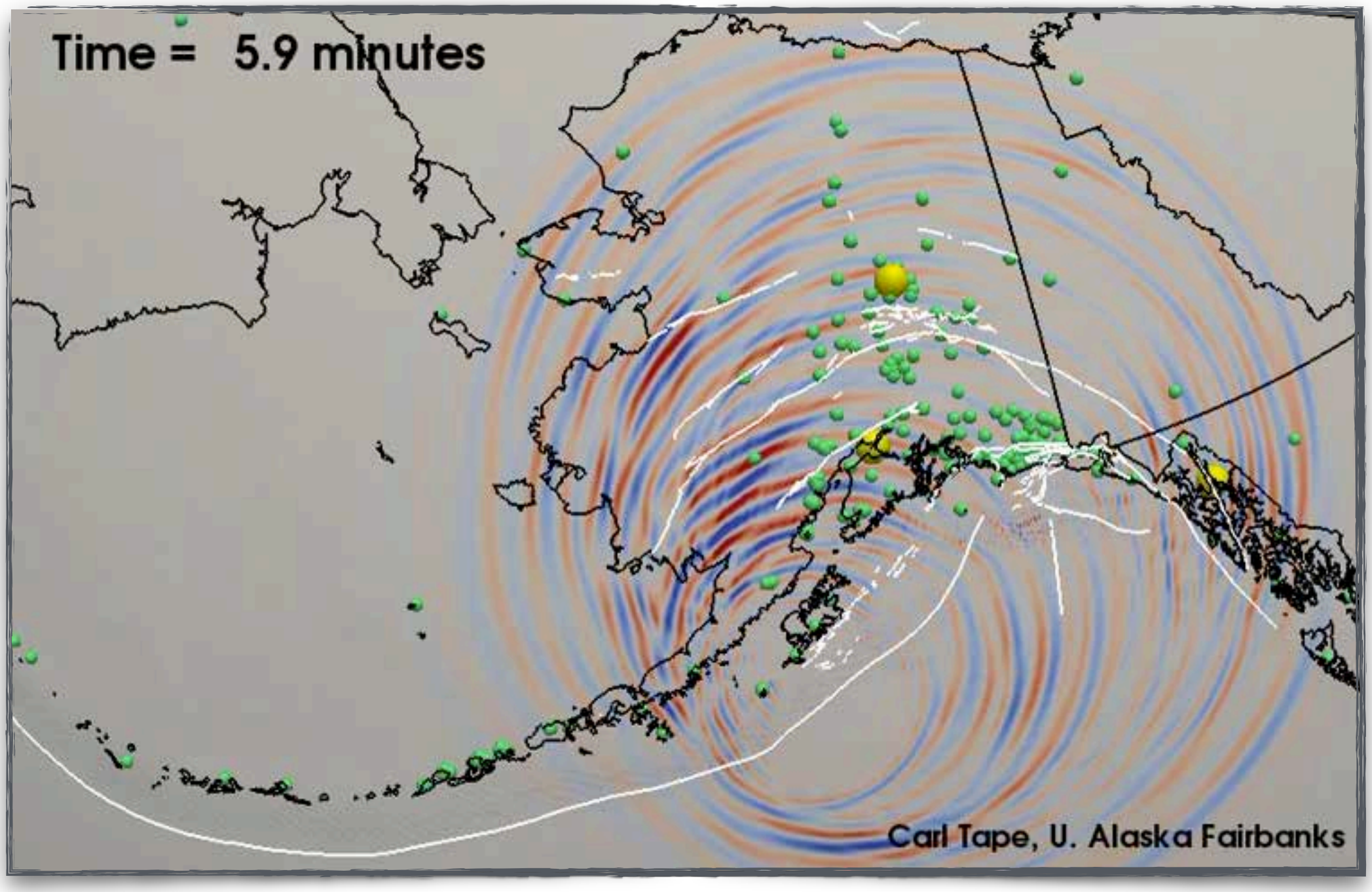

Meshing the Earth

Human time	Simulation workflow	CPU time
15%	Design	0%
80%	Geometry & Meshing	10%
5%	Solver	90%

Source: E. Casarotti, pers. comm.

SPECFEM3D & SW4: Regular meshes

Partitioning: balance between computational load and communication.

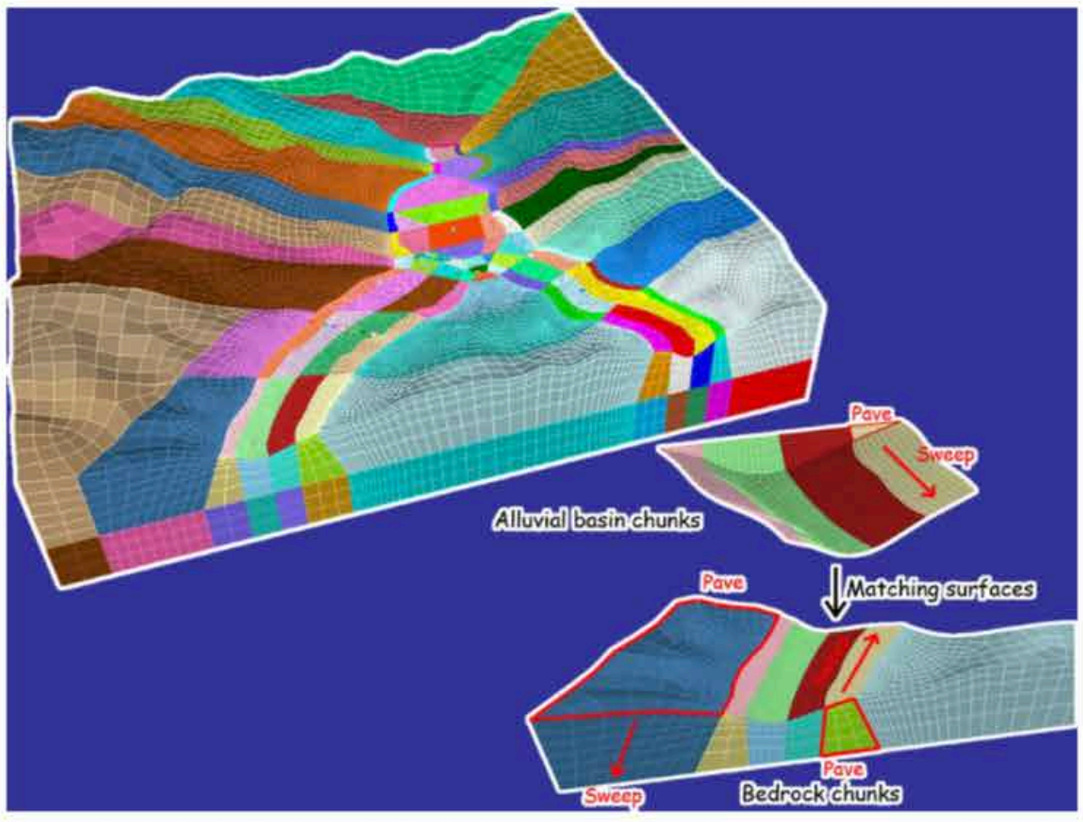

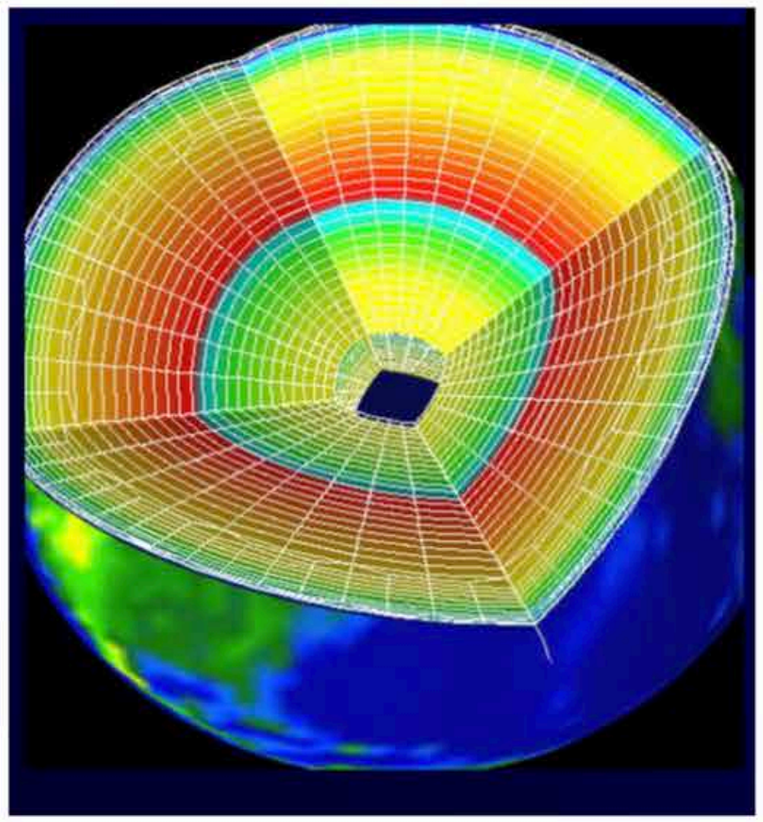

Carene Larmat

Global mesh

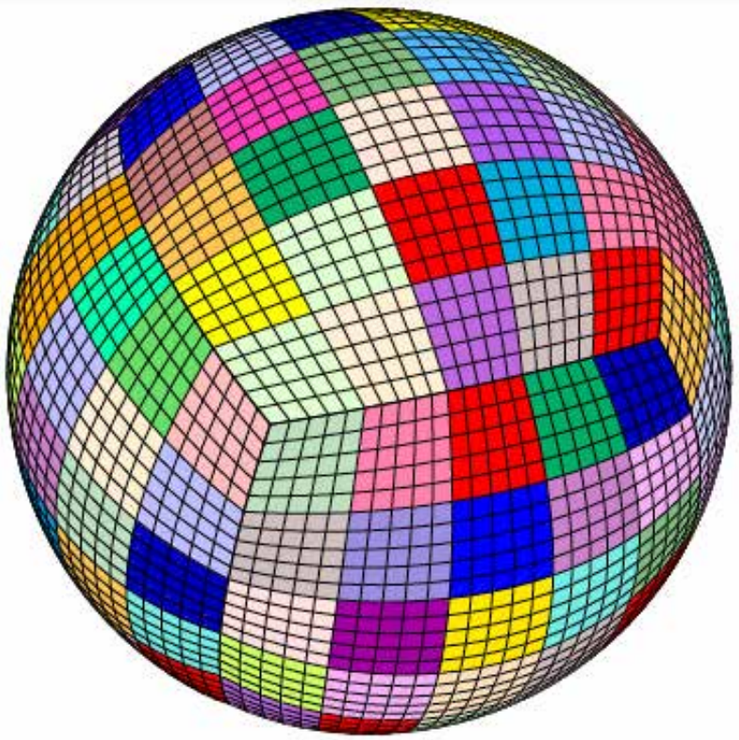

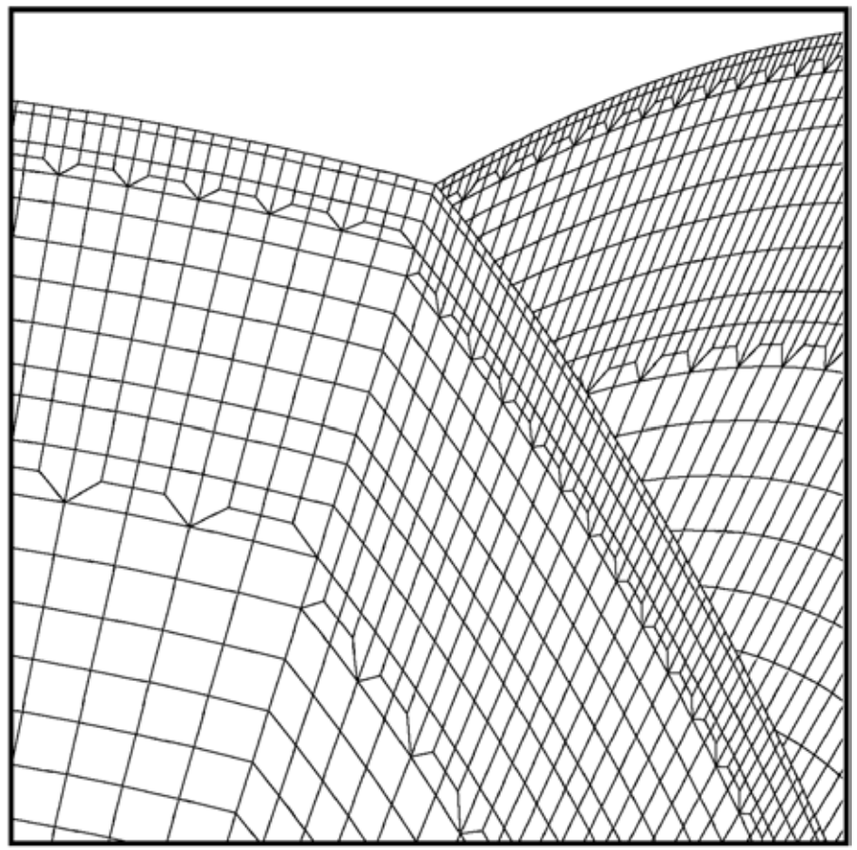

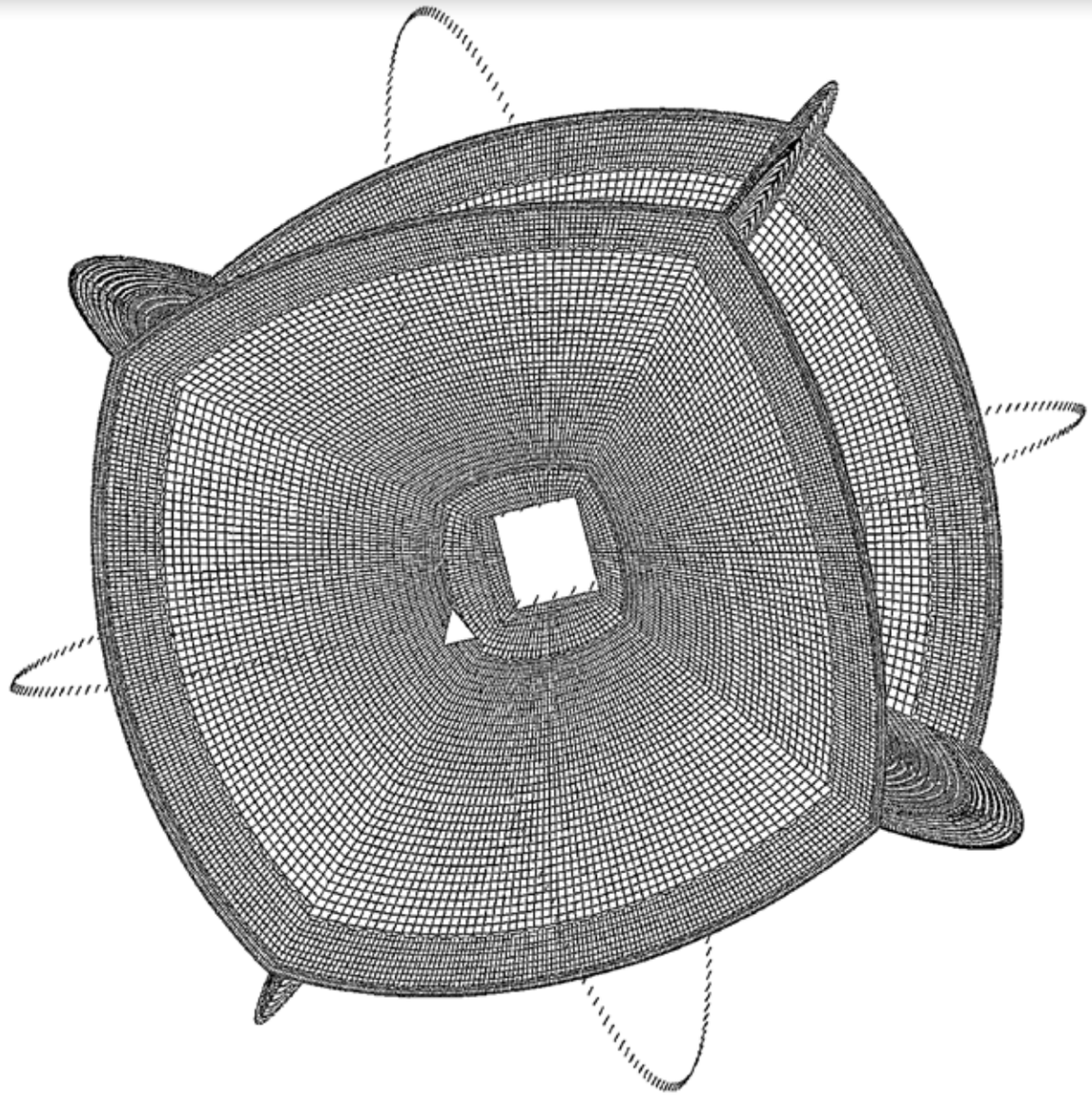

D. Komatitsch & J. Tromp, 2002, GJI

PREM (Preliminary Reference Model)
(A. Dziewonski & D. Anderson, 1981)

3D global wave simulations

February 16, 2018, Oaxaca, Mexico

Mw=7.2, depth=19 km

global.shakemovie.princeton.edu/

Observed vs. 3D seismograms

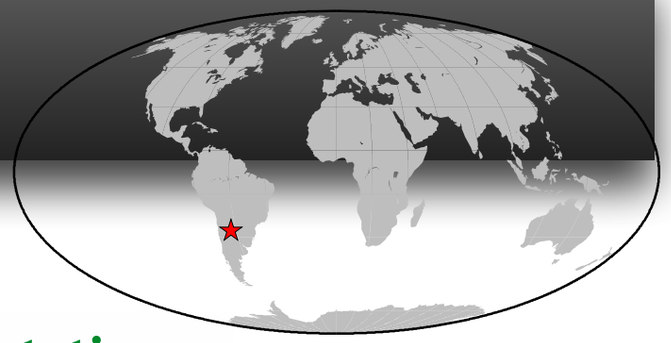

epicentral distance

station codes

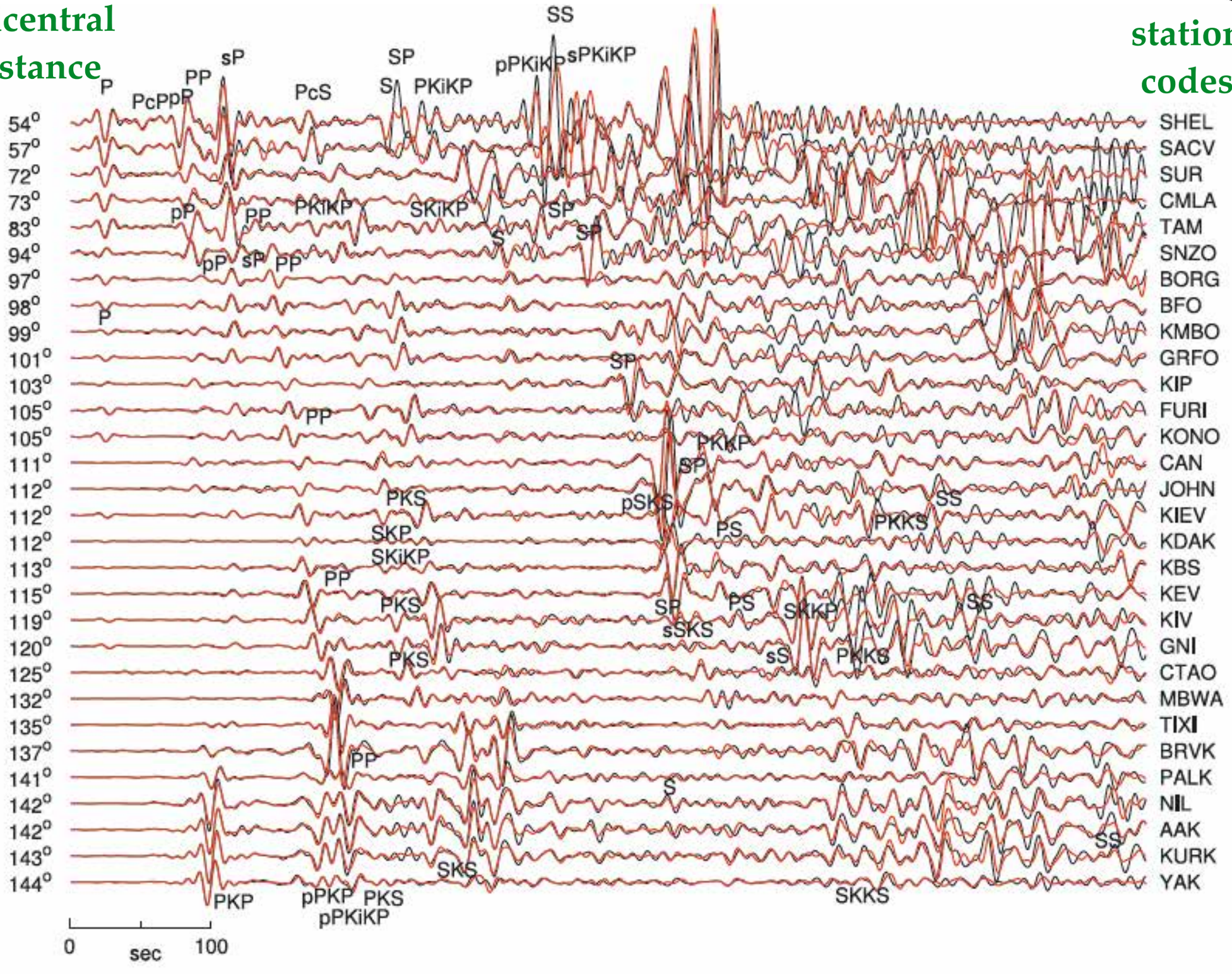

Sept. 3, 2008,
Argentina
Earthquake
$M_w = 6.3$
depth = 571 km

SPECFEM3D_GLOBE

3D Earth model:
S362ANI + Crust2.0
(Kustowski et al. 2007 &
Bassin et al. 2000)

17 - 60 s

Seismic wave simulations on Mars

Daniel Peter & Ebru Bozdag

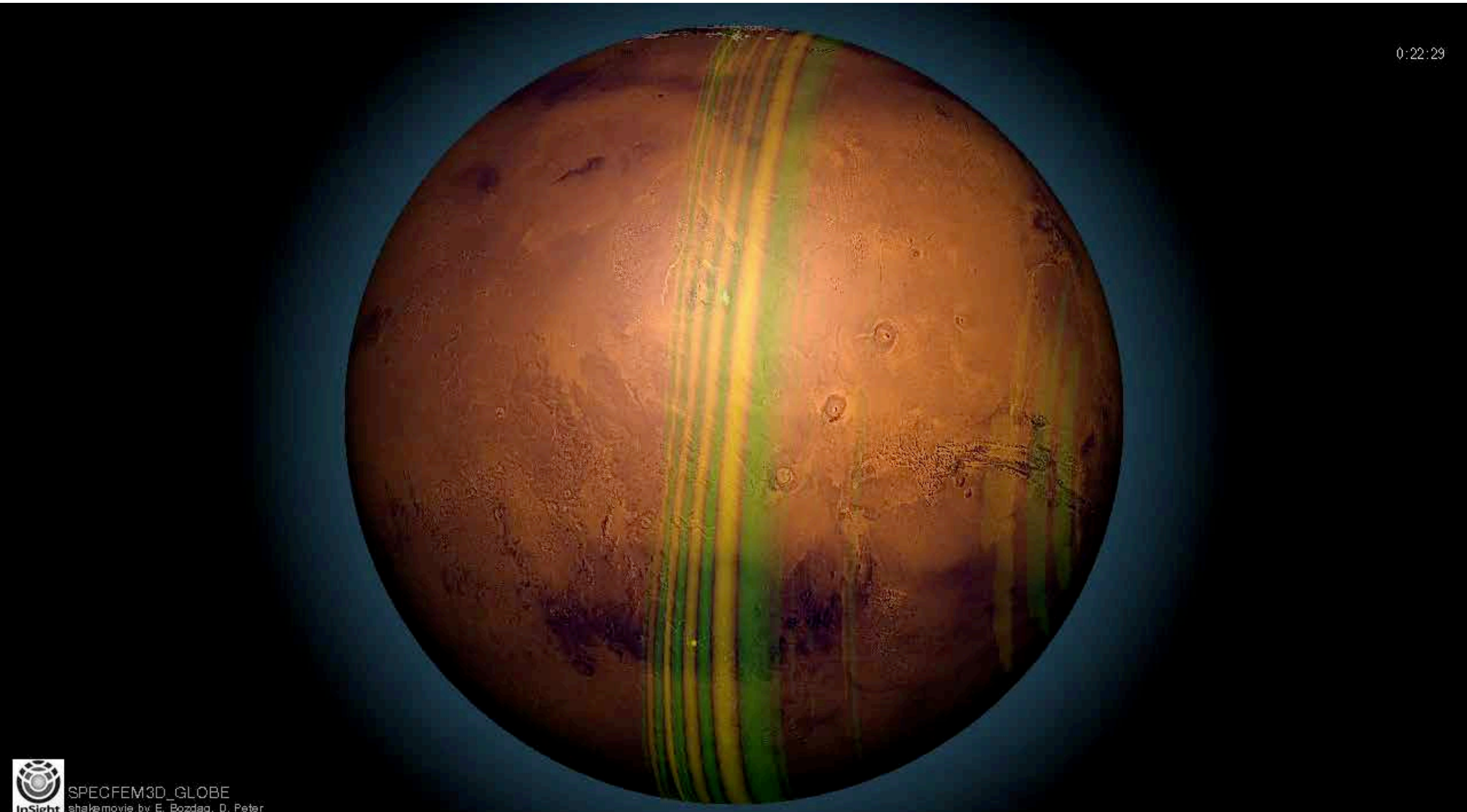

Seismic wave simulations on Mars

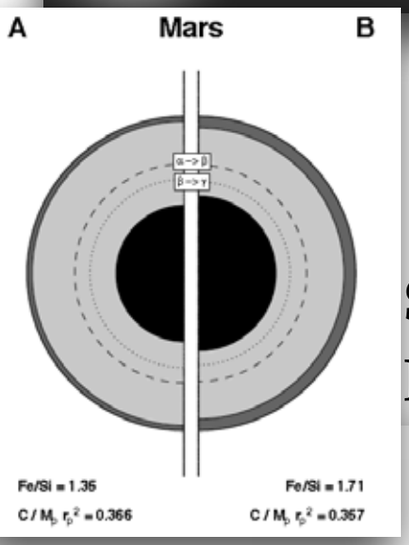

Sohl & Spohn (1997)
Model A

E. Bozdag, Y. Ruan et al. 2017, Space Science Rev.

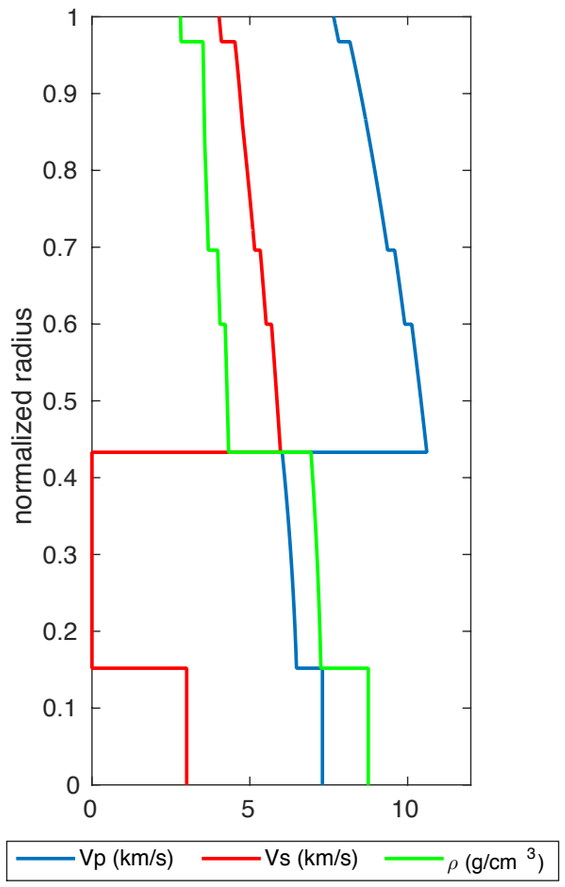

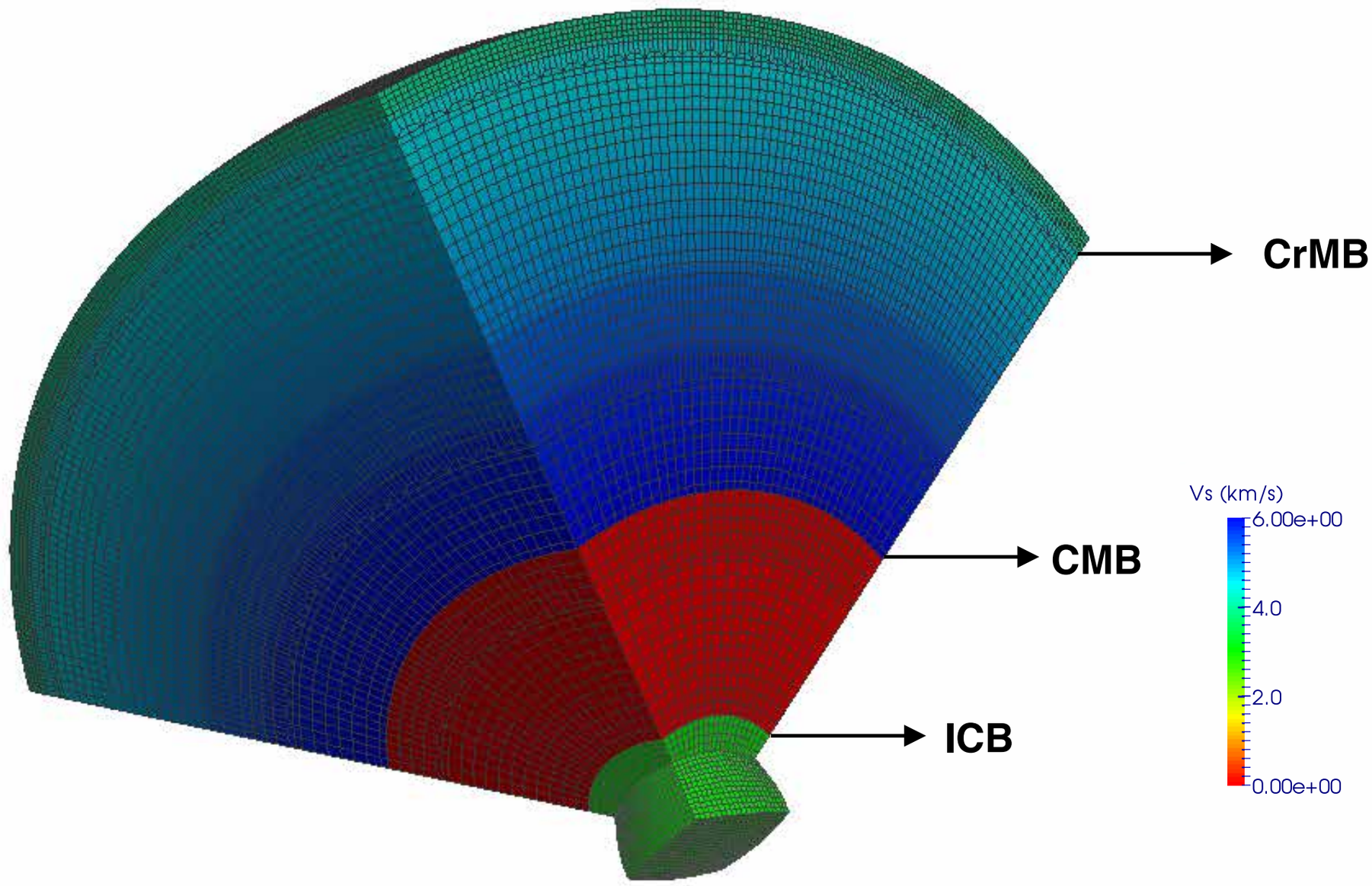

3D crustal mesh

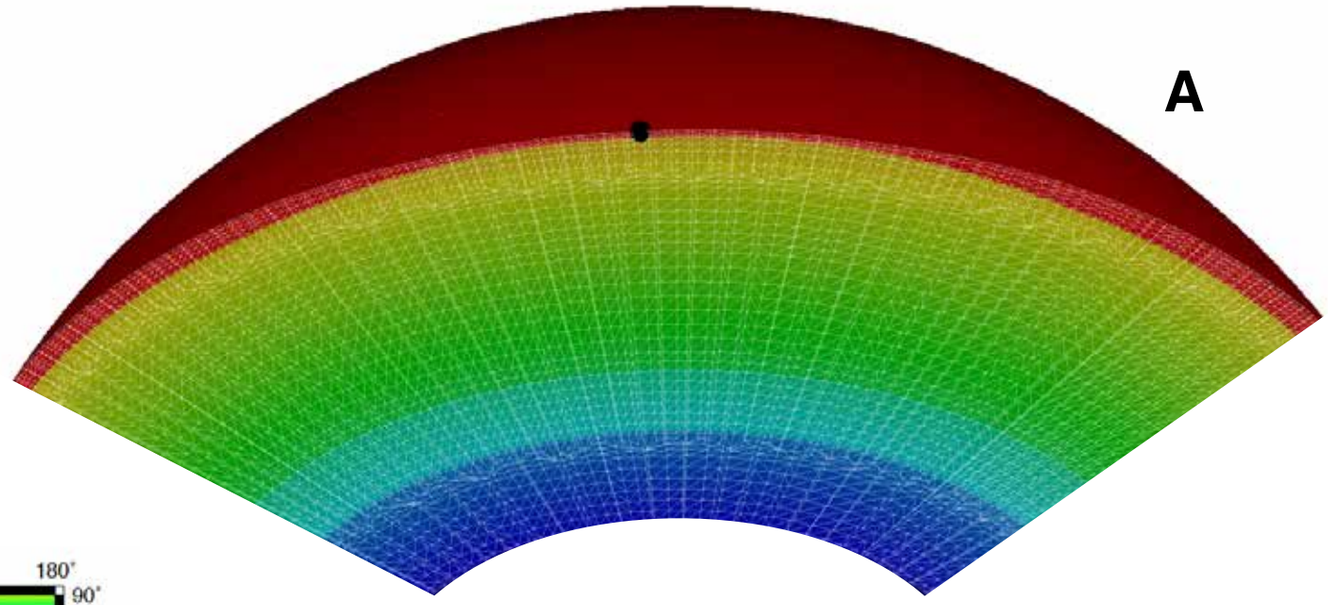

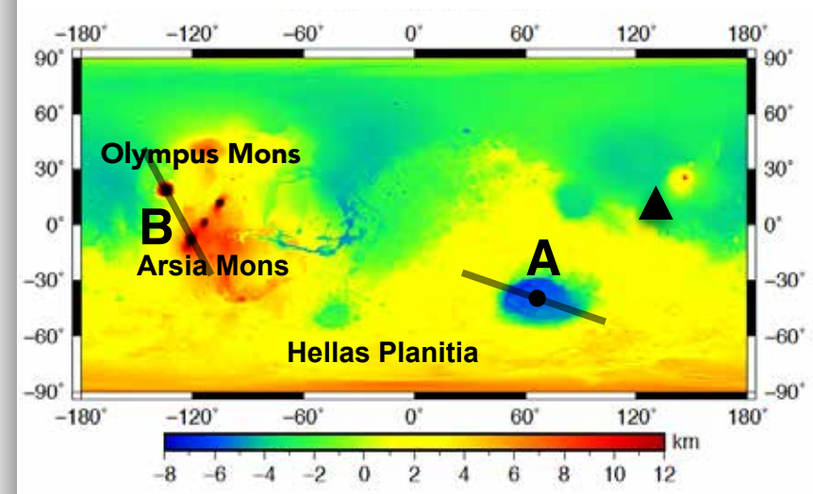

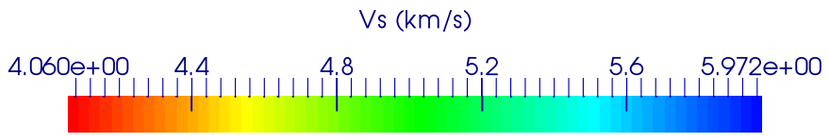

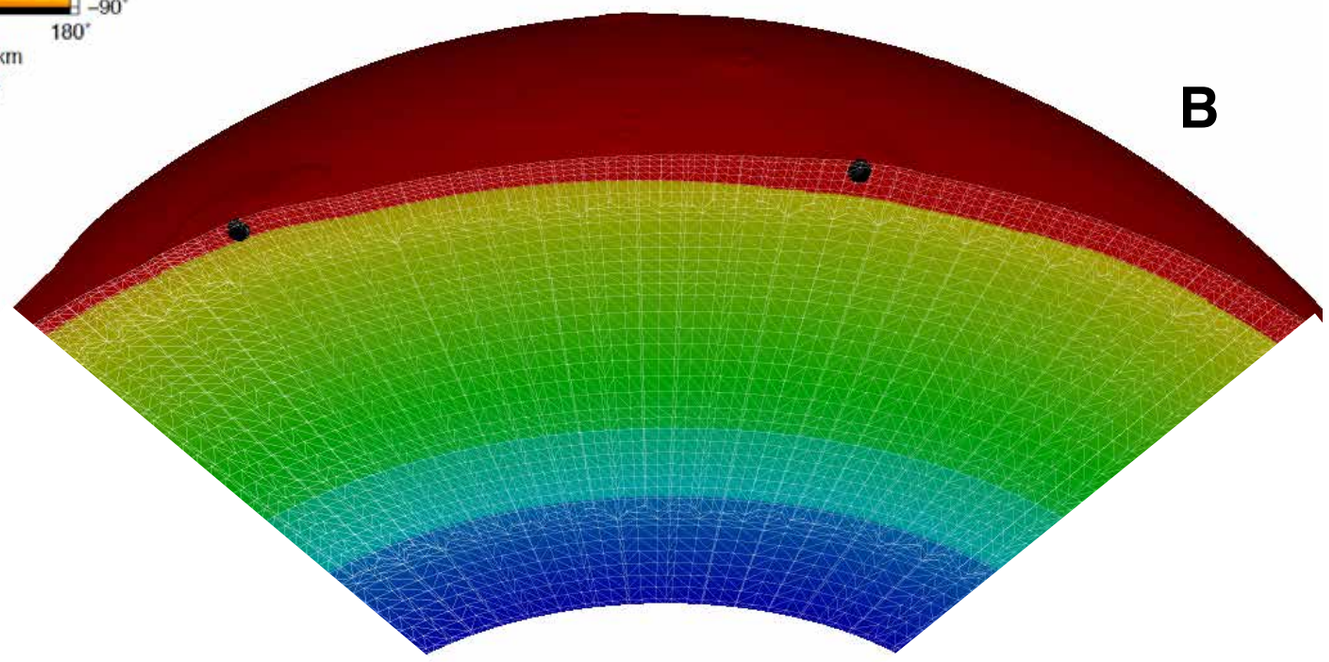

Bozdag, Yuan et al. 2017

3D crustal effects

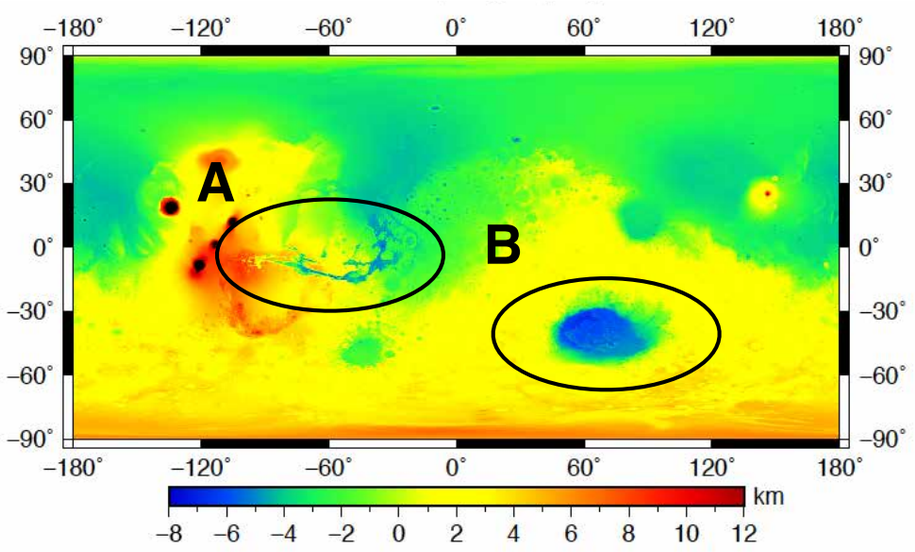

A

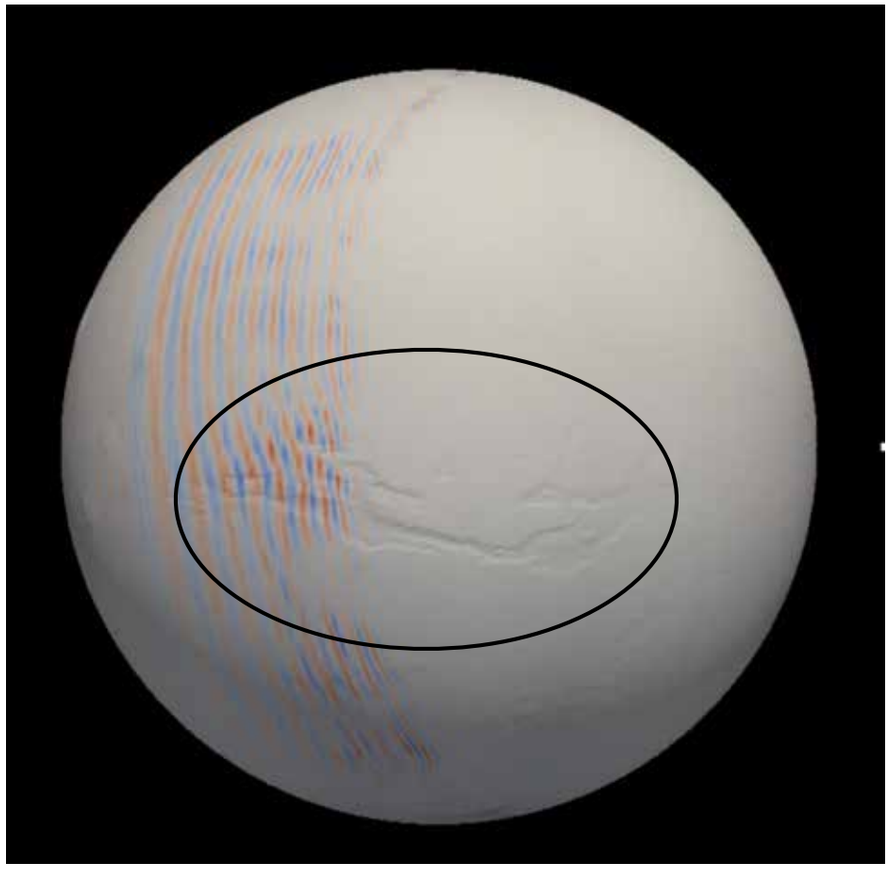

B

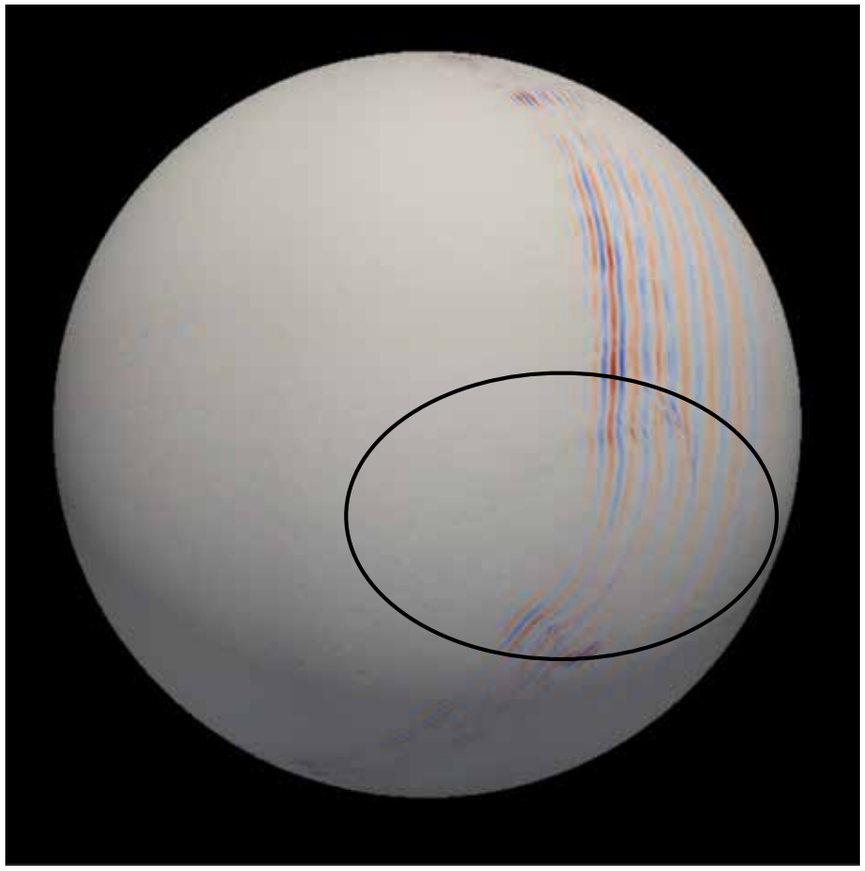

Bozdag, Yuan et al. 2017

3D vs. 1D Martian seismograms

InSight

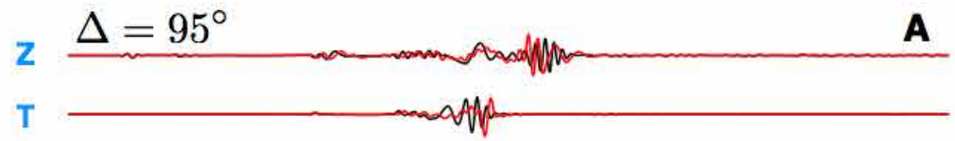

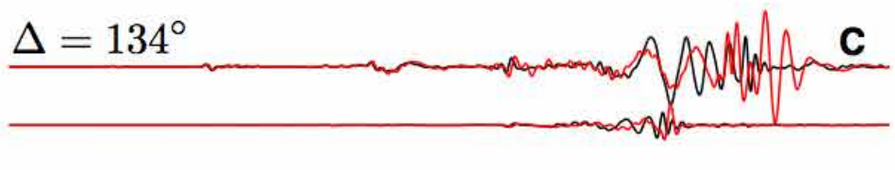

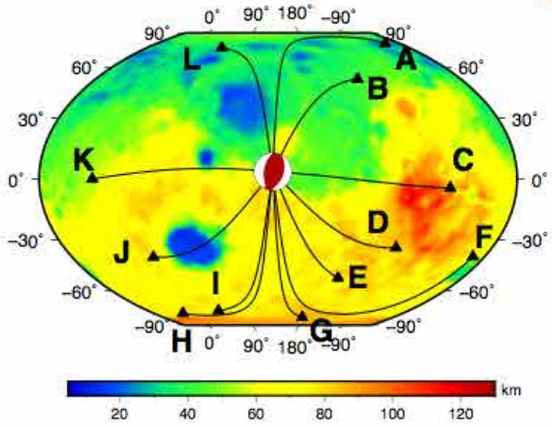

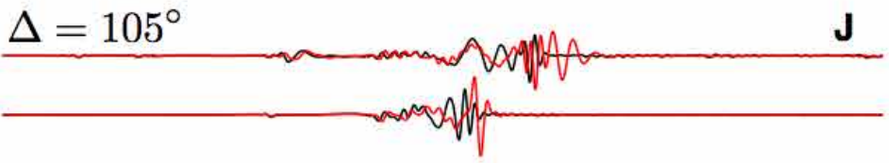

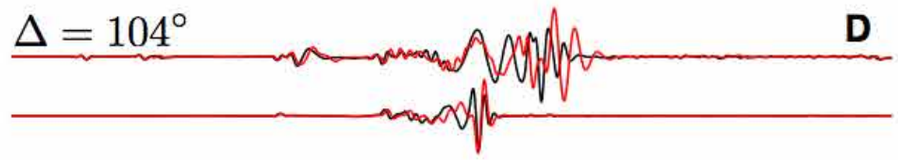

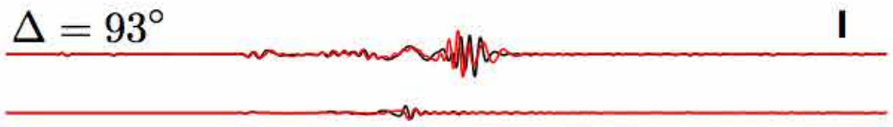

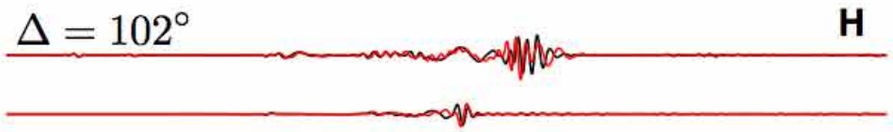

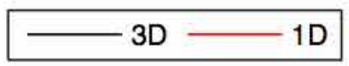

Bozdag et al. 2017

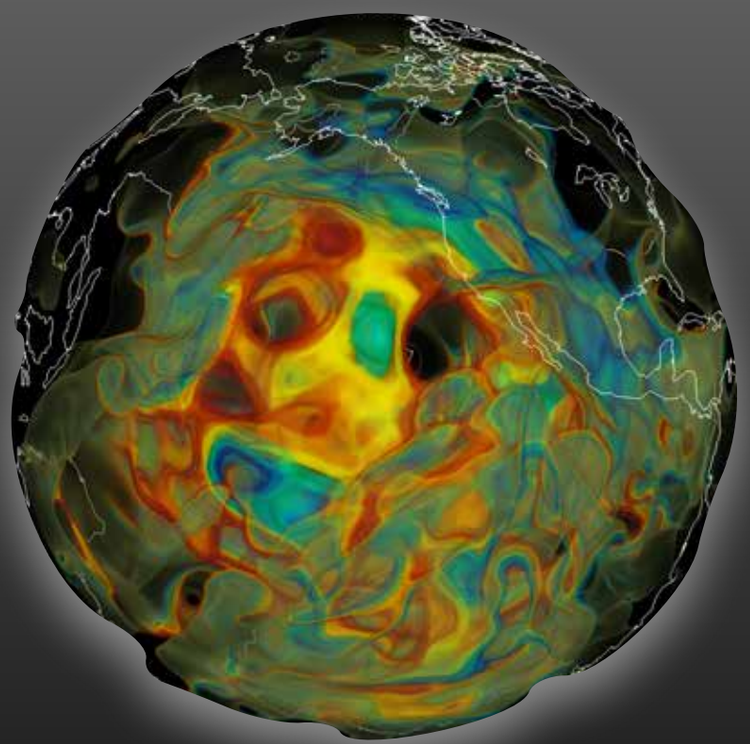

3D wave simulations in seismic tomography

Classical global seismic tomography

PREM
(Dziewonski & Anderson 1981)

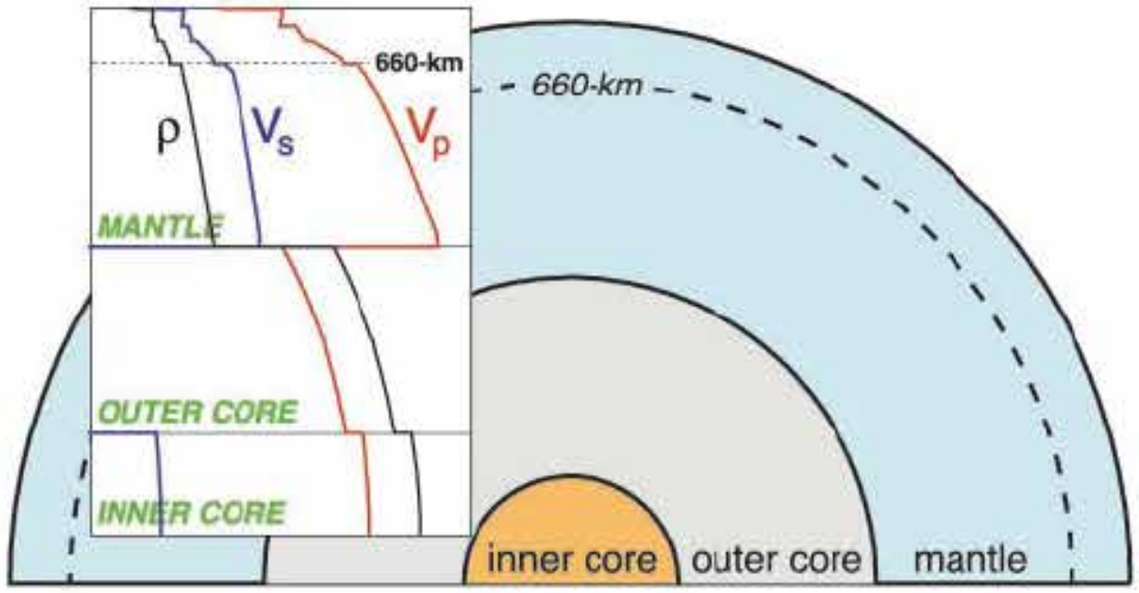

S20RTS
(Ritsema et al. 1999)

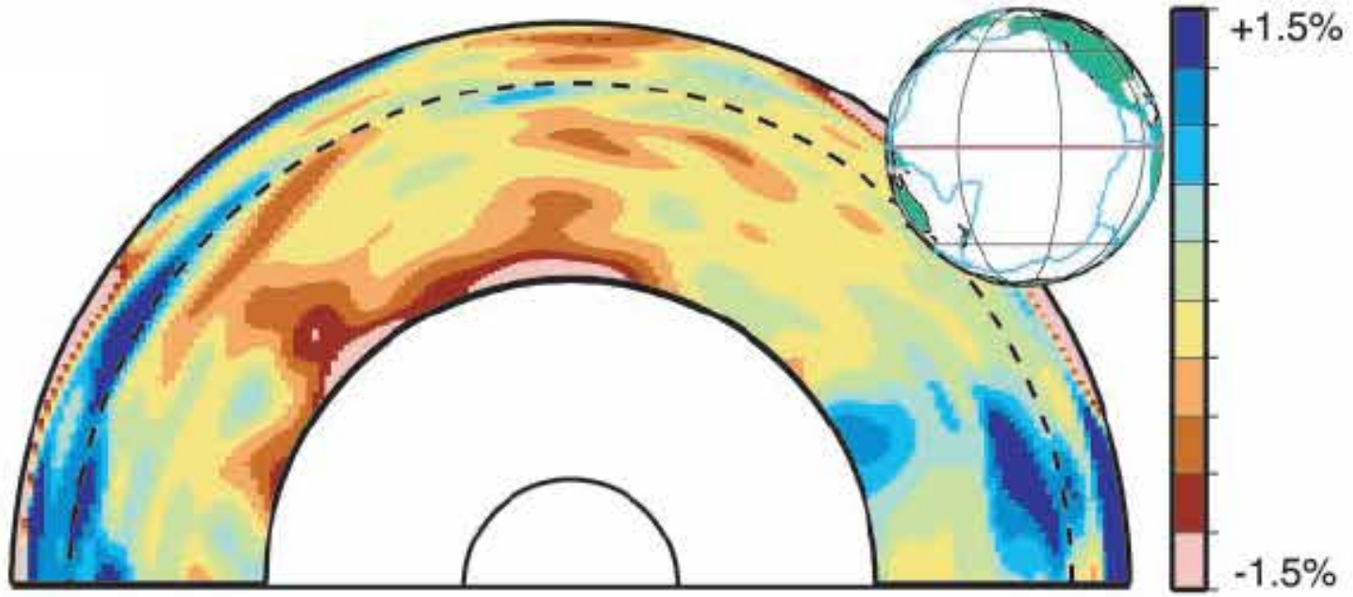

V(r)
1D reference velocity model

seismic modeling

δV(r,θ,φ)
3D velocity structure

from D. Komatitsch, J. Ritsema & J. Tromp, 2002, Science

- **Ray theory, finite-freq. theory based on 1D background models, 3D synthetics with asymptotic kernels**
- **Data coverage: Combination of different data types**
- **Crustal corrections**

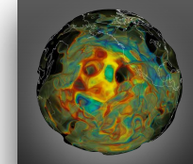

Challenges in global tomography

- **We are at a stage where details matter!**
  - ***Avoid approximations as much as possible***

Challenges in global tomography

- **We are at a stage where details matter!**
  - ***Avoid approximations as much as possible***

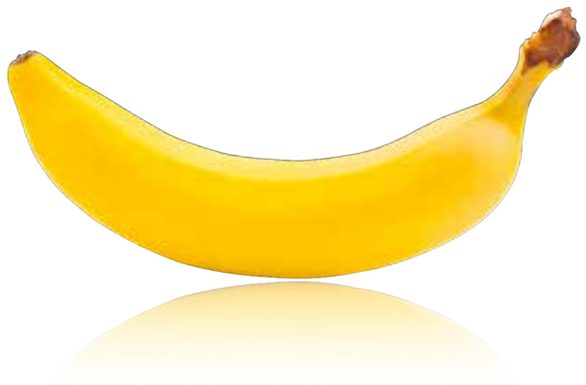

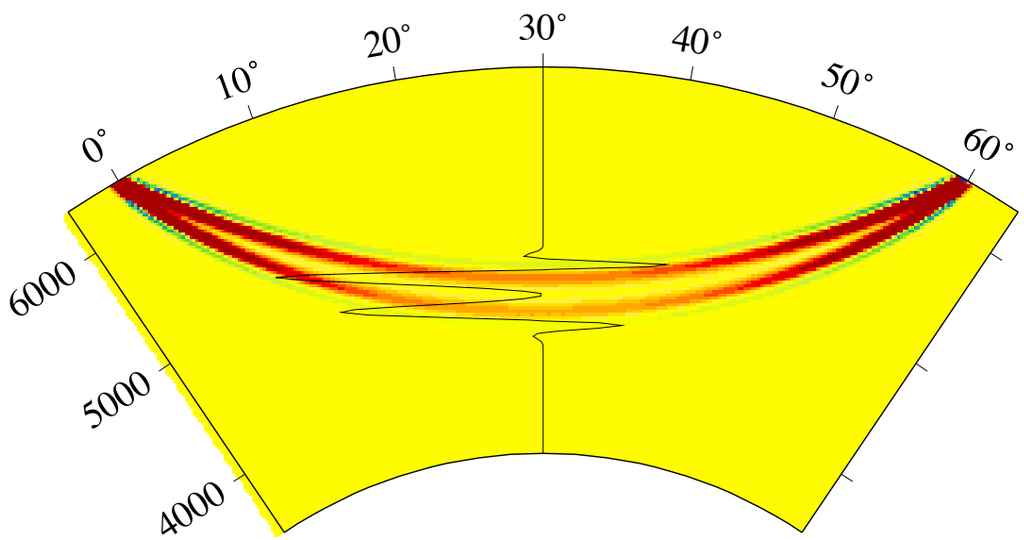

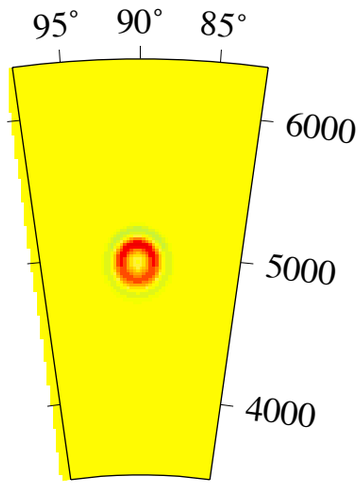

from Hung, Dahlen & Nolet, 2000, GJI

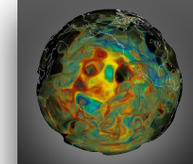

Challenges in global tomography

- **We are at a stage where details matter!**
  - ***Avoid approximations as much as possible***
  - **Seismograms & Fréchet sensitivity kernels need to be calculated numerically in a realistic 3D Earth model**

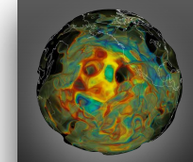

Challenges in global tomography

- **We are at a stage where details matter!**
  - ***Avoid approximations as much as possible***
  - **Seismograms & Fréchet sensitivity kernels need to be calculated numerically in a realistic 3D Earth model**
- **Data coverage**

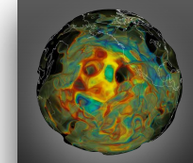

Earthquakes

ISC locations since 1960

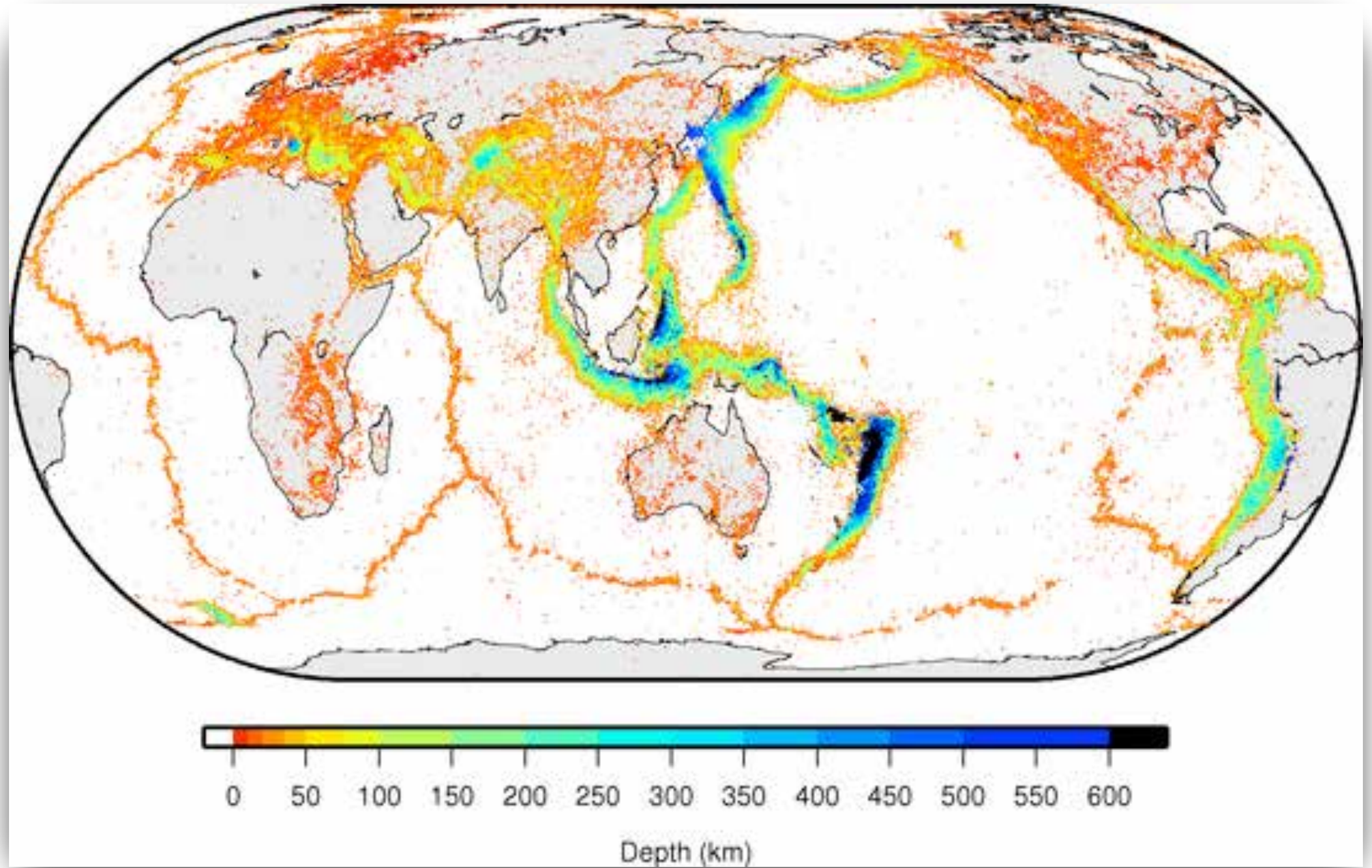

http://www.isc.ac.uk/

Seismic stations

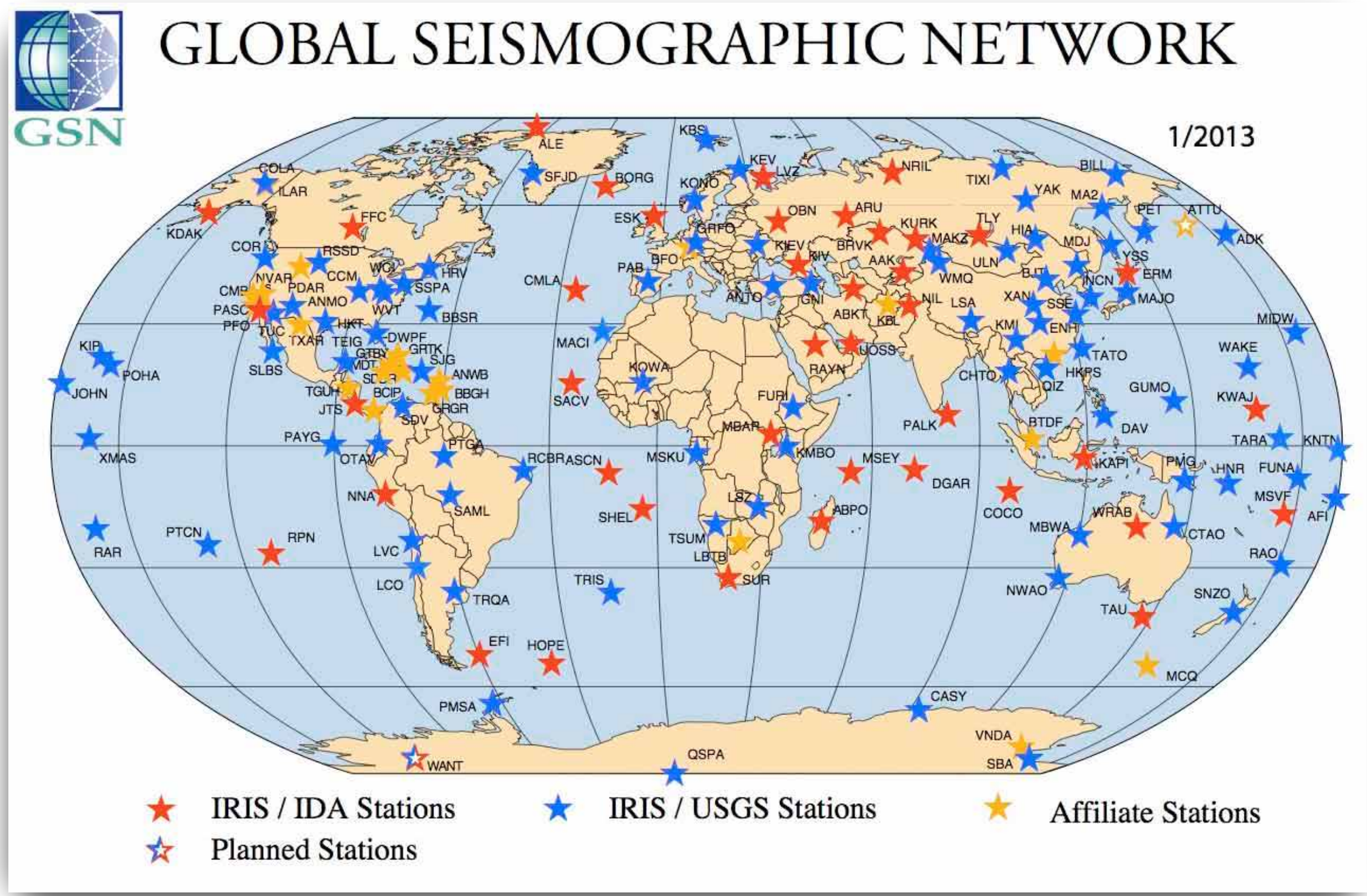

Seismic stations

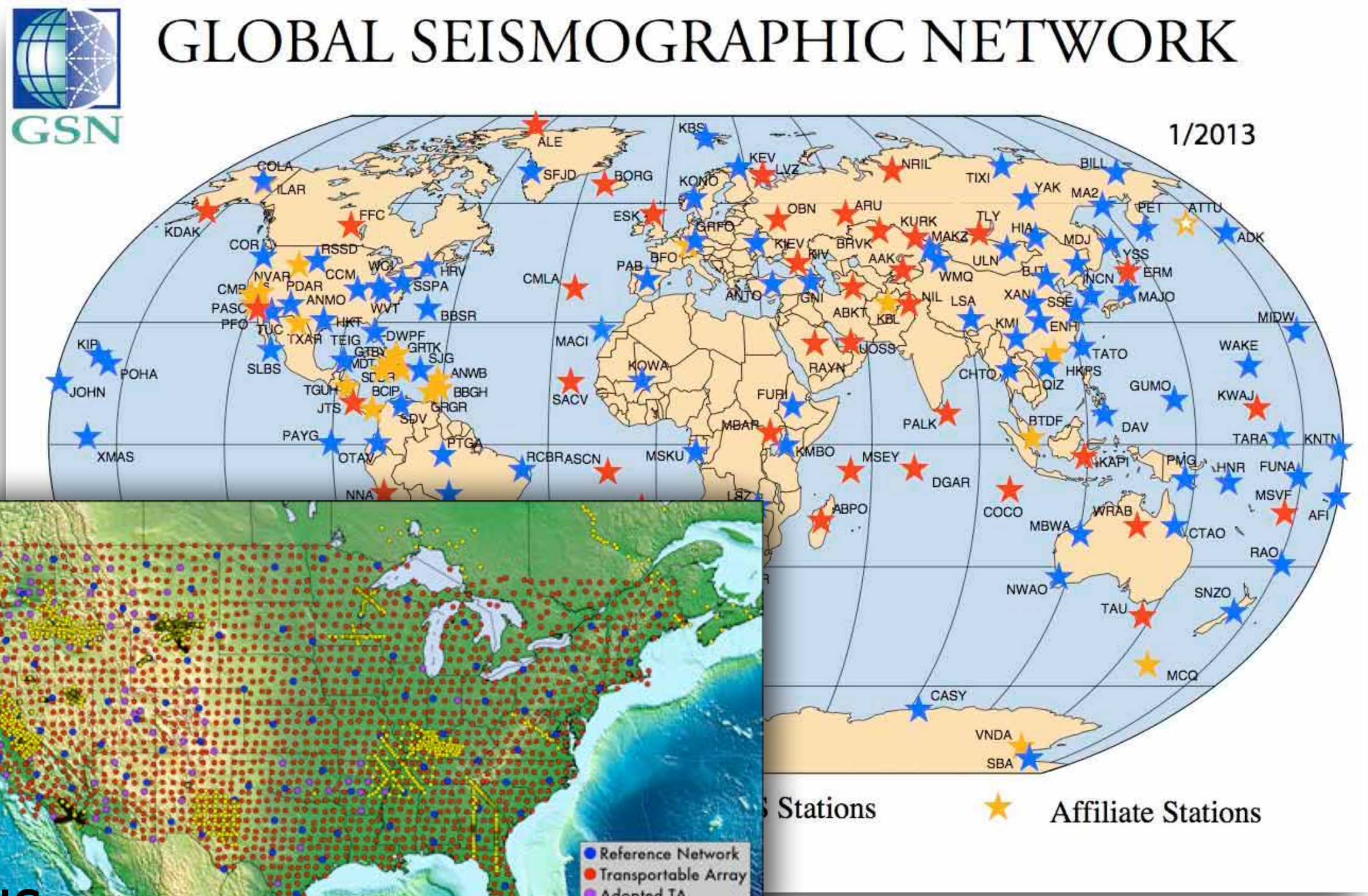

Seismic stations

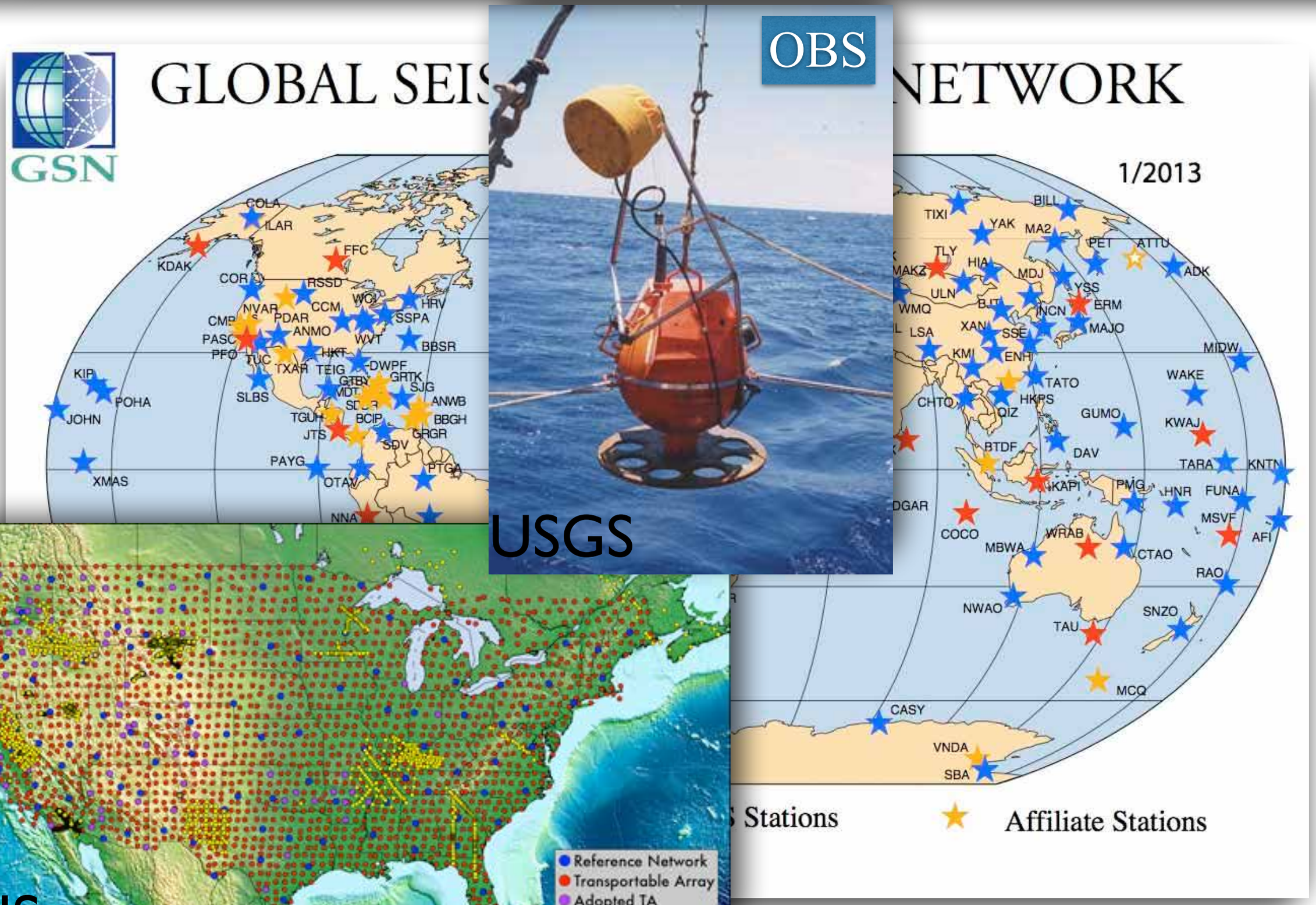

Seismic stations

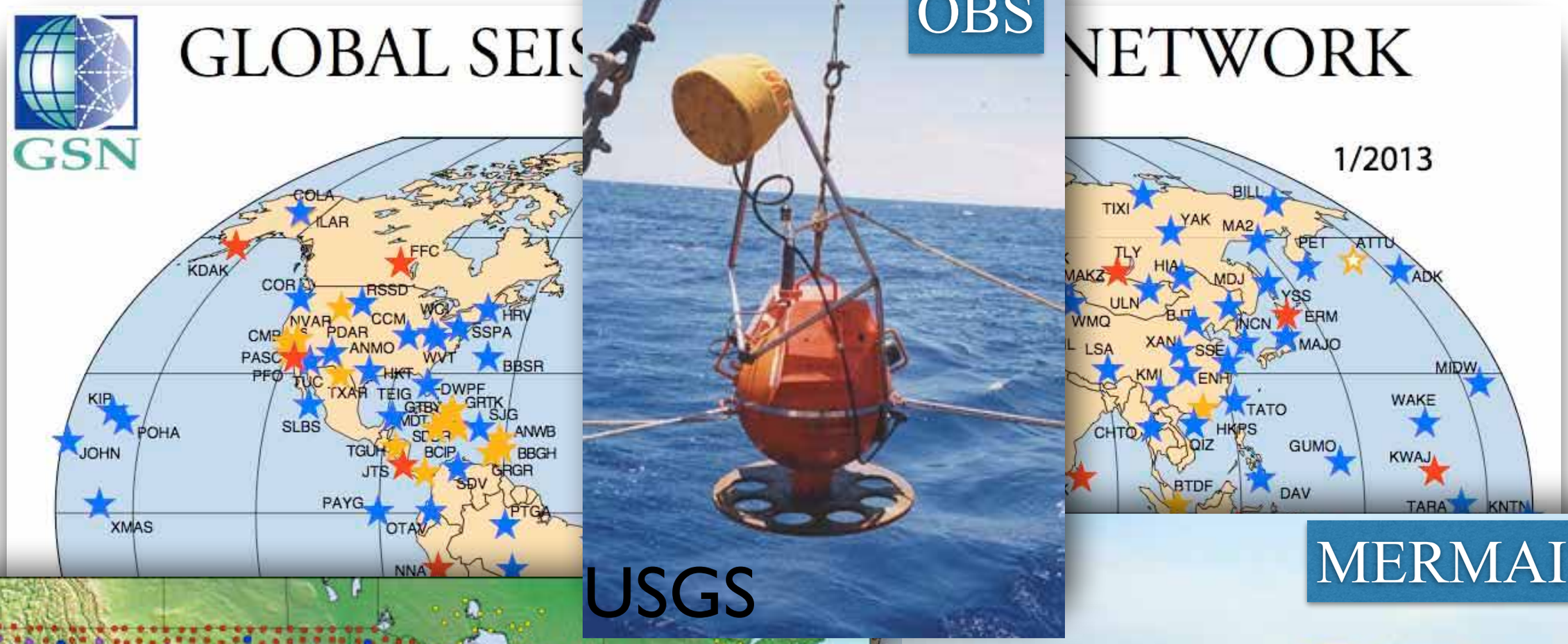

OBS

USGS

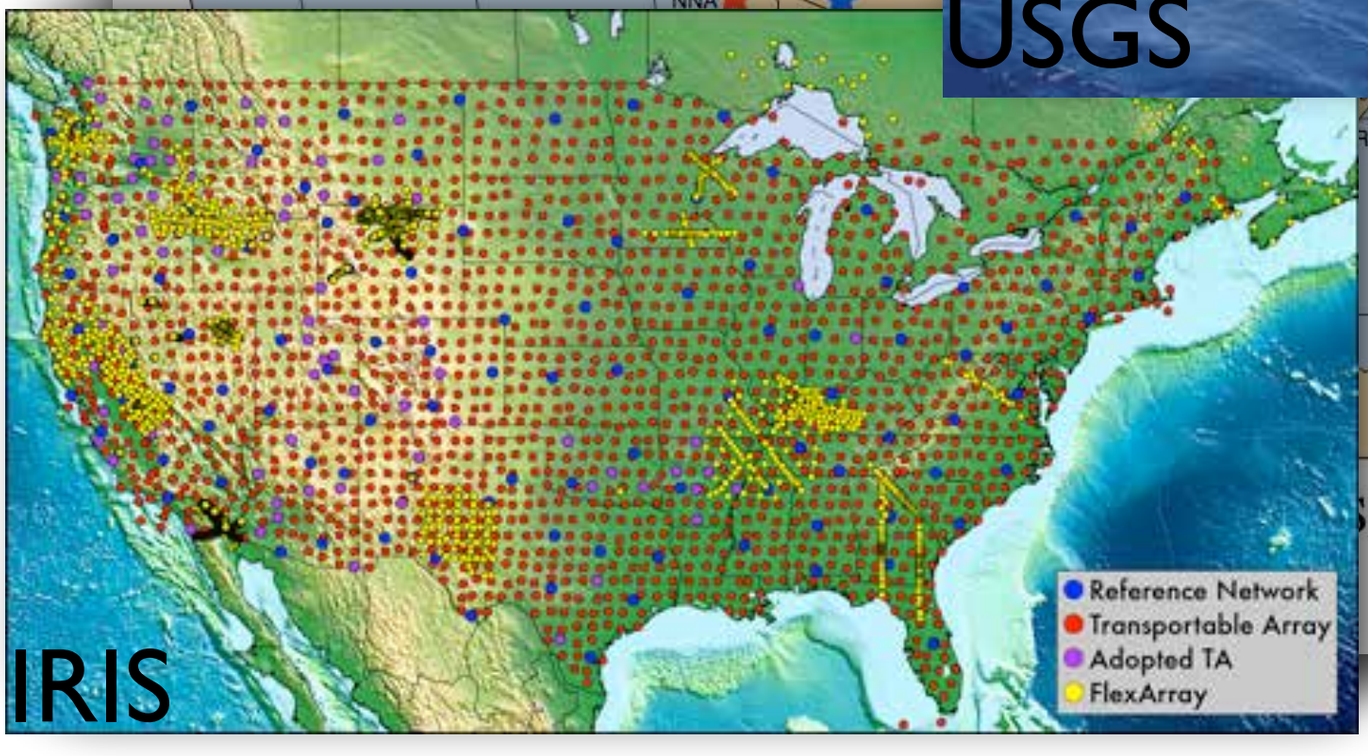

IRIS

MERMAIDS

Courtesy *Guust Nolet*

Data used in classical global tomography

Body-wave traveltimes

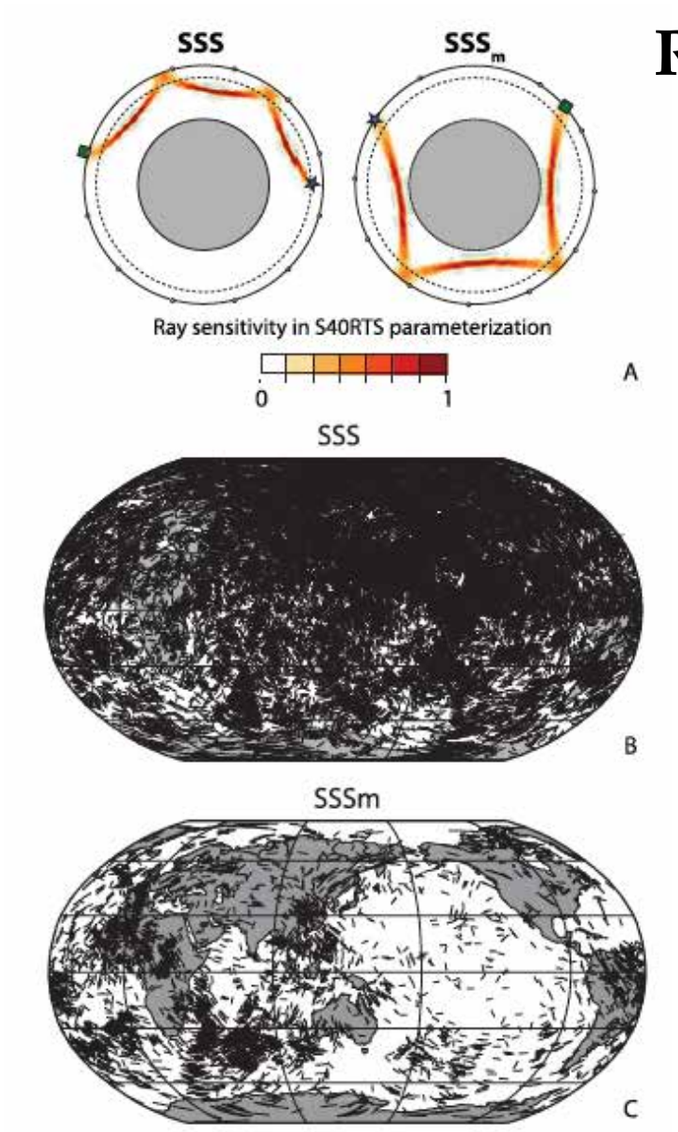

Ritsema et al. (2011)

Normal modes

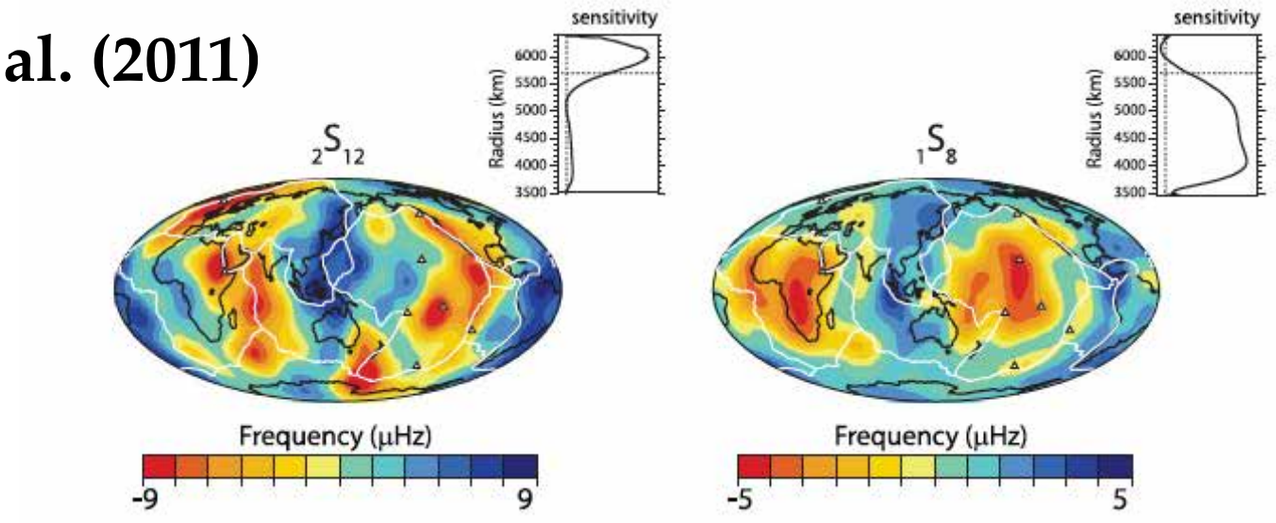

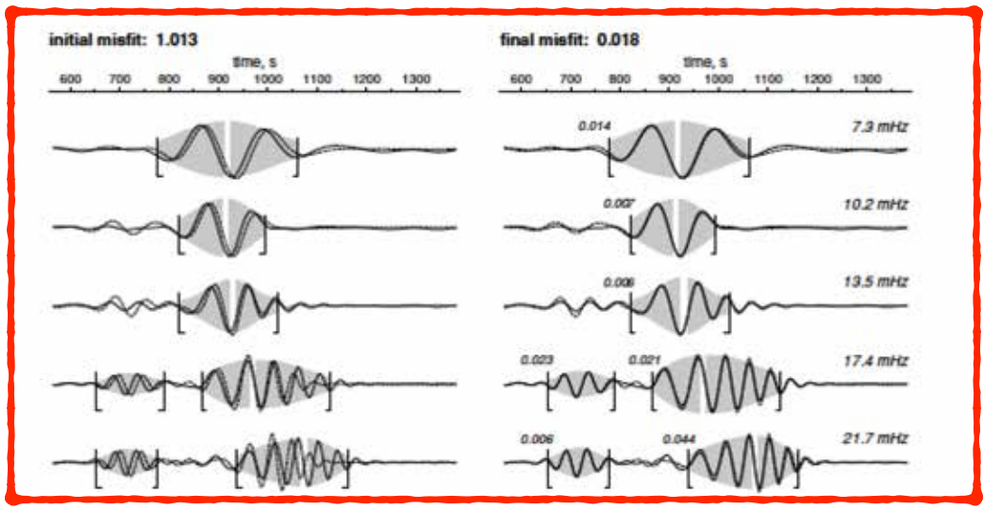

Waveforms

Lebedev et al. (2005)

Minor- & major-arc surface-wave phase/group speeds

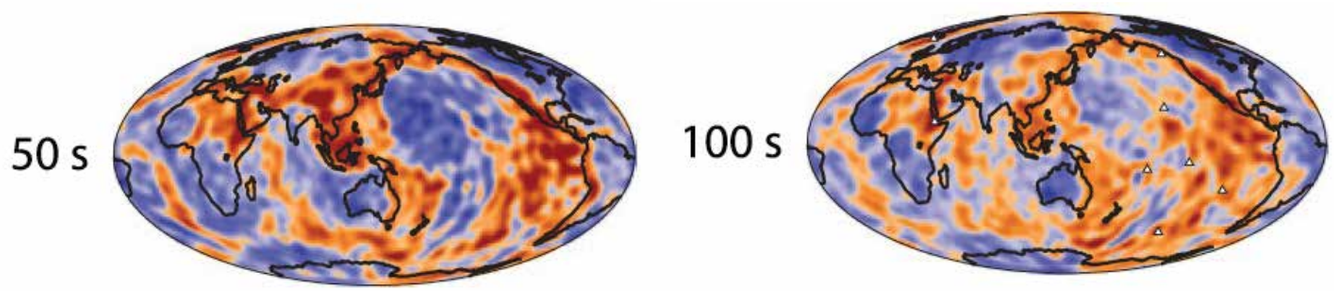

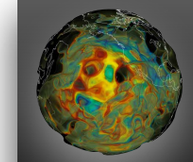

Challenges in global tomography

- **We are at a stage where details matter!**
  - ***Avoid approximations as much as possible***
  - **Seismograms & Fréchet sensitivity kernels need to be calculated numerically in a realistic 3D Earth model**
- **Data coverage**
  - **Source-station distribution can not be changed, but we can change the amount of information that we get from every seismogram**

We can use complete seismograms

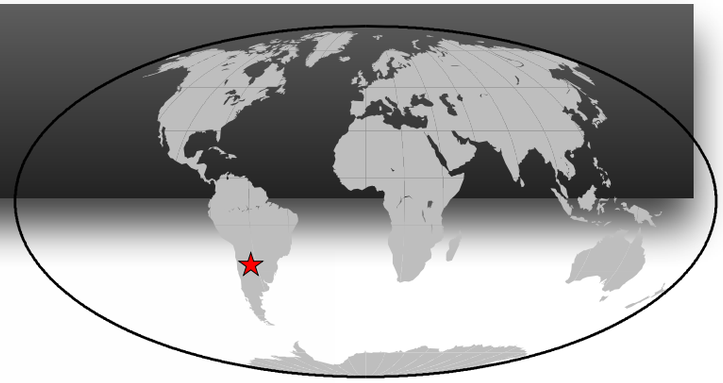

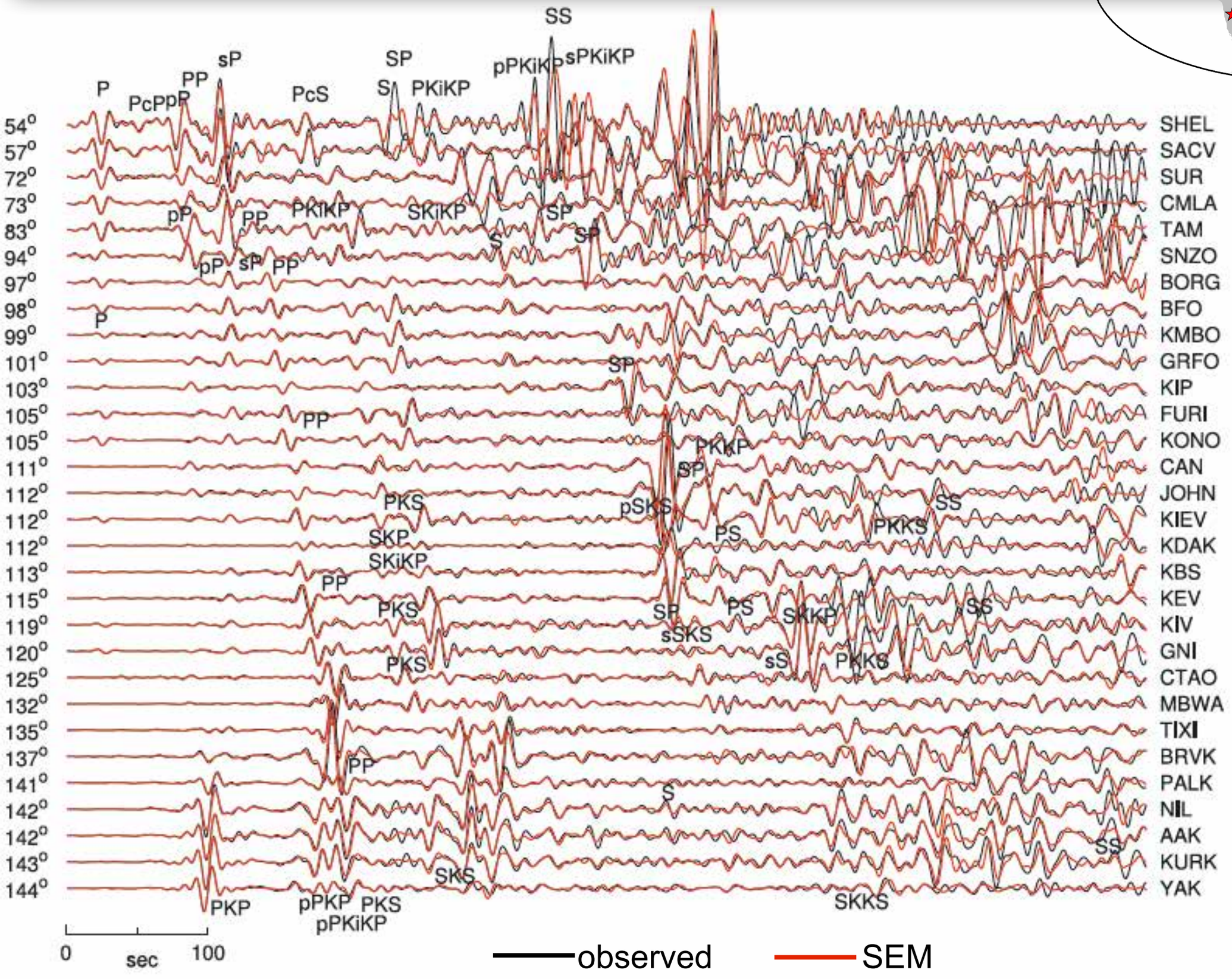

Sept. 3, 2008, Argentina Earthquake

M_w = 6.3

= 571 km

SPECFEM3D_GLOBE

3D Earth model: S362ANI + Crust2.0

17 - 60 s

3D seismograms with NACT kernels

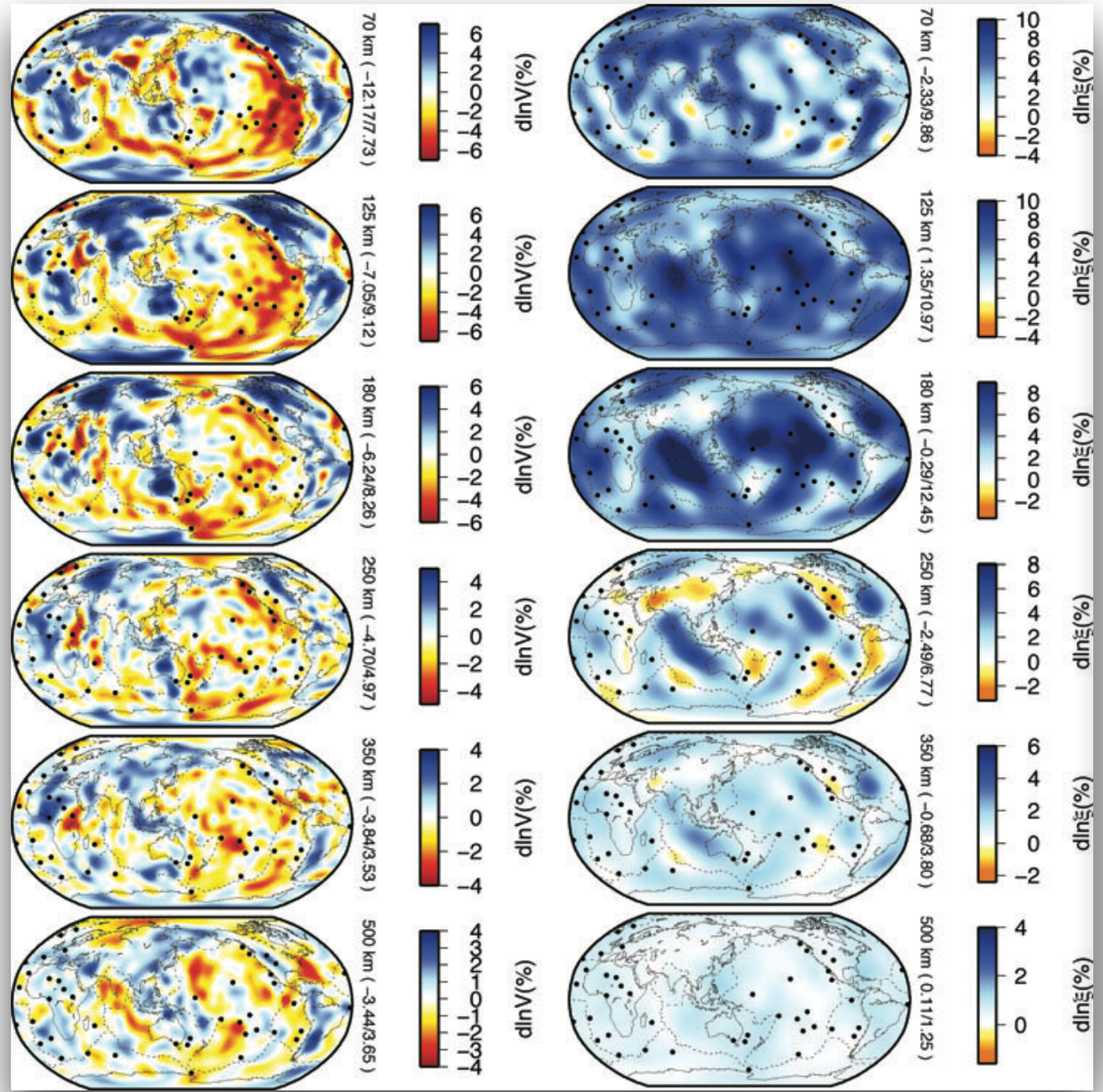

V. Lekic & B. Romanowicz, 2011, GJI

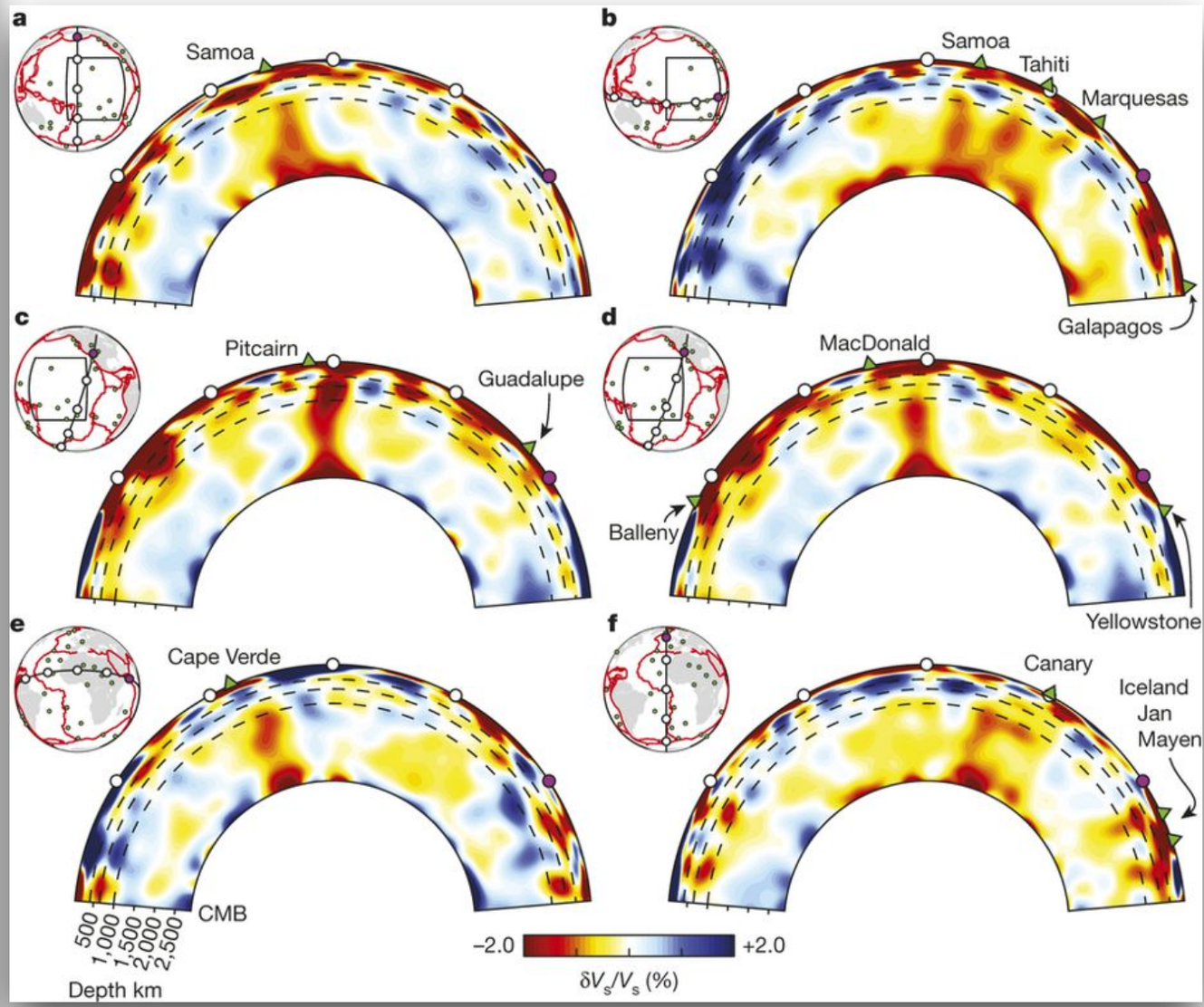

S. French & B. Romanowicz, 2015, Science

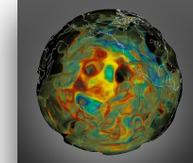

Challenges in global tomography

- **We are at a stage where details matter!**
  - ***Avoid approximations as much as possible***
  - **Seismograms & Fréchet sensitivity kernels need to be calculated numerically in a realistic 3D Earth model**
- **Data coverage**
  - **Source-station distribution can not be changed, but we can change the amount of information that we get from every seismogram**
- **Crust can be highly nonlinear**

Smoothed Moho depths

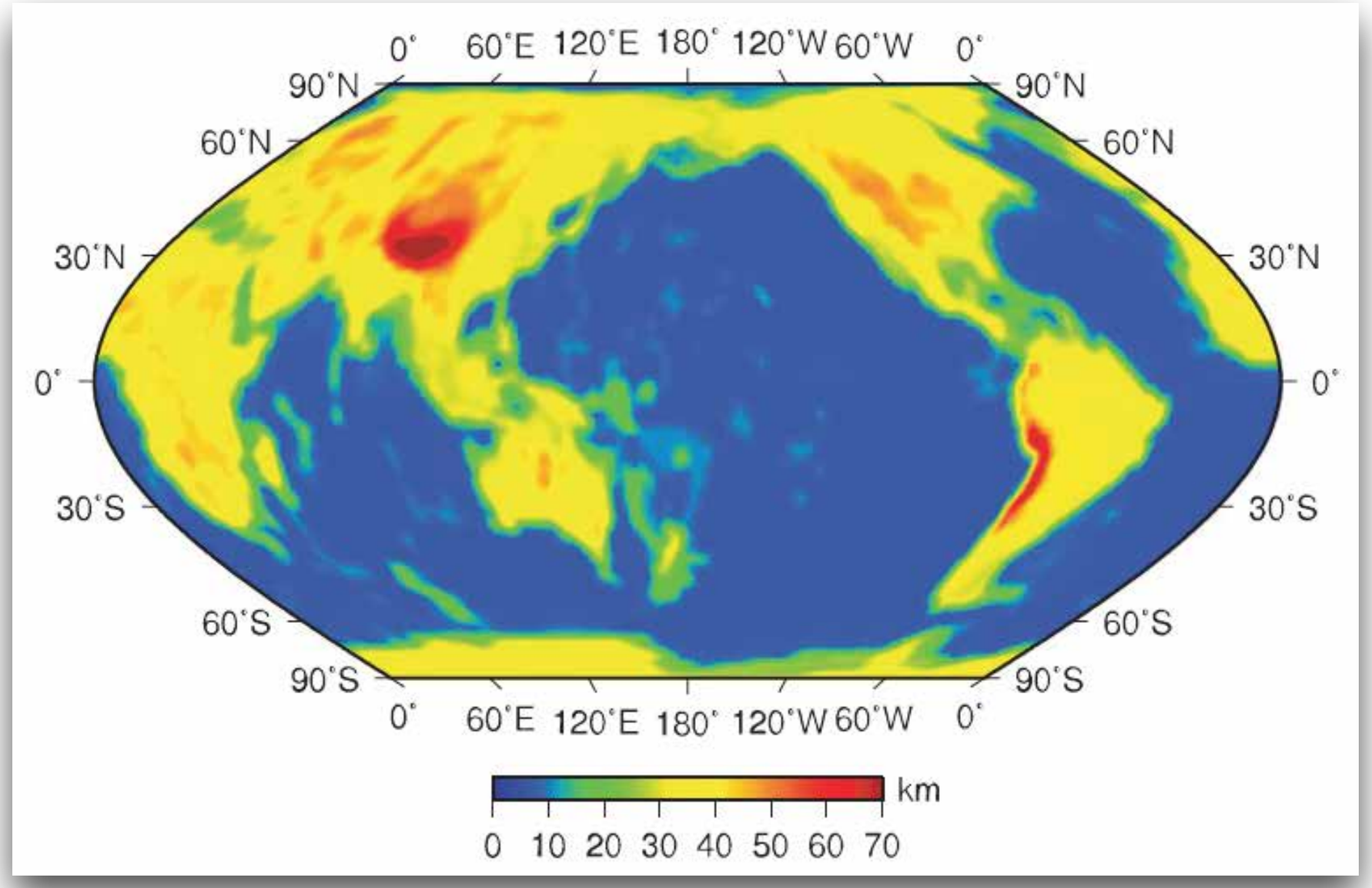

Crust2.0 (Bassin et al. 2000)

Radial anisotropy

$$\xi = \frac{V_{SH}^2}{V_{SV}^2}$$

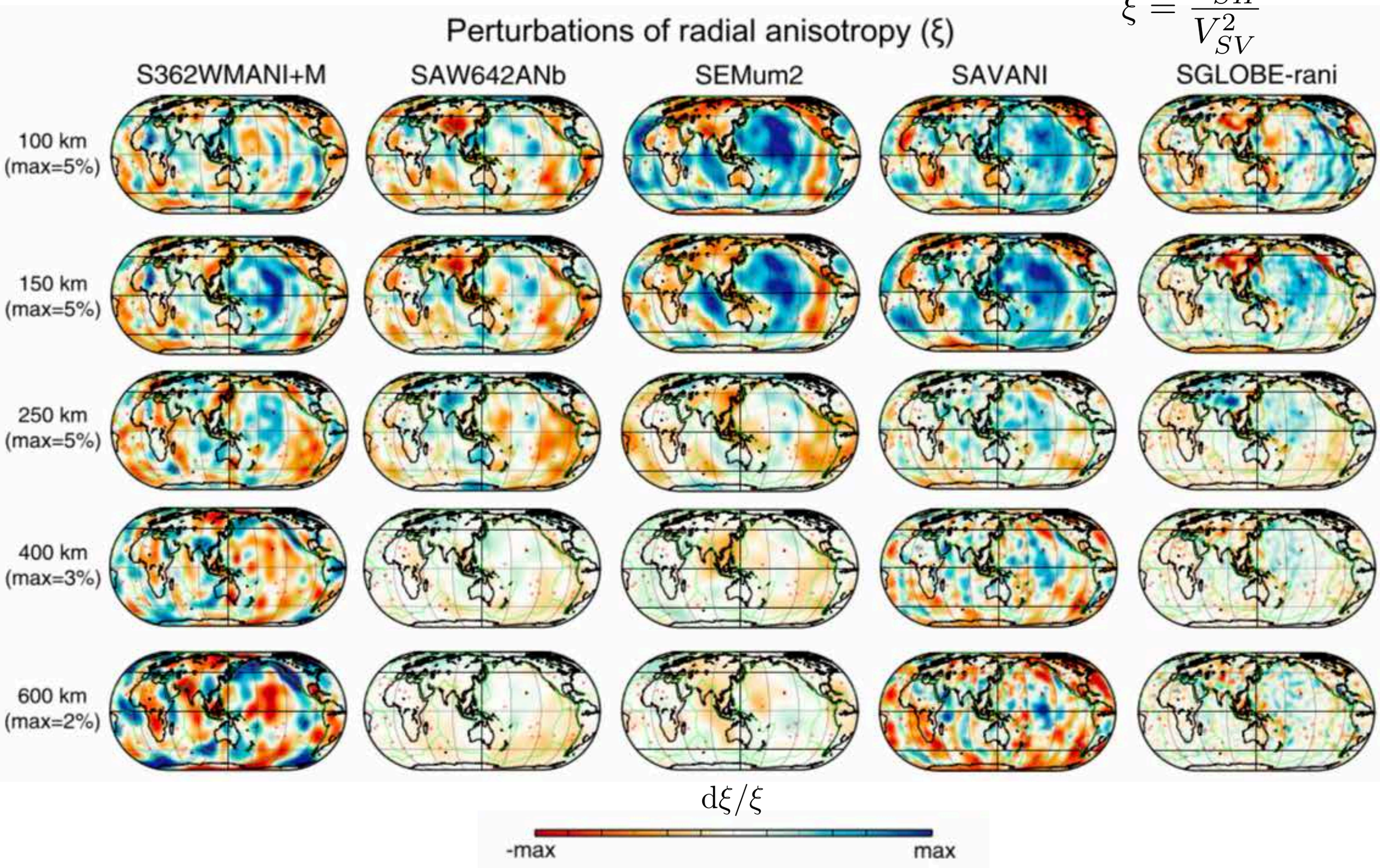

S-J. Chang, A. M. G. Ferreira, J. Ritsema, H. J. van Heijst, J. H. Woodhouse, 2015, JGR

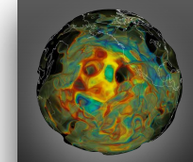

Challenges in global tomography

- **We are at a stage where details matter!**
  - ***Avoid approximations as much as possible***
  - **Seismograms & Fréchet sensitivity kernels need to be calculated numerically in a realistic 3D Earth model**
- **Data coverage**
  - **Source-station distribution can not be changed, but we can change the amount of information that we get from every seismogram**
- **Crust can be highly nonlinear**
  - **Crustal corrections are questionable**
  - **Crust must be addressed properly in inversions**

Dealing with crust in global simulations

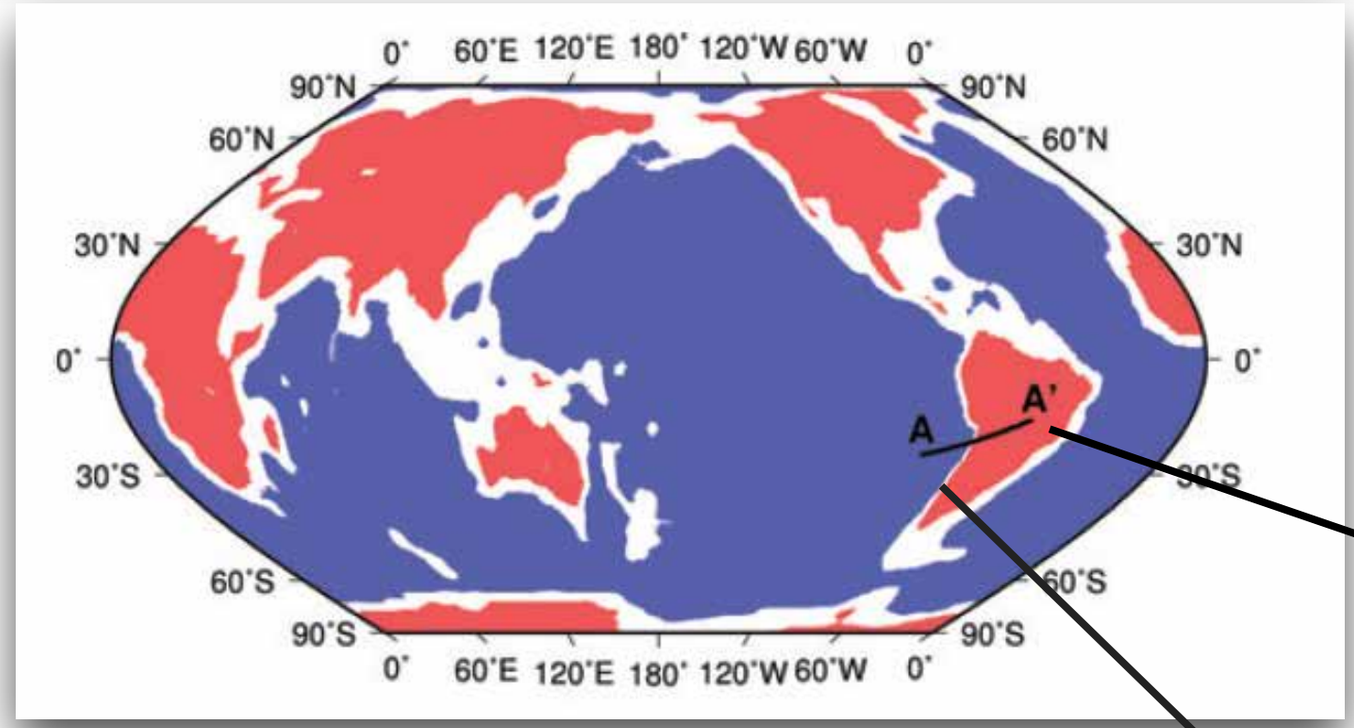

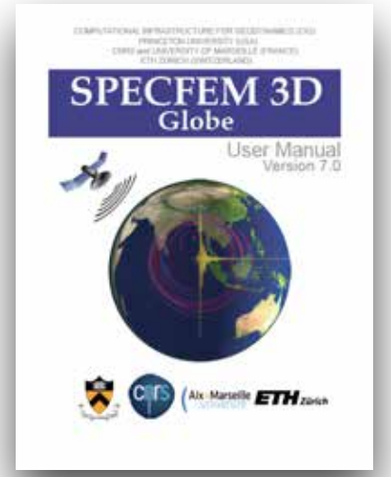

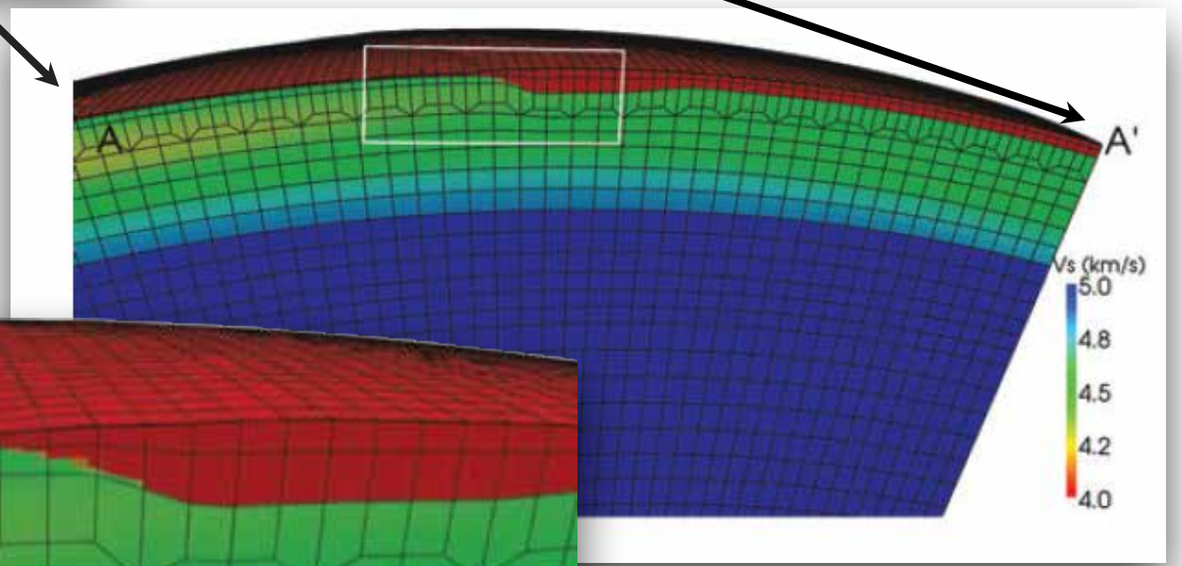

Moho is honored if crustal thickness is ≤15 km and ≥35 km.

J. Tromp et al. 2011, GJI

Homogenization

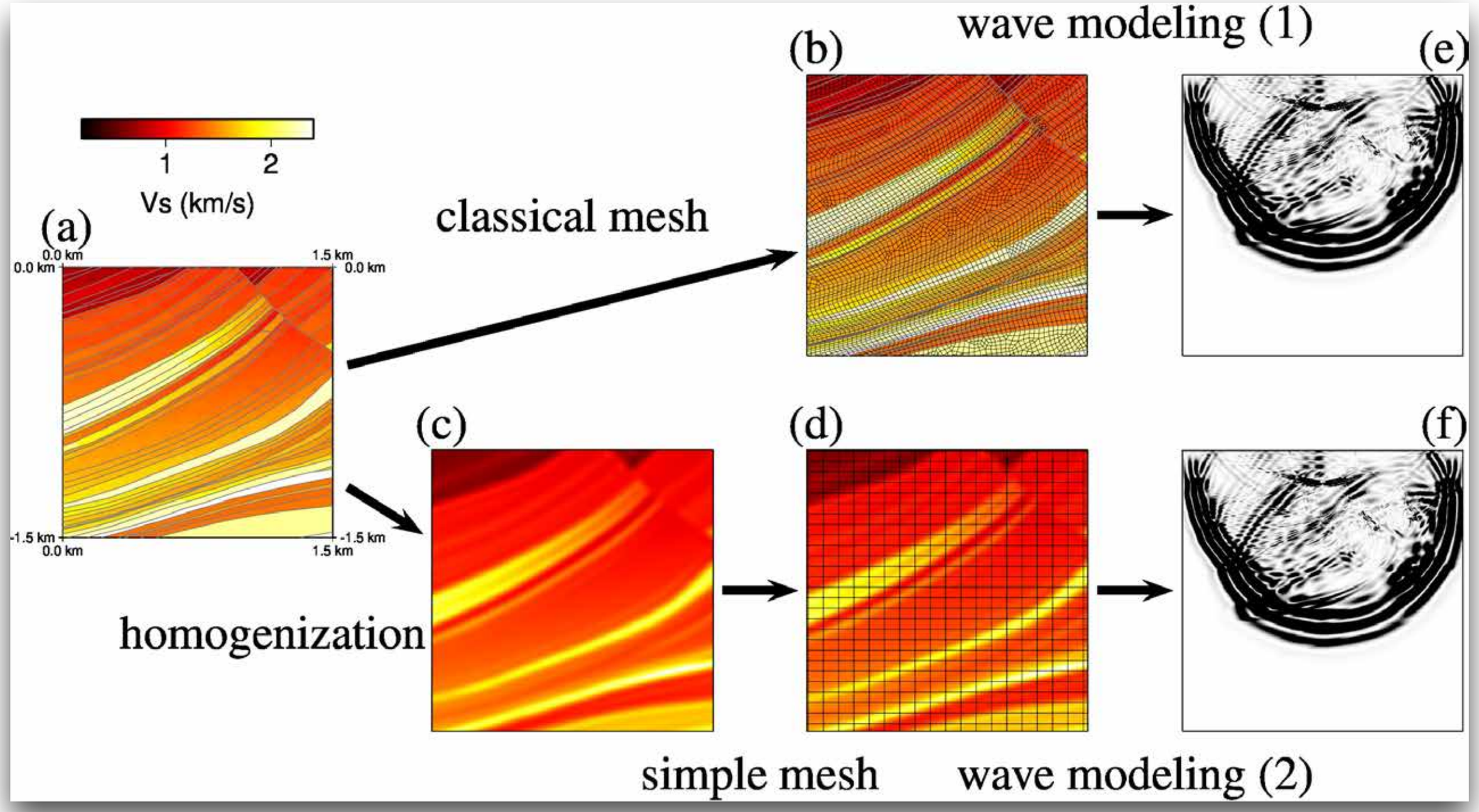

Y. Capdeville & Cance, GJI, 2015

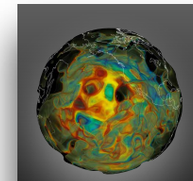

Non-linear inverse problems

$\mathbf{m}$ **is an initial model**

$\mathbf{m} + \delta\mathbf{m}$ **let's perturb it a bit!**

χ **a misfit function (waveform difference, traveltime difference, etc.)**

Taylor expansion $\chi(\mathbf{m} + \delta m) \approx \chi(\mathbf{m}) + \mathbf{g}(\mathbf{m})^{\mathbf{T}} \delta\mathbf{m} + \frac{1}{2}\delta\mathbf{m}^T \mathbf{H}(\mathbf{m}) \delta\mathbf{m}$

gradient $\longleftarrow \mathbf{g}(\mathbf{m}) = \left.\frac{\partial \chi}{\partial \mathbf{m}}\right|_{\mathbf{m}}$ Hessian $\longleftarrow \mathbf{H}(\mathbf{m}) = \left.\frac{\partial^2 \chi}{\partial \mathbf{m} \partial \mathbf{m}}\right|_{\mathbf{m}}$

$$\mathbf{g}(\mathbf{m} + \delta\mathbf{m}) \approx \mathbf{g}(\mathbf{m}) + \mathbf{H}(\mathbf{m}) \delta\mathbf{m}$$

- **If we have the Hessian & the gradient ==> Gauss-Newton method**
- **What if we do not have access to the Hessian?**

see C. Tape, Q. Liu & J. Tromp 2007, GJI

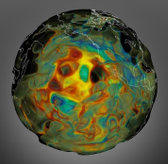

Gradient-based optimizations

- **Steepest descent**
- **Conjugate gradient**
- **BFGS (Broyden–Fletcher–Goldfarb–Shanno)**
- **L-BFGS (Limited-memory BFGS)**
- **…**

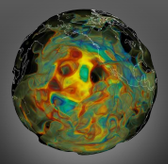

Gradient-based optimizations

calculate misfit

$$\chi(\mathbf{m}^0) \longrightarrow \text{initial model}$$

calculate gradient

$$\mathbf{g}^0 = \partial\chi/\partial\mathbf{m}\ (\mathbf{m}^0)$$

calculate gradient search directions

$$\mathbf{p}^0 = -\mathbf{g}^0$$

perform a line search

$$\tilde{\chi}^k(\nu) = \chi(\mathbf{m}^k + \nu\mathbf{p}^k)$$

$$\tilde{g}^k(\nu) = \frac{\partial\tilde{\chi}^k}{\partial\nu} = \frac{\partial\chi}{\partial\mathbf{m}}\left(\mathbf{m}^k + \nu\mathbf{p}^k\right)\cdot\mathbf{p}^k$$

calculate test models

$$\mathbf{m}_t^k = \mathbf{m}^k + \nu_t^k\mathbf{p}^k$$

calculate $\chi(\mathbf{m}_t^k)$ **for cubic interpolation**

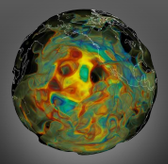

Gradient-based optimizations

update the model

$$\mathbf{m}^{k+1} = \mathbf{m}^k + \nu^k \mathbf{p}^k$$

recalculate the gradient

$$\mathbf{g}^{k+1} = \partial \chi / \partial \mathbf{m} \, (\mathbf{m}^{k+1})$$

recalculate the search direction

$$\mathbf{p}^{k+1} = -\mathbf{g}^{k+1} \longrightarrow \text{steepest descent}$$

conjugate gradient ←

$$\mathbf{p}^{k+1} = -\mathbf{g}^{k+1} + \beta^{k+1} \mathbf{p}^k$$

$$\beta^{k+1} = \mathbf{g}^{k+1} \cdot (\mathbf{g}^{k+1} - \mathbf{g}^k) / (\mathbf{g}^k \cdot \mathbf{g}^k)$$

L-BFGS (Limited-memory BFGS)

$$\text{If } ||\mathbf{p}^{k+1}|| < \epsilon \longrightarrow \mathbf{m}^{k+1} \text{ is the desired model}$$

Nocedal & Wright, 1999, Numerical Optimization, Springer

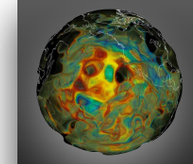

Adjoint tomography

misfit function

$$\chi = \frac{1}{2} \sum_{r=1}^{N} \int_0^T [\mathbf{s}(\mathbf{x}_r, t, \mathbf{m}) - \mathbf{d}(\mathbf{x}_r, t)]^2 dt$$

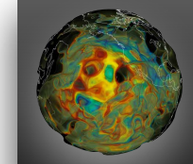

Adjoint tomography

misfit function

$$\chi = \frac{1}{2}\sum_{r=1}^{N}\int_0^T [\mathbf{s}(\mathbf{x}_r,t,\mathbf{m}) - \mathbf{d}(\mathbf{x}_r,t)]^2 dt$$

gradient

$$\delta\chi = \sum_{r=1}^{N}\int_0^T [\mathbf{s}(\mathbf{x}_r,t,\mathbf{m}) - \mathbf{d}(\mathbf{x}_r,t)]\delta\mathbf{s}(\mathbf{x}_r,t,\mathbf{m})dt$$

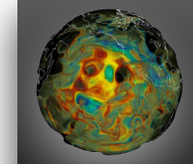

Adjoint tomography

misfit function

$$\chi = \frac{1}{2}\sum_{r=1}^{N}\int_0^T [\mathbf{s}(\mathbf{x}_r,t,\mathbf{m}) - \mathbf{d}(\mathbf{x}_r,t)]^2 dt$$

gradient

$$\delta\chi = \sum_{r=1}^{N}\int_0^T [\mathbf{s}(\mathbf{x}_r,t,\mathbf{m}) - \mathbf{d}(\mathbf{x}_r,t)]\,\delta\mathbf{s}(\mathbf{x}_r,t,\mathbf{m})\,dt$$

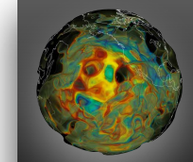

Adjoint tomography

misfit function

$$\chi = \frac{1}{2}\sum_{r=1}^{N}\int_0^T [\mathbf{s}(\mathbf{x}_r,t,\mathbf{m}) - \mathbf{d}(\mathbf{x}_r,t)]^2 dt$$

gradient

$$\delta\chi = \sum_{r=1}^{N}\int_0^T [\mathbf{s}(\mathbf{x}_r,t,\mathbf{m}) - \mathbf{d}(\mathbf{x}_r,t)]\,\delta\mathbf{s}(\mathbf{x}_r,t,\mathbf{m})\,dt$$

$$\delta\chi = -\sum_{r=1}^{N}\int_0^T [s_i(\mathbf{x}_r,t) - d_i(\mathbf{x}_r,t)] \int_0^t \int_V [\delta\rho(\mathbf{x}')G_{ij}(\mathbf{x}_r,\mathbf{x}';t-t')\partial_{t'}^2 s_j(\mathbf{x}',t')$$
$$+\delta c_{jklm}(\mathbf{x}')\partial_k' G_{ij}(\mathbf{x}_r,\mathbf{x}';t-t')\partial_l' s_m(\mathbf{x}',t')]d^3\mathbf{x}'\,dt'\,dt.$$

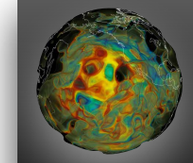

Adjoint tomography

misfit function

$$\chi = \frac{1}{2}\sum_{r=1}^{N}\int_0^T [\mathbf{s}(\mathbf{x}_r,t,\mathbf{m}) - \mathbf{d}(\mathbf{x}_r,t)]^2 dt$$

gradient

$$\delta\chi = \sum_{r=1}^{N}\int_0^T [\mathbf{s}(\mathbf{x}_r,t,\mathbf{m}) - \mathbf{d}(\mathbf{x}_r,t)]\delta\mathbf{s}(\mathbf{x}_r,t,\mathbf{m})dt$$

$$\delta\chi = -\sum_{r=1}^{N}\int_0^T [s_i(\mathbf{x}_r,t) - d_i(\mathbf{x}_r,t)]\int_0^t\int_V [\delta\rho(\mathbf{x}')G_{ij}(\mathbf{x}_r,\mathbf{x}';t-t')\partial_{t'}^2 s_j(\mathbf{x}',t')$$
$$+\delta c_{jklm}(\mathbf{x}')\partial_k' G_{ij}(\mathbf{x}_r,\mathbf{x}';t-t')\partial_l' s_m(\mathbf{x}',t')]d^3\mathbf{x}'\,dt'\,dt.$$

$$G_{ij}(\mathbf{x},\mathbf{x}';t-t') = G_{ji}(\mathbf{x}',\mathbf{x};t'-t)$$

$$t \longrightarrow T - t$$

Adjoint tomography

misfit function

$$\chi = \frac{1}{2}\sum_{r=1}^{N}\int_0^T [\mathbf{s}(\mathbf{x}_r,t,\mathbf{m}) - \mathbf{d}(\mathbf{x}_r,t)]^2 dt$$

gradient

$$\delta\chi = \sum_{r=1}^{N}\int_0^T [\mathbf{s}(\mathbf{x}_r,t,\mathbf{m}) - \mathbf{d}(\mathbf{x}_r,t)]\delta\mathbf{s}(\mathbf{x}_r,t,\mathbf{m})dt$$

$$\delta\chi = -\sum_{r=1}^{N}\int_0^T [s_i(\mathbf{x}_r,t) - d_i(\mathbf{x}_r,t)]\int_0^t\int_V [\delta\rho(\mathbf{x}')G_{ij}(\mathbf{x}_r,\mathbf{x}';t-t')\partial_{t'}^2 s_j(\mathbf{x}',t')$$
$$+\delta c_{jklm}(\mathbf{x}')\partial_k' G_{ij}(\mathbf{x}_r,\mathbf{x}';t-t')\partial_l' s_m(\mathbf{x}',t')]d^3\mathbf{x}'\,dt'\,dt.$$

$$G_{ij}(\mathbf{x},\mathbf{x}';t-t') = G_{ji}(\mathbf{x}',\mathbf{x};t'-t)$$

$$t \longrightarrow T - t$$

adjoint wavefield

$$s_k^\dagger(\mathbf{x}',t') = \sum_{r=1}^{N}\int_0^{t'}\int_V G_{ki}(\mathbf{x}',\mathbf{x}_r;t'-t)[s_i(\mathbf{x}_r,T-t) - d_i(\mathbf{x}_r,T-t)]d^3\mathbf{x}dt$$

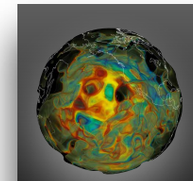

Adjoint tomography

misfit function

$$\chi = \frac{1}{2}\sum_{r=1}^{N}\int_0^T [\mathbf{s}(\mathbf{x}_r,t,\mathbf{m}) - \mathbf{d}(\mathbf{x}_r,t)]^2 dt$$

gradient

$$\delta\chi = \sum_{r=1}^{N}\int_0^T [\mathbf{s}(\mathbf{x}_r,t,\mathbf{m}) - \mathbf{d}(\mathbf{x}_r,t)]\delta\mathbf{s}(\mathbf{x}_r,t,\mathbf{m})dt$$

$$\delta\chi = -\sum_{r=1}^{N}\int_0^T [s_i(\mathbf{x}_r,t) - d_i(\mathbf{x}_r,t)]\int_0^t\int_V [\delta\rho(\mathbf{x}')G_{ij}(\mathbf{x}_r,\mathbf{x}';t-t')\partial_{t'}^2 s_j(\mathbf{x}',t')$$

$$+\delta c_{jklm}(\mathbf{x}')\partial_k' G_{ij}(\mathbf{x}_r,\mathbf{x}';t-t')\partial_l' s_m(\mathbf{x}',t')]d^3\mathbf{x}'dt'dt.$$

$$G_{ij}(\mathbf{x},\mathbf{x}';t-t') = G_{ji}(\mathbf{x}',\mathbf{x};t'-t)$$

$$t \longrightarrow T - t$$

adjoint wavefield

$$s_k^\dagger(\mathbf{x}',t') = \sum_{r=1}^{N}\int_0^{t'}\int_V G_{ki}(\mathbf{x}',\mathbf{x}_r;t'-t)[s_i(\mathbf{x}_r,T-t) - d_i(\mathbf{x}_r,T-t)]d^3\mathbf{x}dt$$

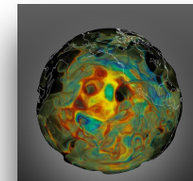

Adjoint tomography

misfit function

$$\chi = \frac{1}{2}\sum_{r=1}^{N}\int_0^T [\mathbf{s}(\mathbf{x}_r,t,\mathbf{m}) - \mathbf{d}(\mathbf{x}_r,t)]^2 dt$$

gradient

$$\delta\chi = \sum_{r=1}^{N}\int_0^T [\mathbf{s}(\mathbf{x}_r,t,\mathbf{m}) - \mathbf{d}(\mathbf{x}_r,t)]\delta\mathbf{s}(\mathbf{x}_r,t,\mathbf{m})dt$$

$$\delta\chi = -\sum_{r=1}^{N}\int_0^T [s_i(\mathbf{x}_r,t) - d_i(\mathbf{x}_r,t)]\int_0^t\int_V [\delta\rho(\mathbf{x}')G_{ij}(\mathbf{x}_r,\mathbf{x}';t-t')\partial_{t'}^2 s_j(\mathbf{x}',t')$$

$$+\delta c_{jklm}(\mathbf{x}')\partial_k' G_{ij}(\mathbf{x}_r,\mathbf{x}';t-t')\partial_l' s_m(\mathbf{x}',t')]d^3\mathbf{x}'dt'dt.$$

$$G_{ij}(\mathbf{x},\mathbf{x}';t-t') = G_{ji}(\mathbf{x}',\mathbf{x};t'-t) \qquad t \longrightarrow T-t$$

adjoint wavefield

$$s_k^\dagger(\mathbf{x}',t') = \sum_{r=1}^{N}\int_0^{t'}\int_V G_{ki}(\mathbf{x}',\mathbf{x}_r;t'-t)[s_i(\mathbf{x}_r,T-t) - d_i(\mathbf{x}_r,T-t)]d^3\mathbf{x}dt$$

adjoint source

$$f_i^\dagger(\mathbf{x},t) = \sum_{r=1}^{N}[s_i(\mathbf{x}_r,T-t) - d_i(\mathbf{x}_r,T-t)]\delta(\mathbf{x}-\mathbf{x}_r)$$

Tromp et al. 2005

How to compute adjoint kernels?

$$\delta\chi = \int_V [K_\rho(\mathbf{x})\delta \ln \rho(\mathbf{x}) + K_{c_{jklm}}(\mathbf{x})\delta \ln c_{jklm}(\mathbf{x})]\, d^3\mathbf{x}$$

$$K_\rho(\mathbf{x}) = -\int_0^T \rho(\mathbf{x})\mathbf{s}^\dagger(\mathbf{x}, T-t)\cdot\partial_t^2\mathbf{s}(\mathbf{x}, t)\, dt$$

$$K_{c_{jklm}}(\mathbf{x}) = -\int_0^T \epsilon_{jk}^\dagger(\mathbf{x}, T-t)c_{jklm}(\mathbf{x})\epsilon_{lm}(\mathbf{x}, t)\, dt$$

How to compute adjoint kernels?

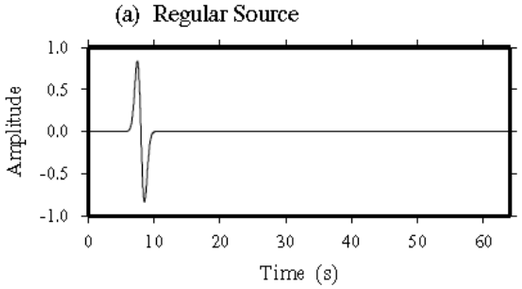

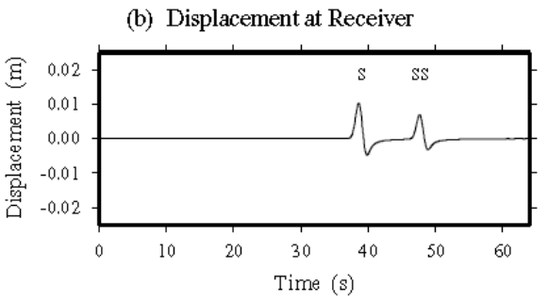

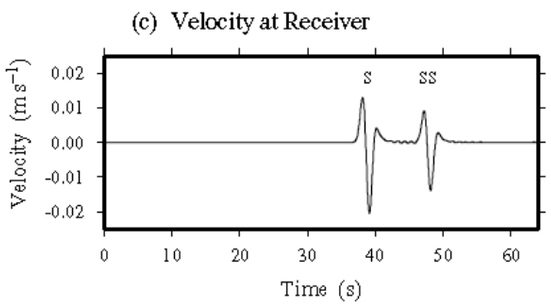

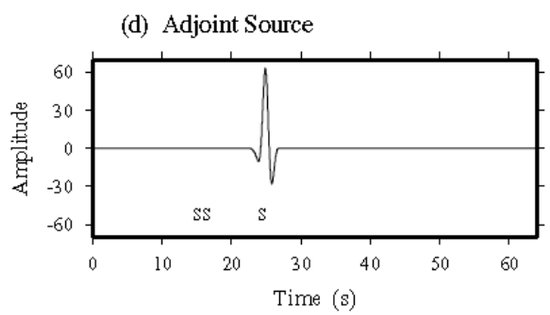

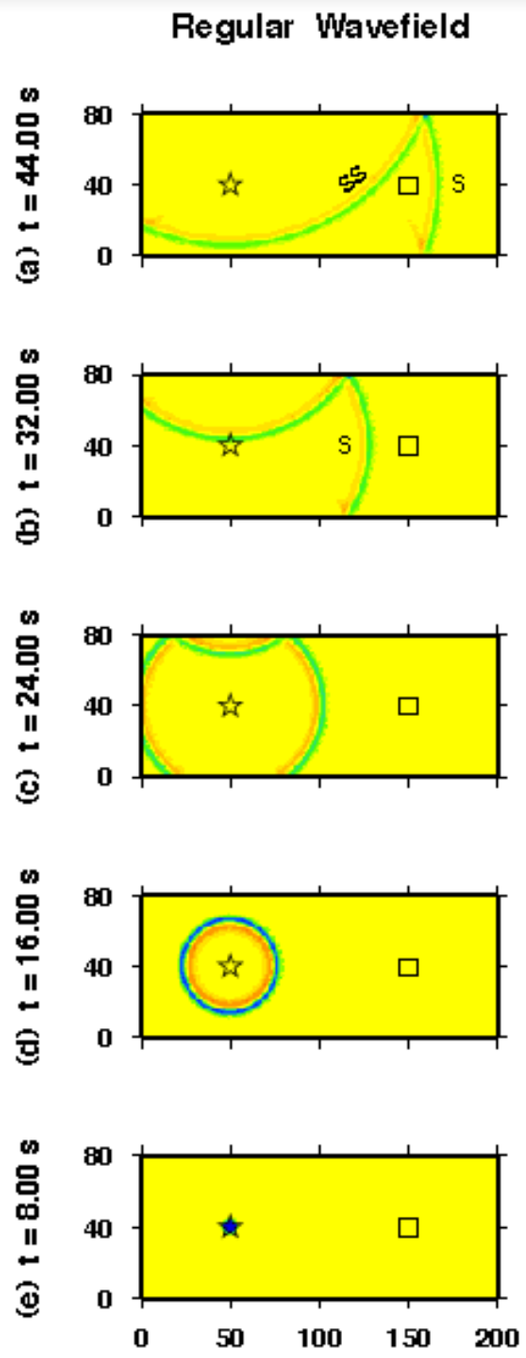

J. Tromp, Q. Liu & C. Tape, 2005, GJI

How to compute adjoint kernels?

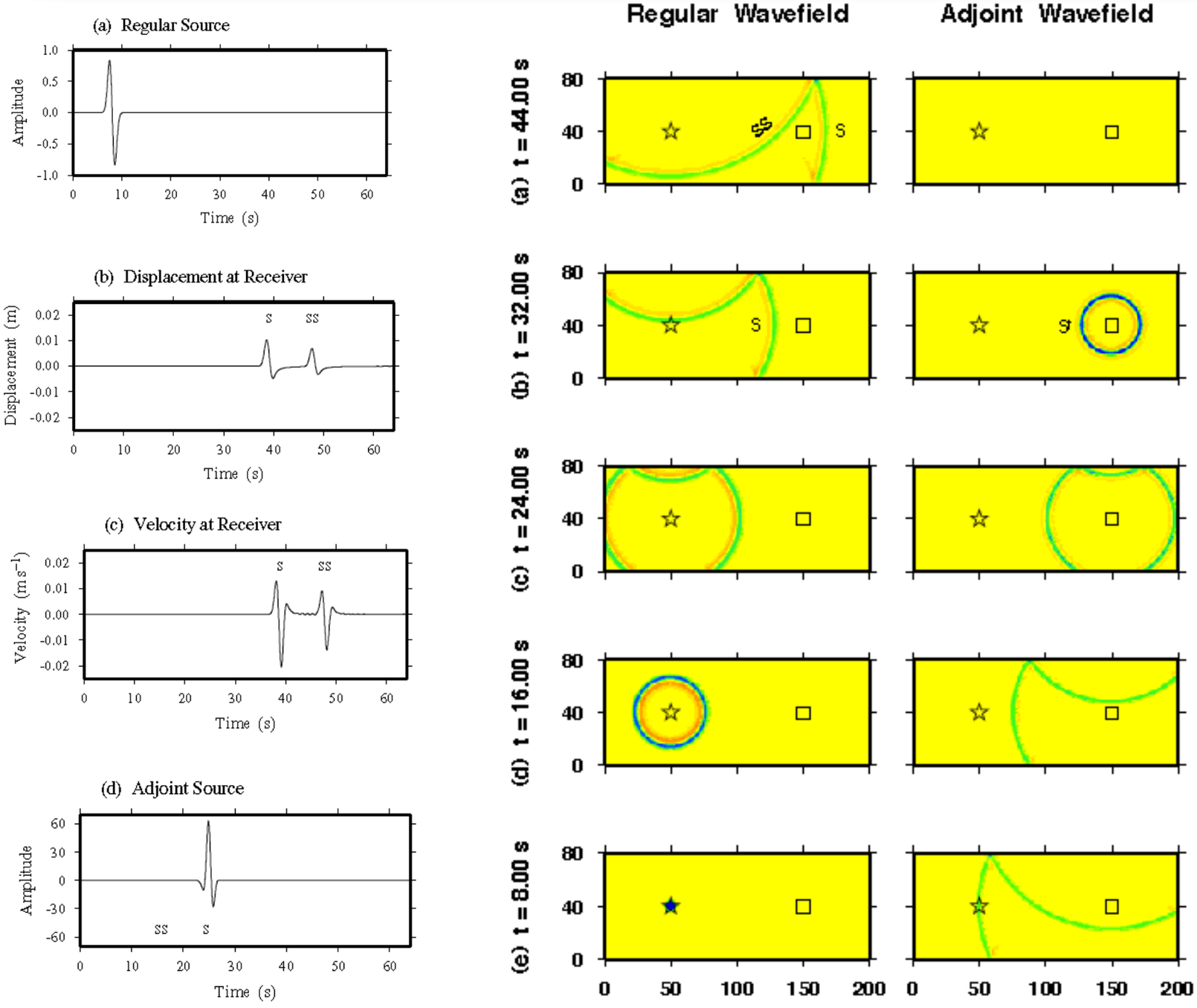

J. Tromp, Q. Liu & C. Tape, 2005, GJI

How to compute adjoint kernels?

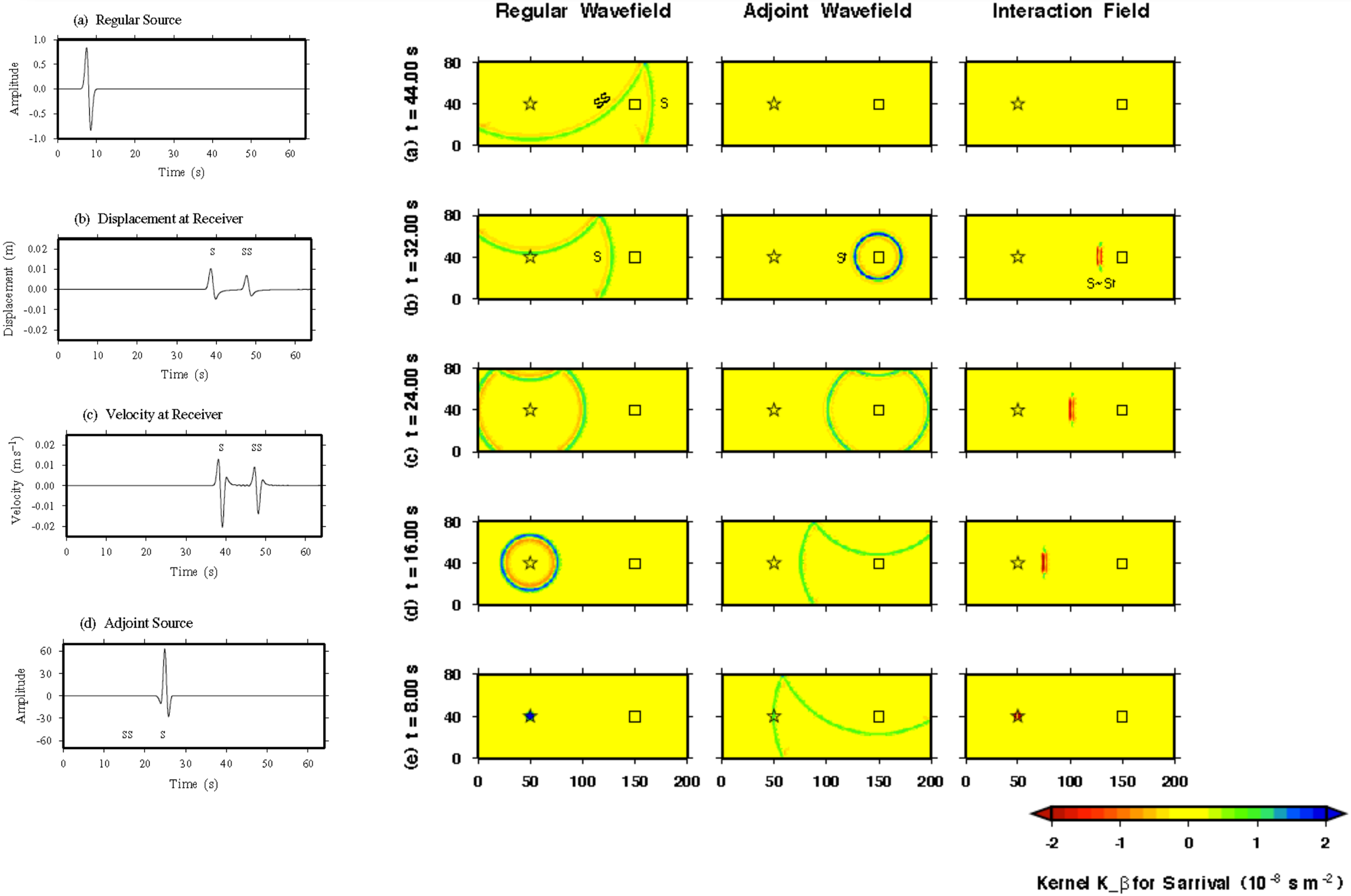

J. Tromp, Q. Liu & C. Tape, 2005, GJI

How to compute adjoint kernels?

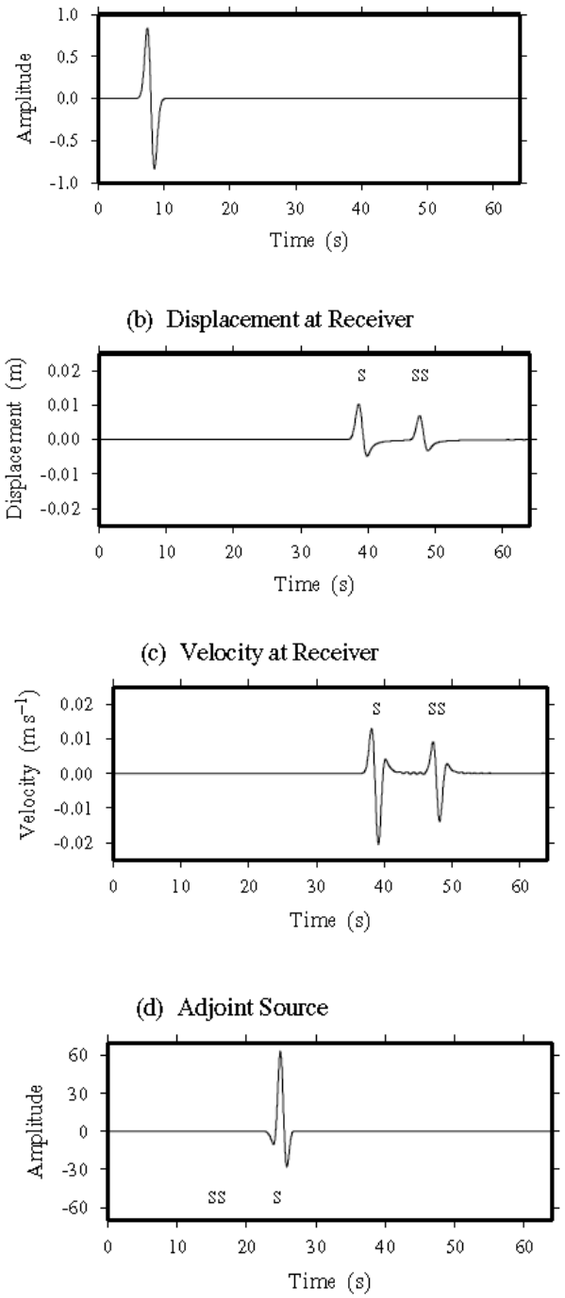

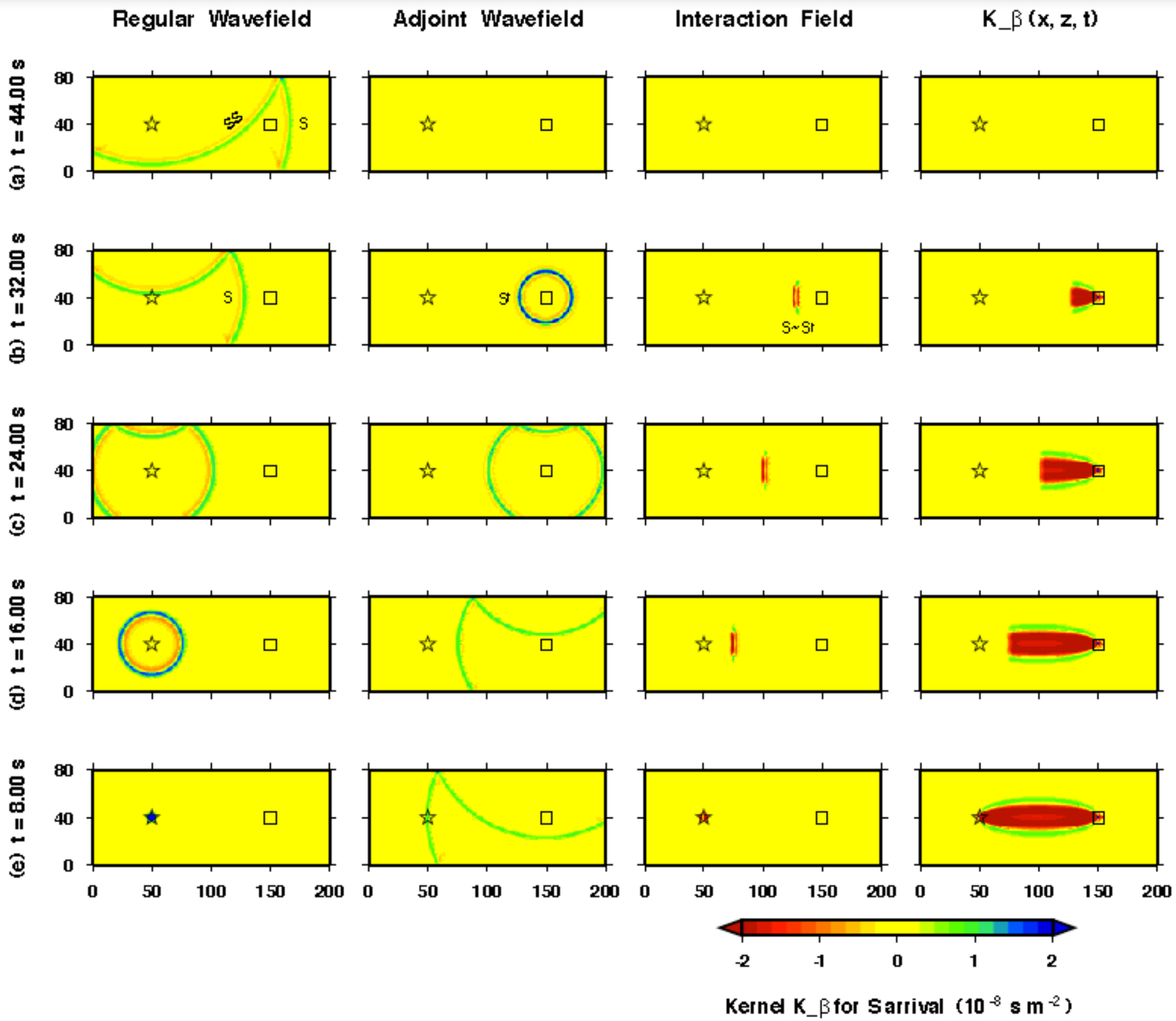

J. Tromp, Q. Liu & C. Tape, 2005, GJI

Banana-doughnuts

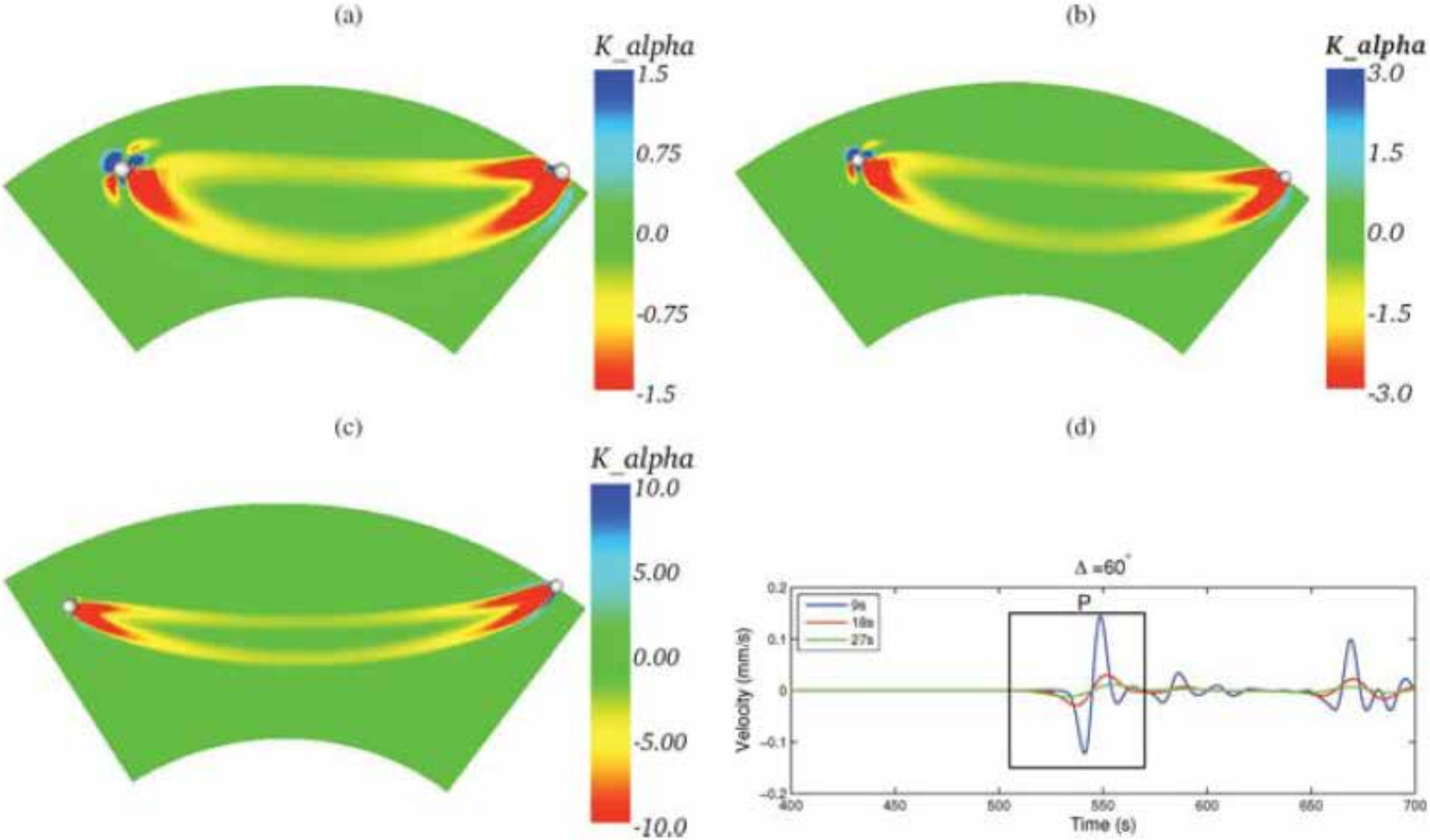

Q. Liu & J. Tromp, 2007, GJI

More banana-doughnuts

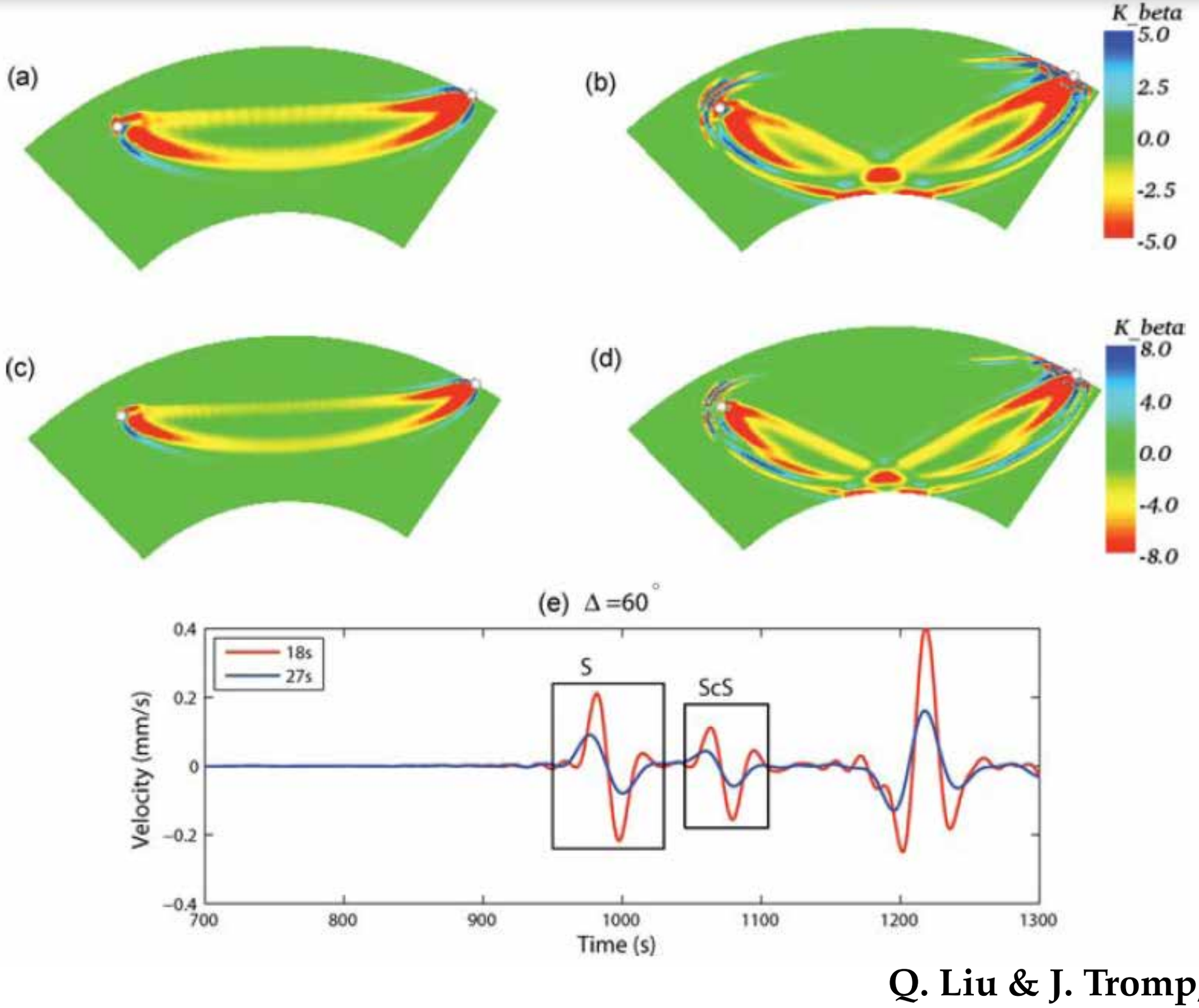

Q. Liu & J. Tromp, 2007, GJI

More banana-doughnuts

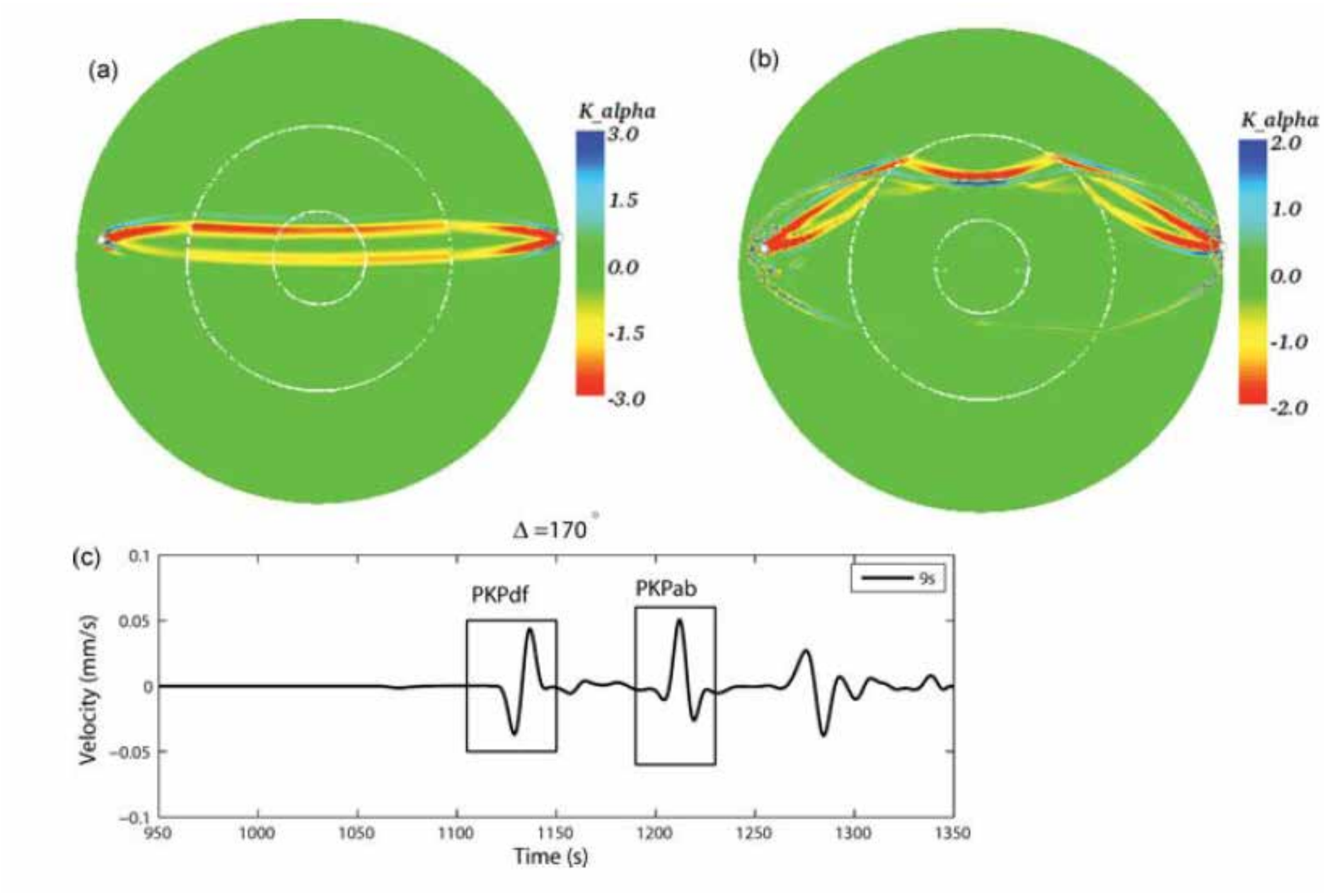

Q. Liu & J. Tromp, 2007, GJI

Surface wave sensitivities

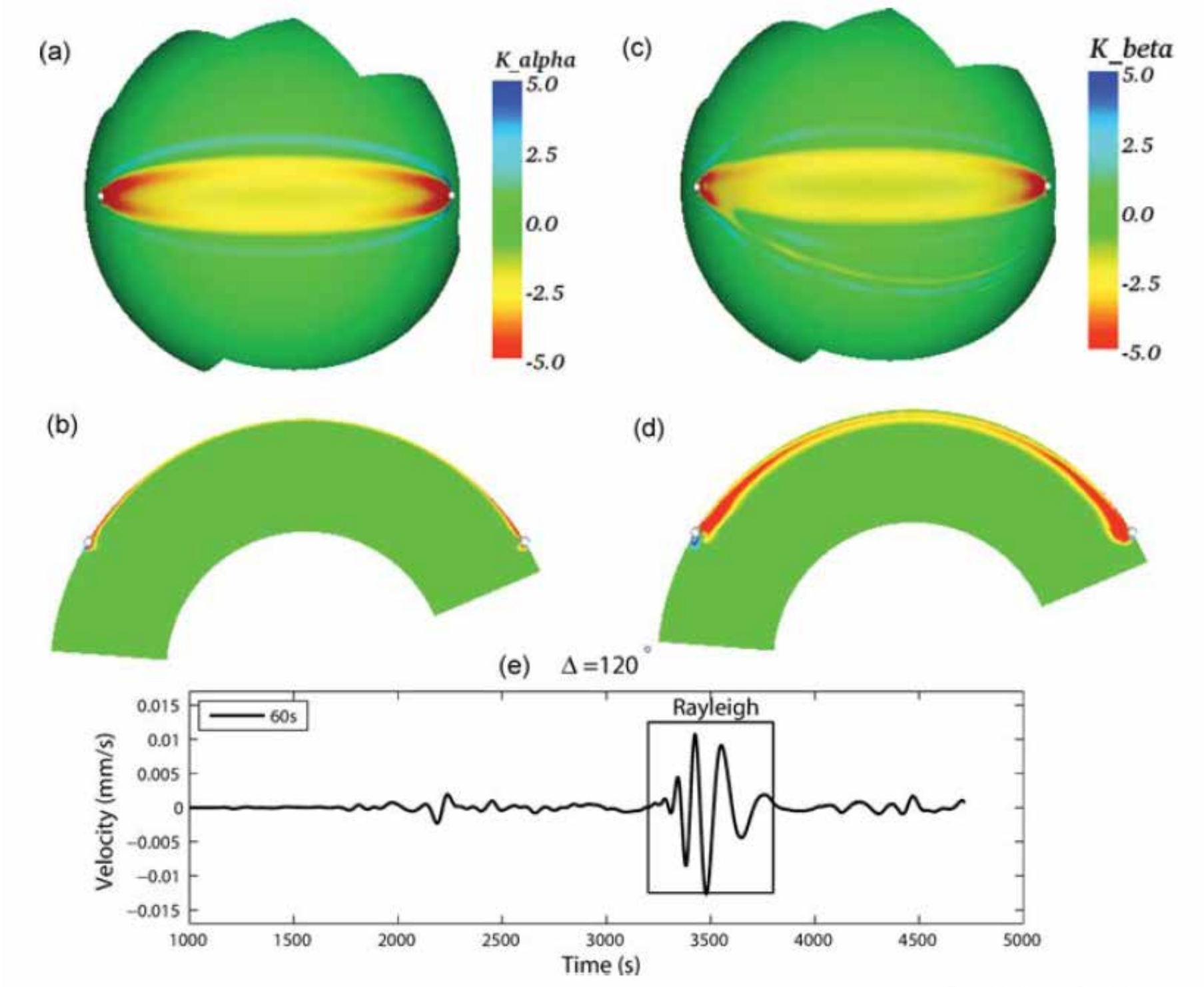

Q. Liu & J. Tromp, 2007, GJI

Sensitivity to upper-mantle discontinuities

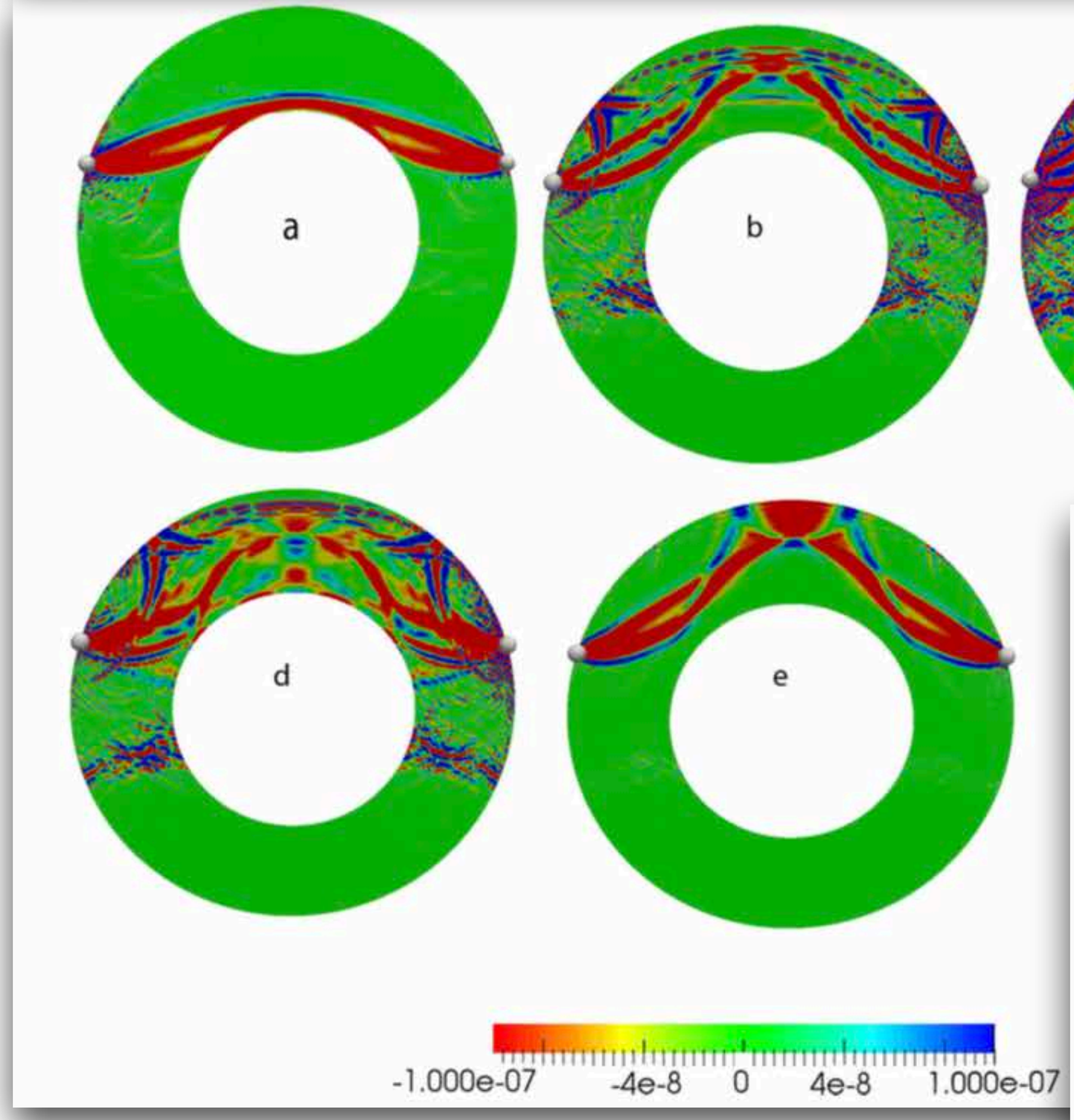

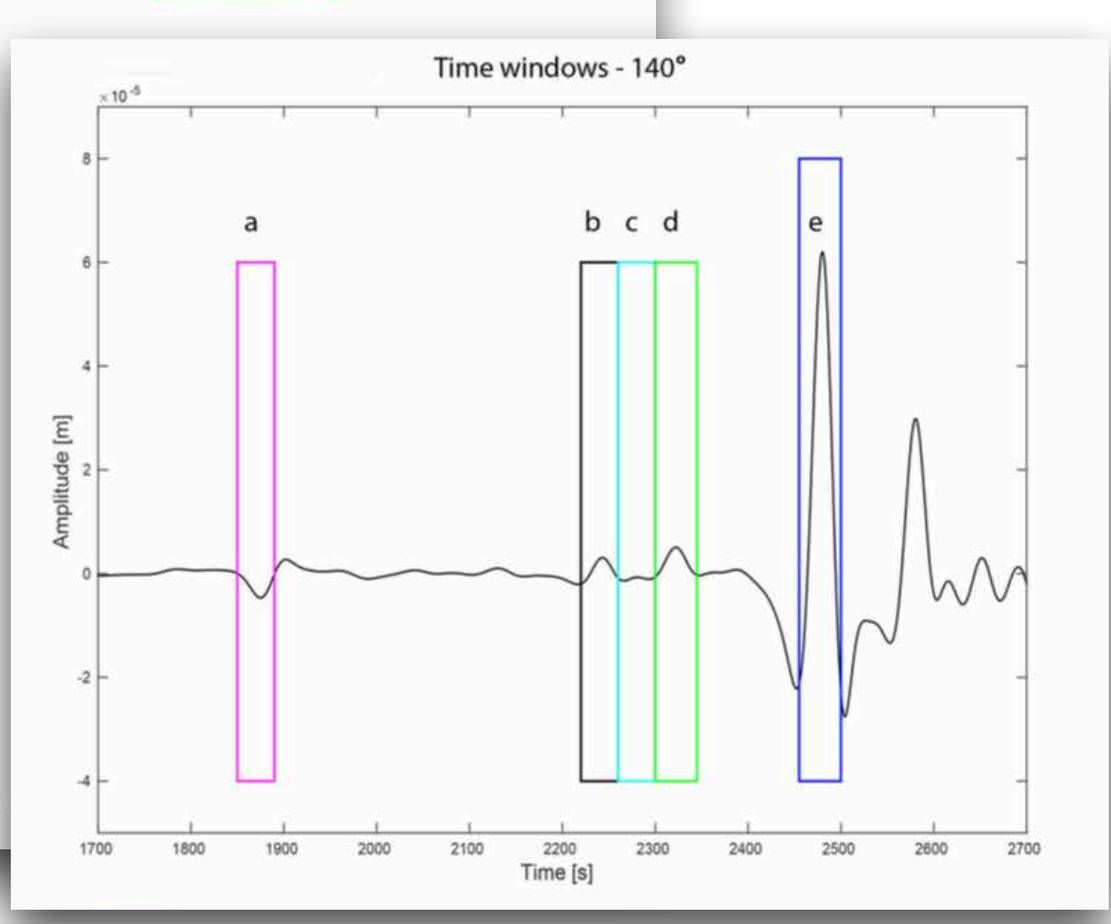

M. Koroni, E. Bozdag, H. Paulssen, J. Trampert, GJI, 2017

First global seismic models

JOURNAL OF GEOPHYSICAL RESEARCH, VOL. 89, NO. B7, PAGES 5953–5986, JULY 10, 1984

Mapping the Upper Mantle: Three-Dimensional Modeling of Earth Structure by Inversion of Seismic Waveforms

JOHN H. WOODHOUSE AND ADAM M. DZIEWONSKI

Department of Geological Sciences, Harvard University, Cambridge, Massachusetts

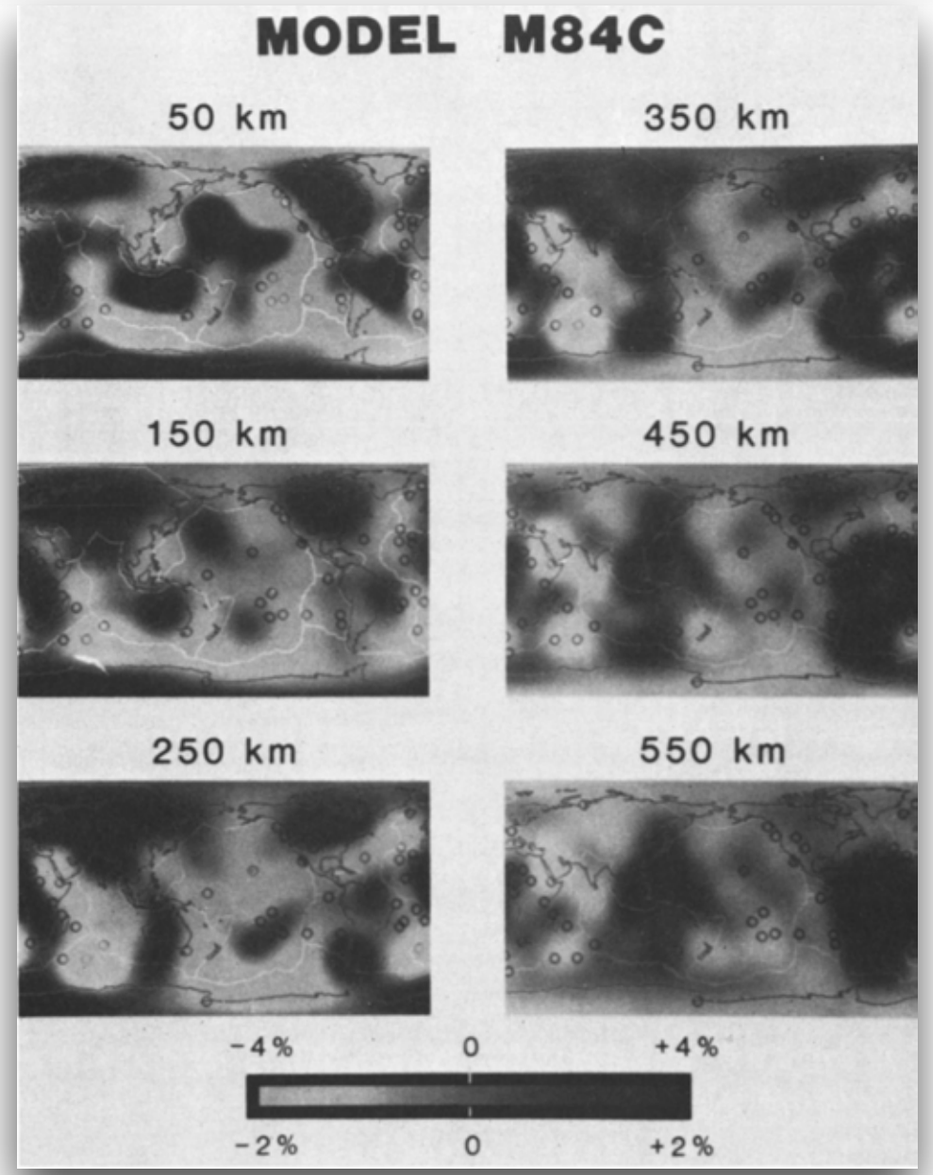

GEOPHYSICAL RESEARCH LETTERS, VOL. 11, NO. 2, PAGES 109-112, FEBRUARY 1984

ANISOTROPY AND SHEAR-VELOCITY HETEROGENEITIES IN THE UPPER MANTLE

H.-C. Nataf[1], I. Nakanishi[2], and Don L. Anderson

Seismological Laboratory, California Institute of Technology, Pasadena, Ca., 91125, USA.

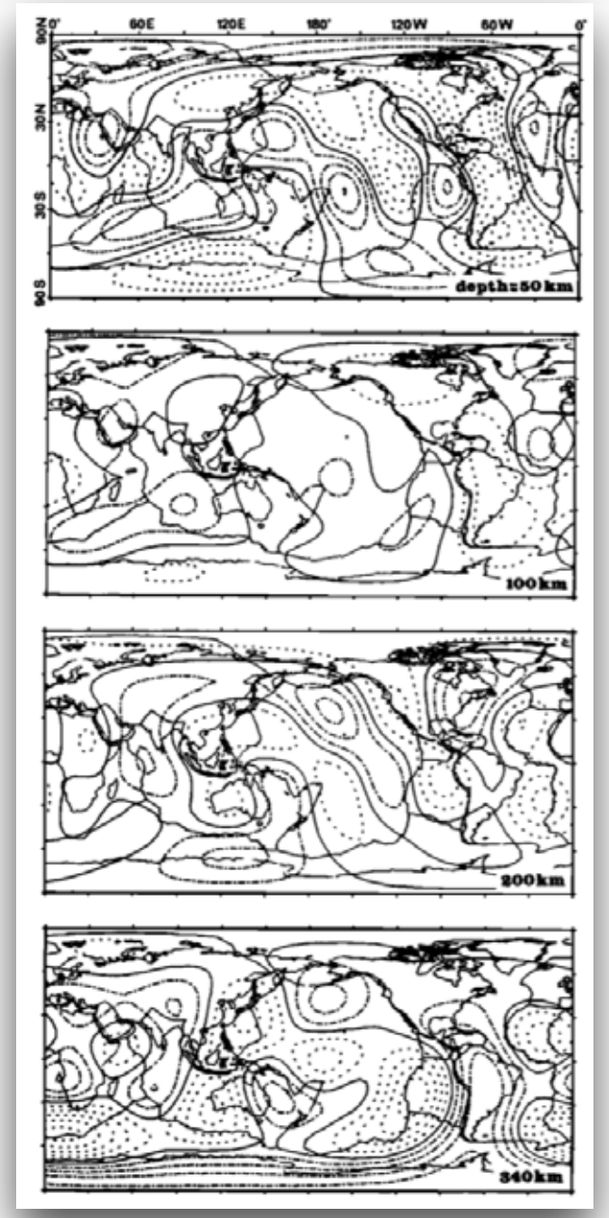

First global seismic models

Global Images of the Earth's Interior

ADAM M. DZIEWONSKI AND JOHN H. WOODHOUSE

Science, New Series, Vol. 236, No. 4797 (Apr. 3, 1987), pp. 37-48

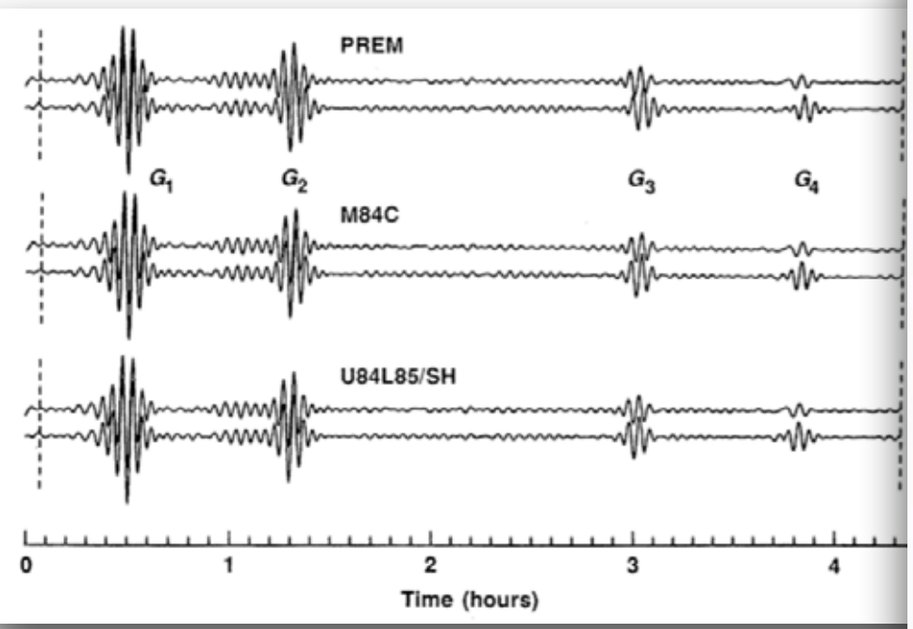

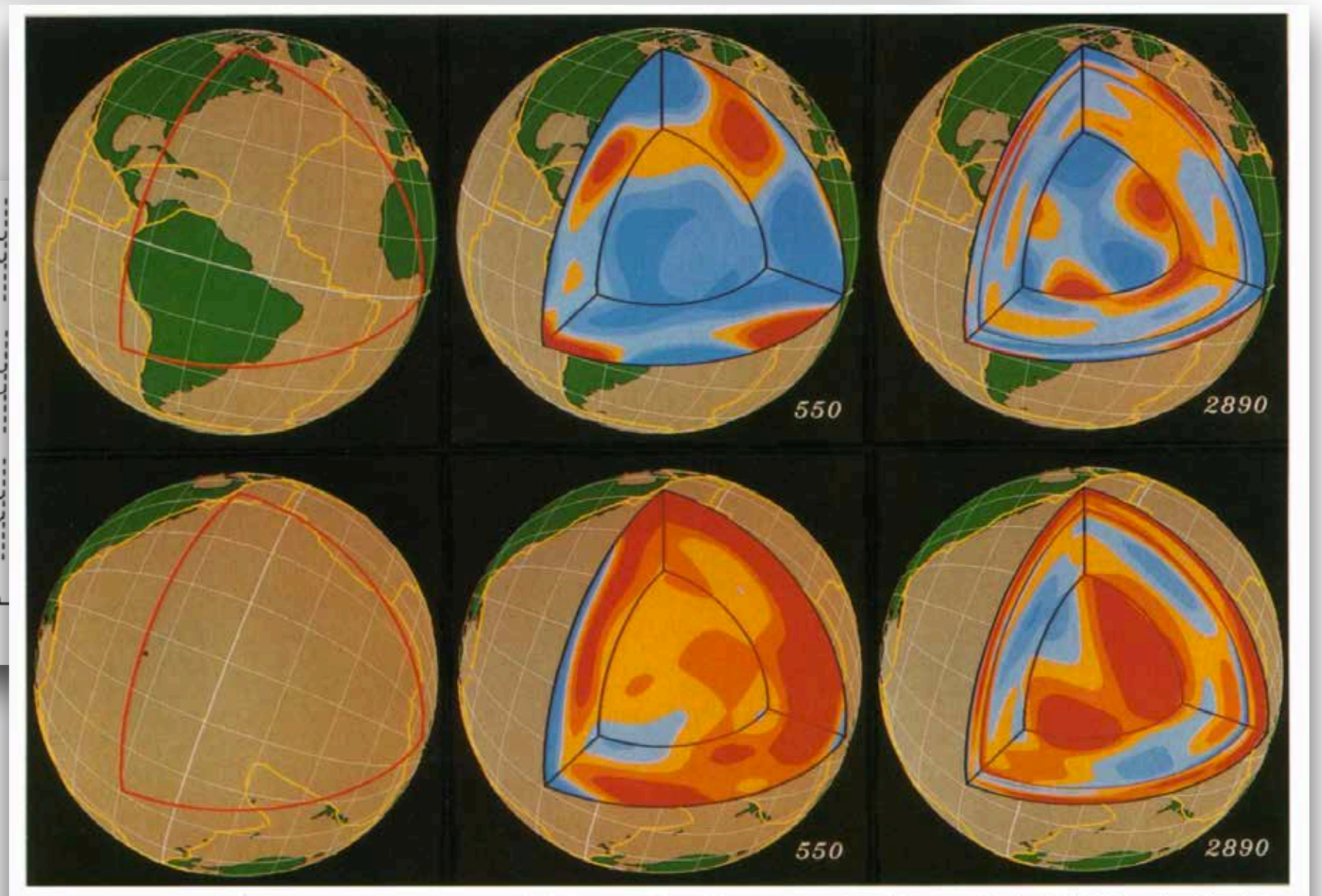

Fig. 12. Windows into the earth. Three-dimensional plots of velocity anomalies under two oceans viewed from an altitude of 35,000 km: the Atlantic (top panels) and the Pacific (bottom panels). Depth to the bottom is indicated in kilometers. In the upper mantle panels (550 km) the depth scale is exaggerated by a factor of 5. Based on models in (*3*) and (*15*). Yellow lines are plate boundaries.

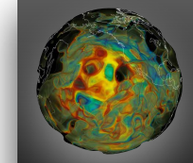

Adjoint tomography

GEOPHYSICS, VOL. 49, NO. 8 (AUGUST 1984); P. 1259–1266.

Inversion of seismic reflection data in the acoustic approximation

Albert Tarantola*

ABSTRACT

The *nonlinear* inverse problem for seismic reflection data is solved in the acoustic approximation. The method is based on the generalized least-squares criterion, and it can handle errors in the data set and a priori information on the model. Multiply reflected energy is naturally taken into account, as well as refracted energy or surface waves. The inverse problem can be solved using an iterative algorithm which gives, at each iteration, updated values of bulk modulus, density, and time source function. Each step of the iterative algorithm essentially consists of a forward propagation of the actual sources in the current model and a forward propagation (backward in time) of the data residuals. The correlation at each point of the space of the two fields thus obtained yields the corrections of the bulk modulus and density models. This shows, in particular, that the general solution of the inverse problem can be attained by methods strongly related to the methods of migration of unstacked data, and commercially competitive with them.

Adjoint tomography

GEOPHYSICS, VOL. 51, NO. 7 (JULY 1986); P. 1387-1403, 16 FIGS.

Two-dimensional nonlinear inversion of seismic waveforms: Numerical results

Odile Gauthier*, Jean Virieux*, and Albert Tarantola*

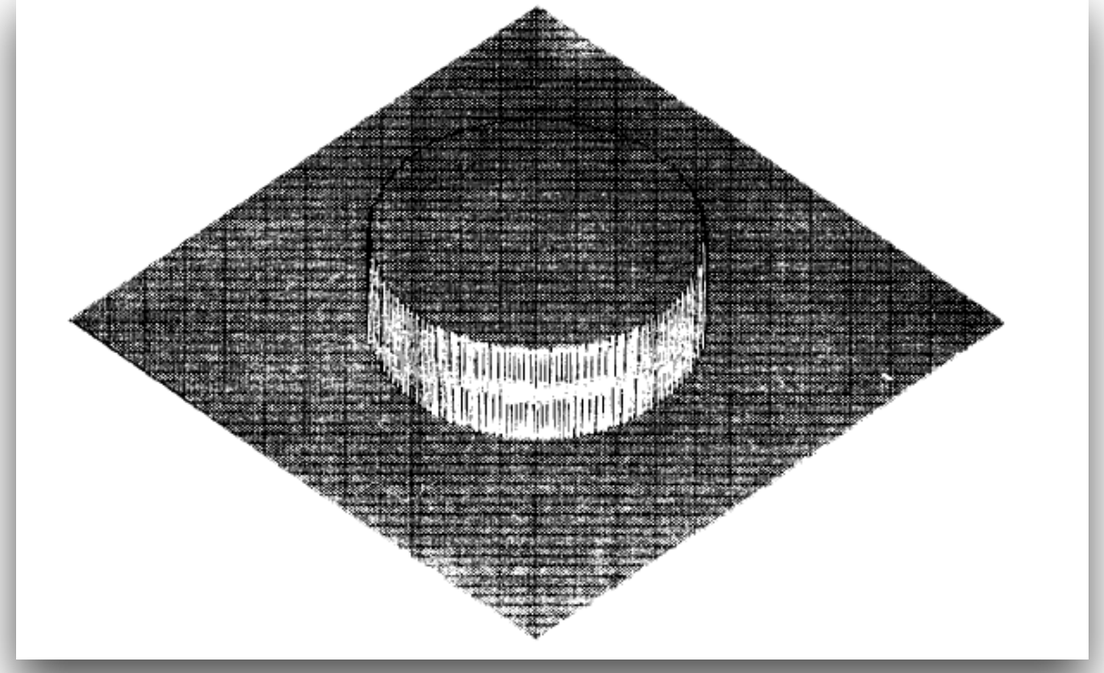

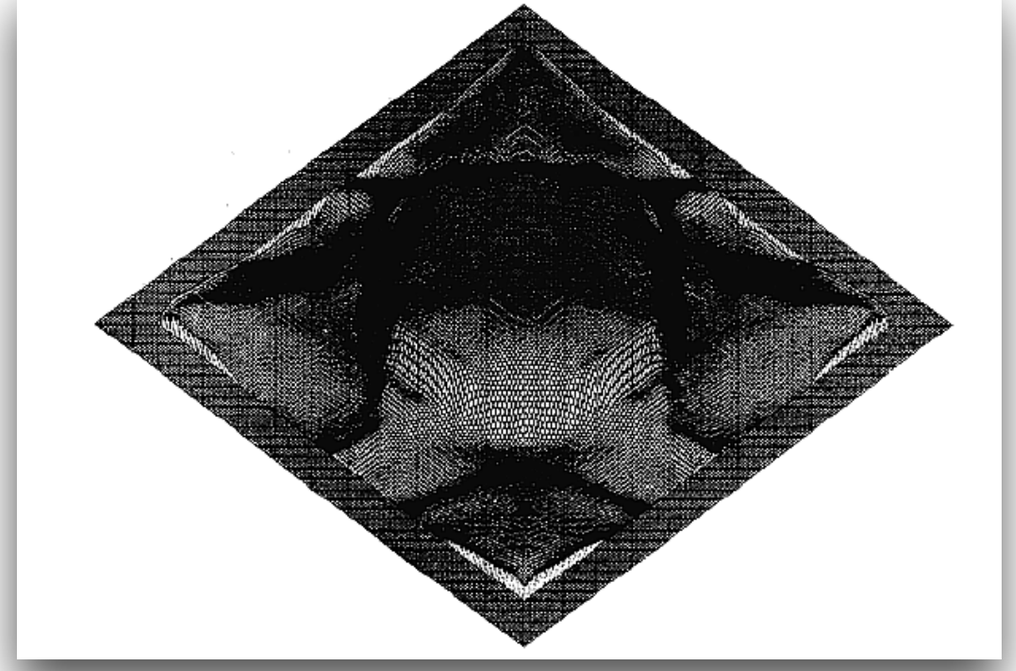

target model

after 5 iterations

Adjoint tomography

GEOPHYSICS, VOL. 51, NO. 7 (JULY 1986); P. 1387-1403, 16 FIGS.

Two-dimensional nonlinear inversion of seismic waveforms: Numerical results

Odile Gauthier*, Jean Virieux*, and Albert Tarantola*

On the other hand, numerical methods based on discretization of the wave equation synthesize the different waves arriving at the station as a whole. This can make physical interpretation of a forward calculation difficult, but it does not prevent inversion. The main limitation of numerical methods is their computational cost, in both time and memory requirements.

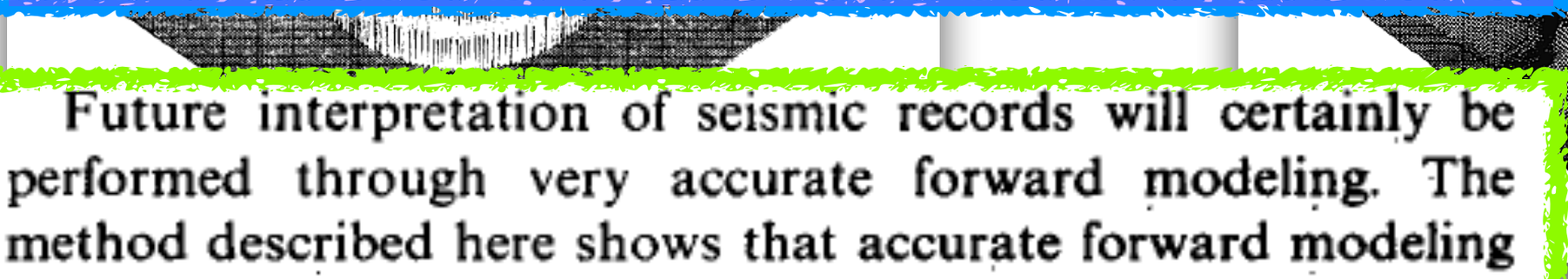

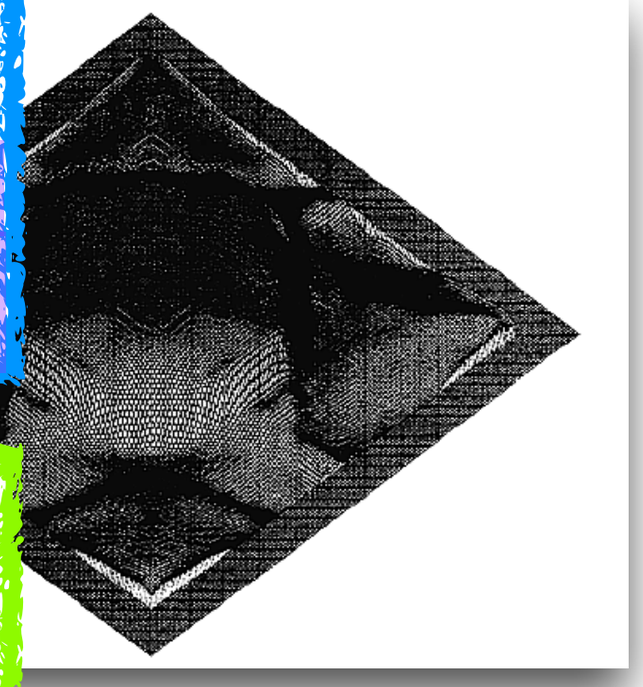

Future interpretation of seismic records will certainly be performed through very accurate forward modeling. The method described here shows that accurate forward modeling codes can be used for waveform matching.

target model

after 5 iterations

Global adjoint tomography

Gauthier et al. 1987

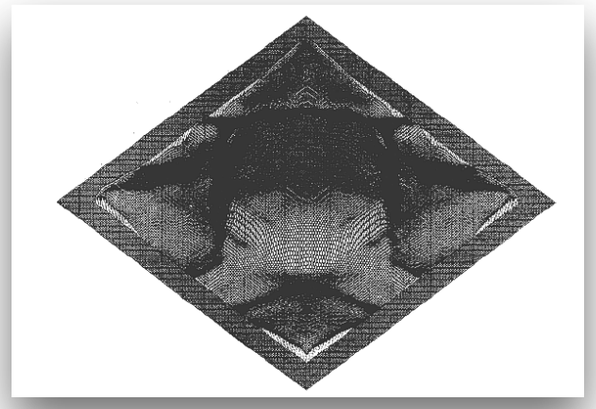

- dx=dz=5 m
- 200x200 grid points
- 8 shots, 400 receivers
- 2D acoustic
- ~8 s seismograms

Bozdağ et al. 2016

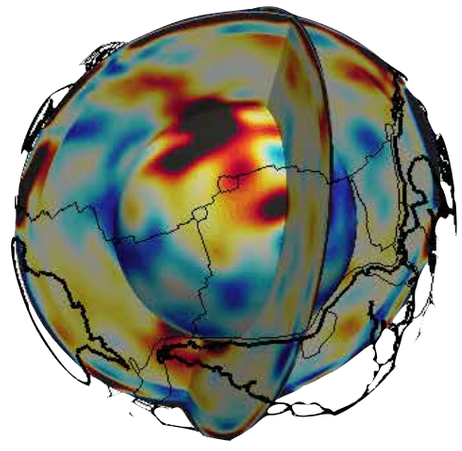

- entire globe
- ~300 millions grid points
- 253 equakes, ~1000 stations/event (>6000 earthquakes)
- 3D anelastic
- 180 m seismograms

GLAD-M15

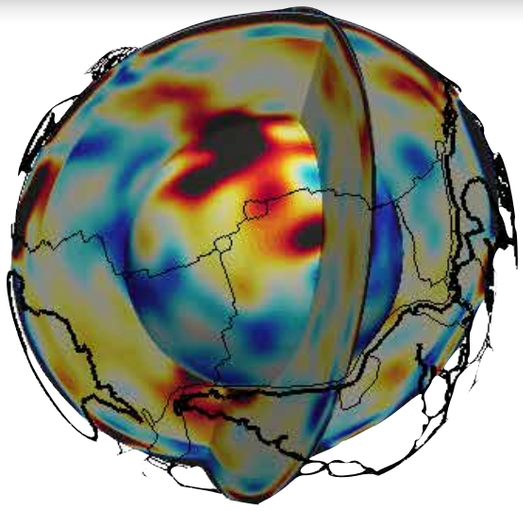

E. Bozdag, D. Peter, M. Lefebvre, D. Komatitsch, J. Tromp, J. Hill, N. Podhorszki, D. Pugmire, 2016, GJI

- **First-generation global adjoint model: TI in upper mantle, *P & S* wavespeeds**

- ***Forward simulations & Fréchet sensitivity kernels* in realistic 3D Earth models using *spectral-element & adjoint methods*.**

- **253 earthquakes and 15 conjugate-gradient iterations**

- **Crust and mantle are inverted simultaneously: *no crustal corrections!***

Numerical simulations

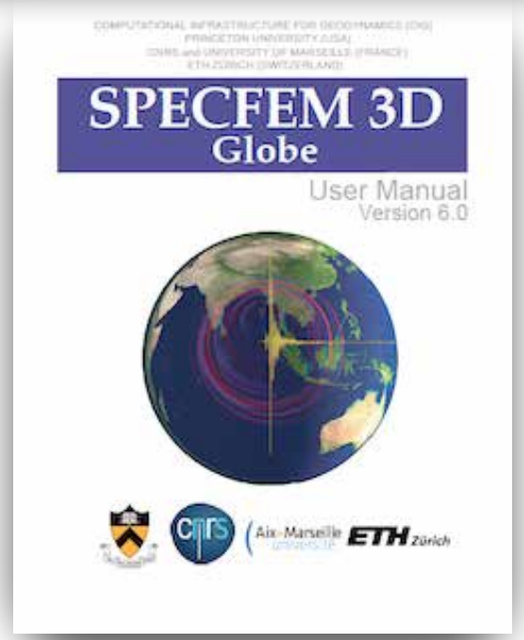

- **SPECFEM3D_GLOBE**

  (Komatitsch & Tromp 2002)

  GPU version by Daniel Peter

- **3D reference model:**

  S362ANI (Kustowski et al. 2008) + Crust2.0 (Bassin et al. 2000)

- **Topography/bathymetry/attenuation/ellipticity/rotation/ gravity (Cowling approx.)/ocean load**

- **Length of seismograms = 100 m-200 m,**
  Tmin = ~27 s, *now* Tmin=~17 s, soon Tmin=~9 s

Earthquakes & seismic stations

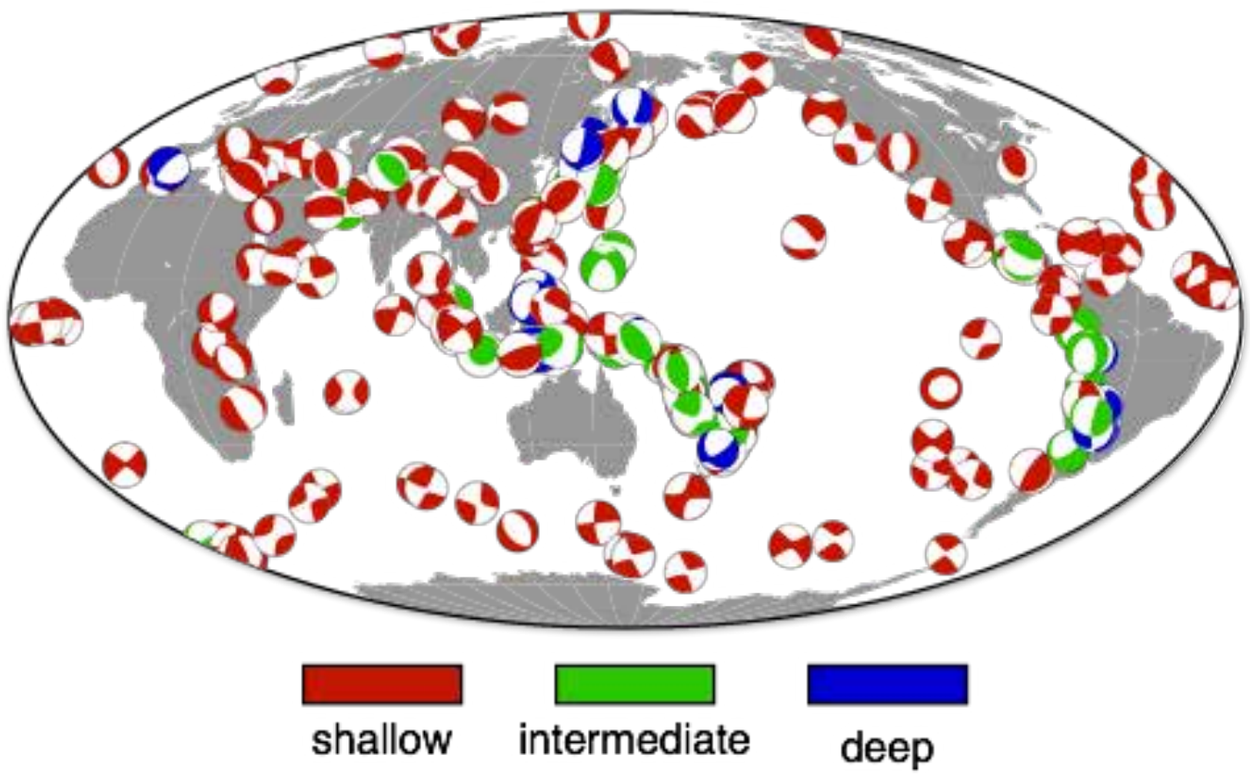

Initially selected 253 CMT events
(5.8 ≤ Mw ≤ 7.0)

shallow: d ≤ 50 km
intermediate: 50 km < d ≤ 300 km
deep: d > 300 km

data from IRIS & ORFEUS
blue: additional local + PASSCAL arrays

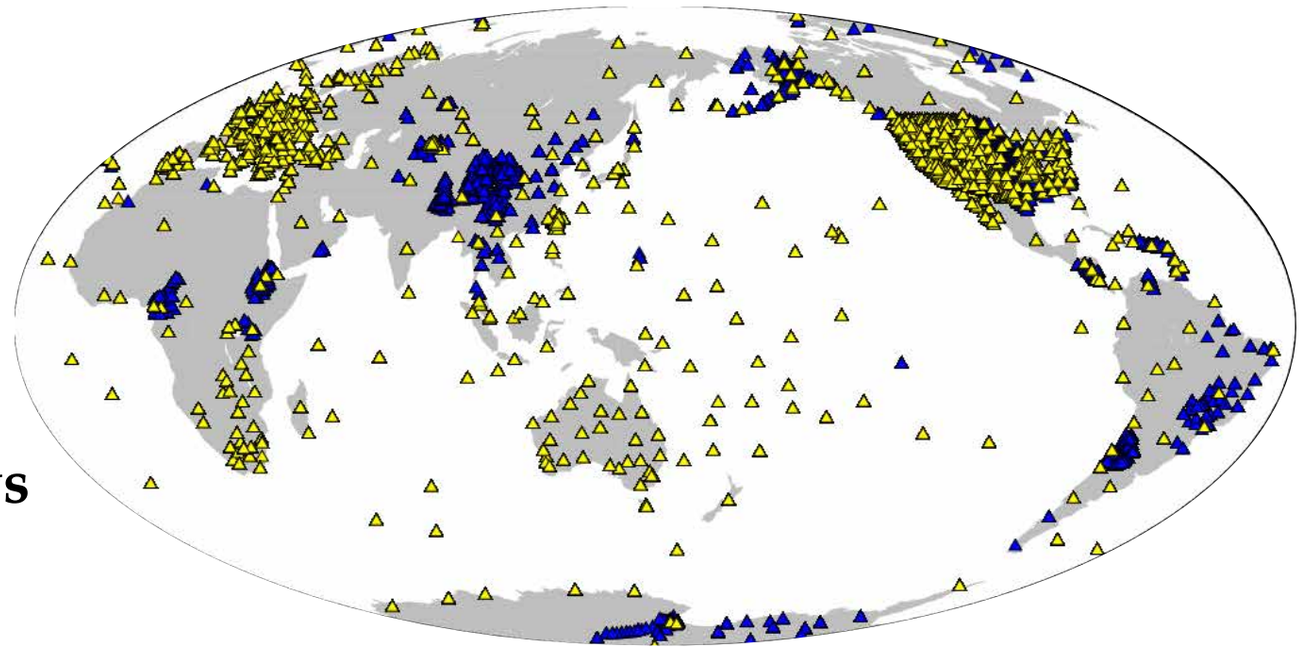

Cross-sections - 250 km

M00: S362ANI

(Kustowski et al. 2007)

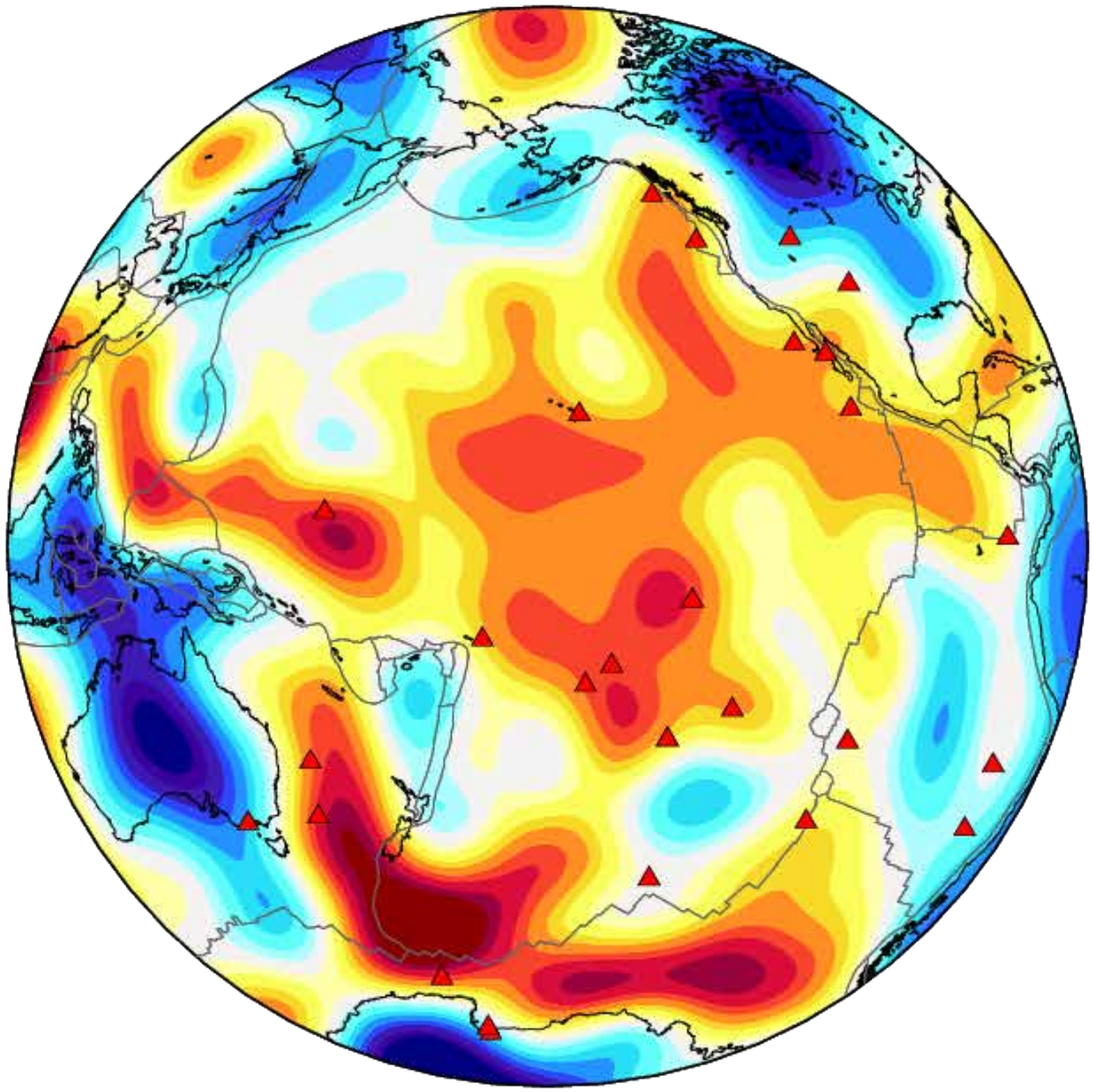

dlnVsv (3%)

min max

Cross-sections - 250 km

M15: GLAD-M15

(Bozdag et al. 2016)

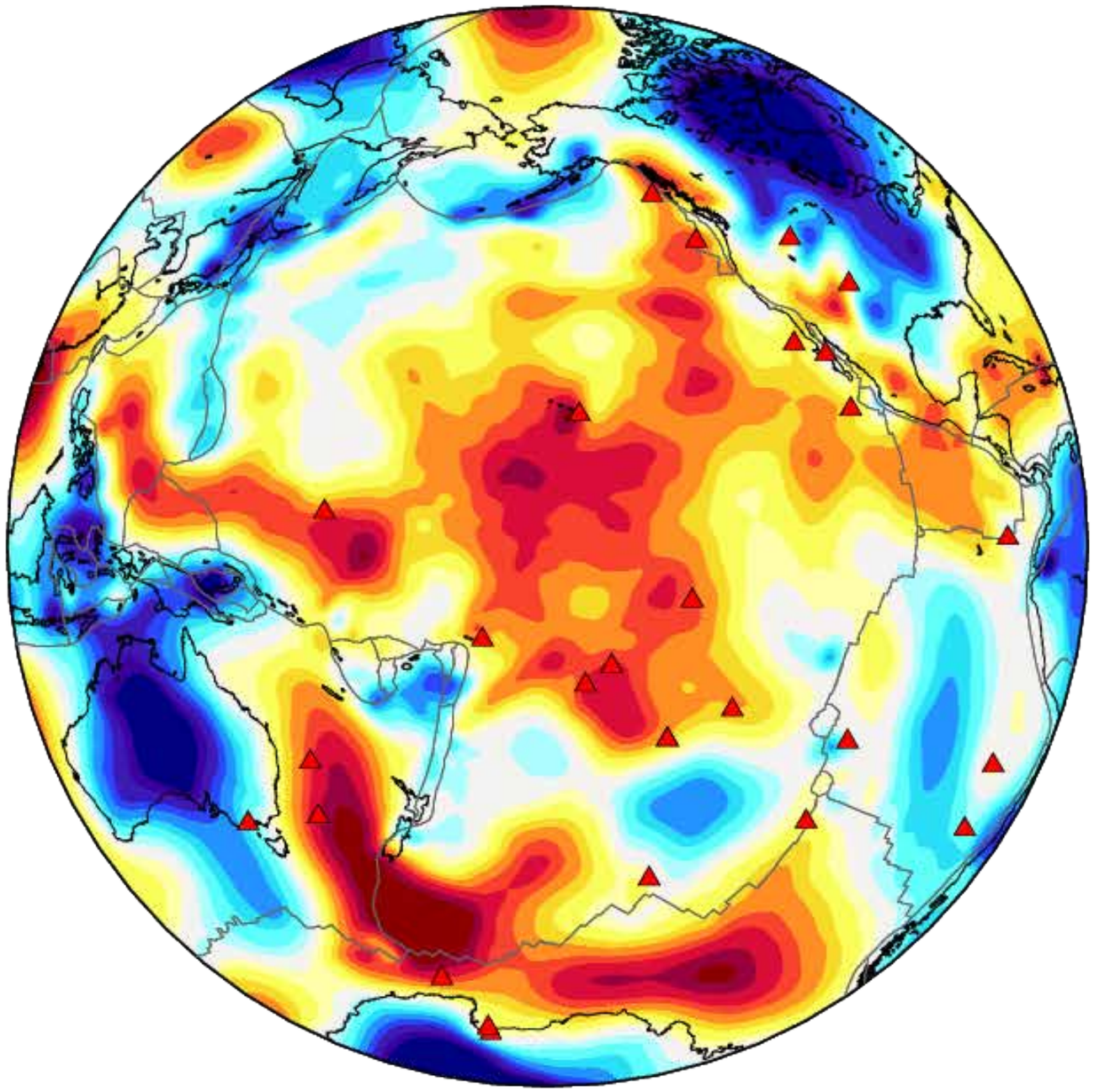

dlnVsv (3%)

min max

Cross-sections - 250 km

M15: GLAD-M15

(Bozdag et al. 2016)

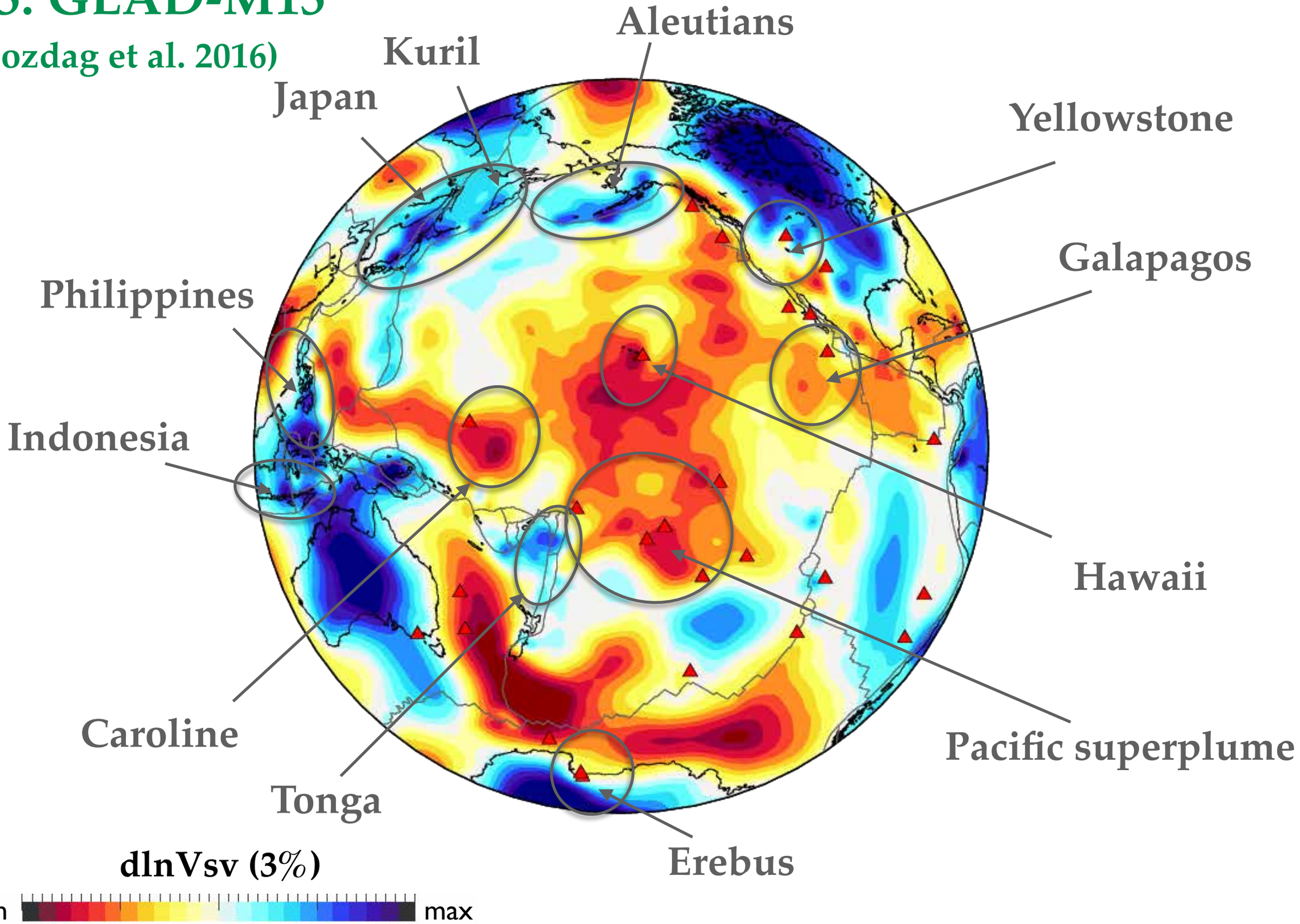

More sections

M00 - 1DREF

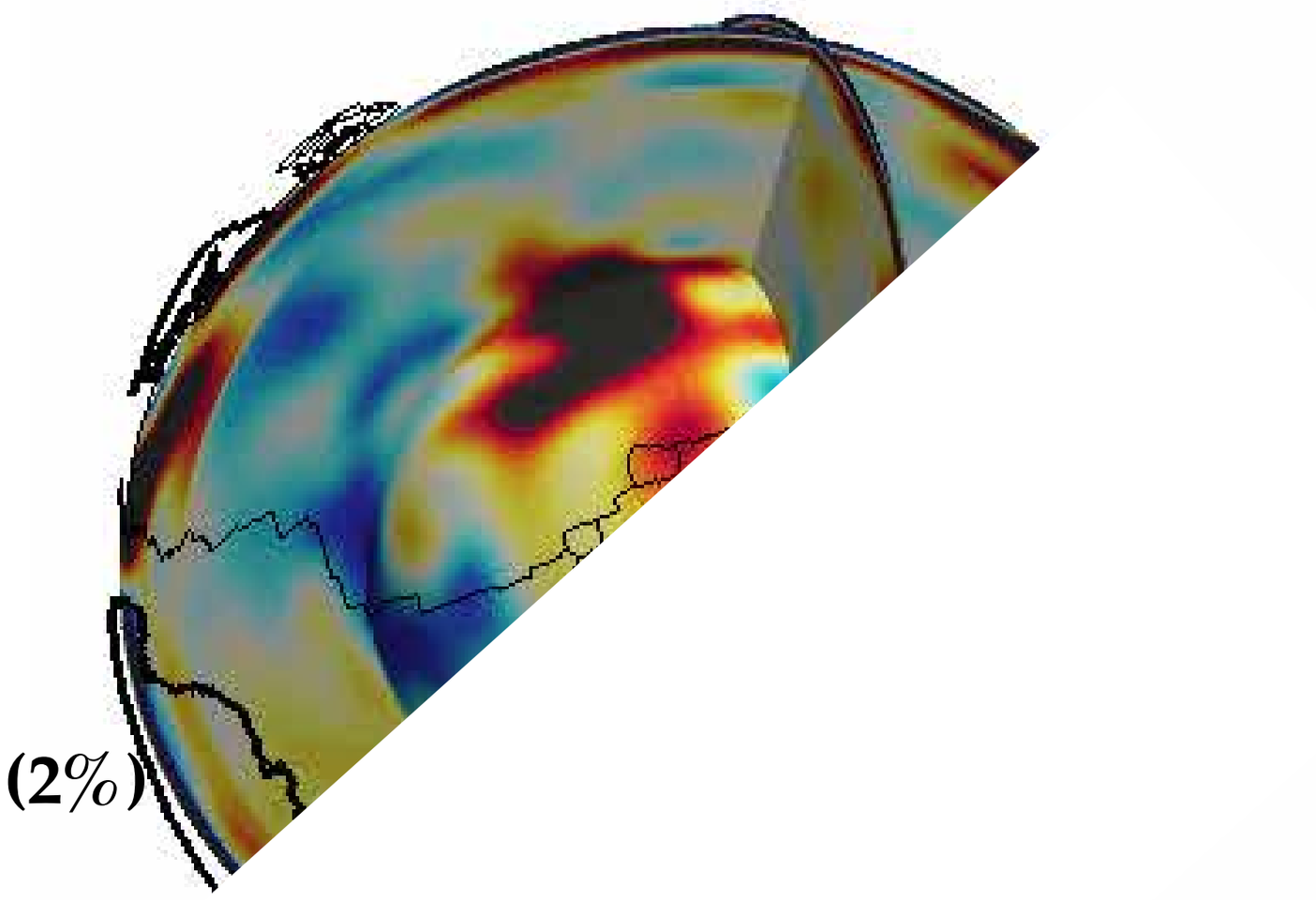

dlnVsv

min max

More sections

M15 - 1DREF

Samoa

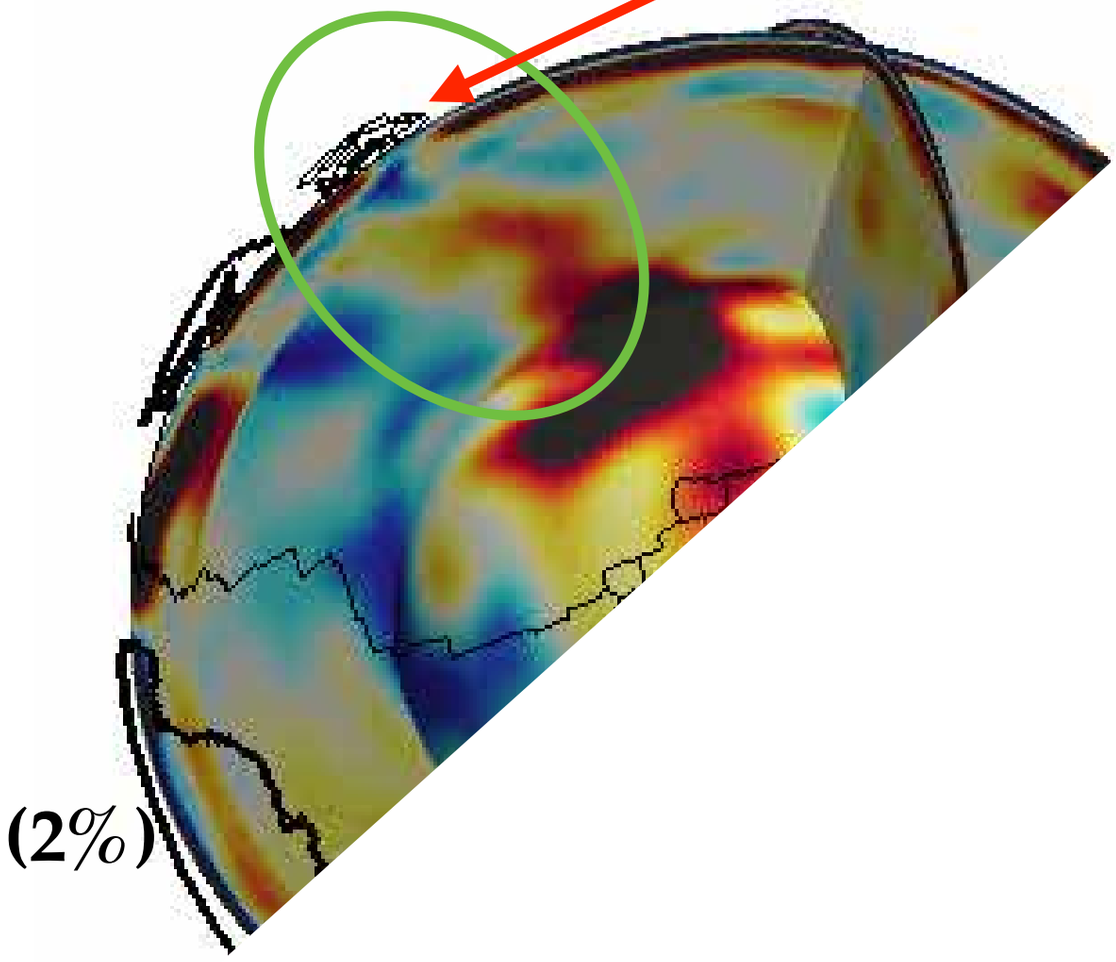

(2%)

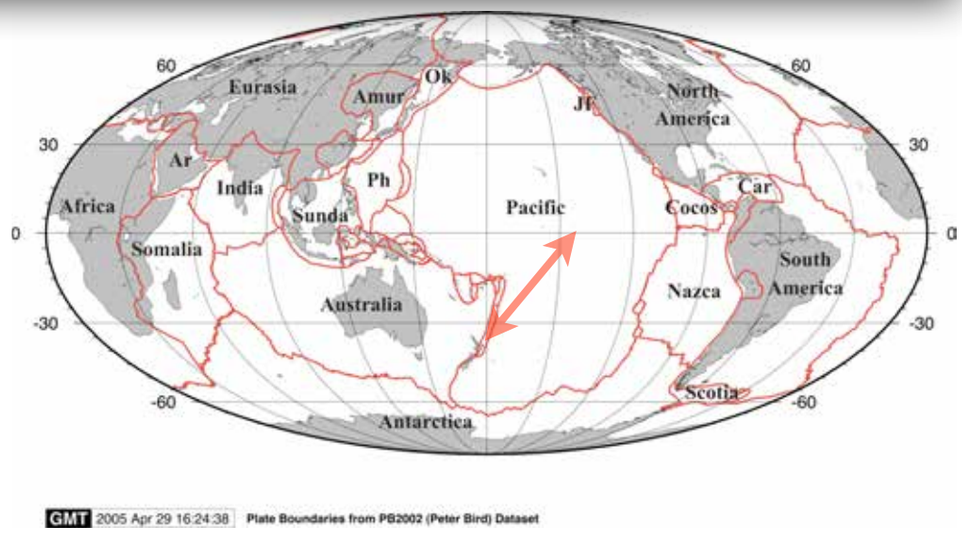

dlnVsv

min — max

More sections

M15 - 1DREF

Samoa

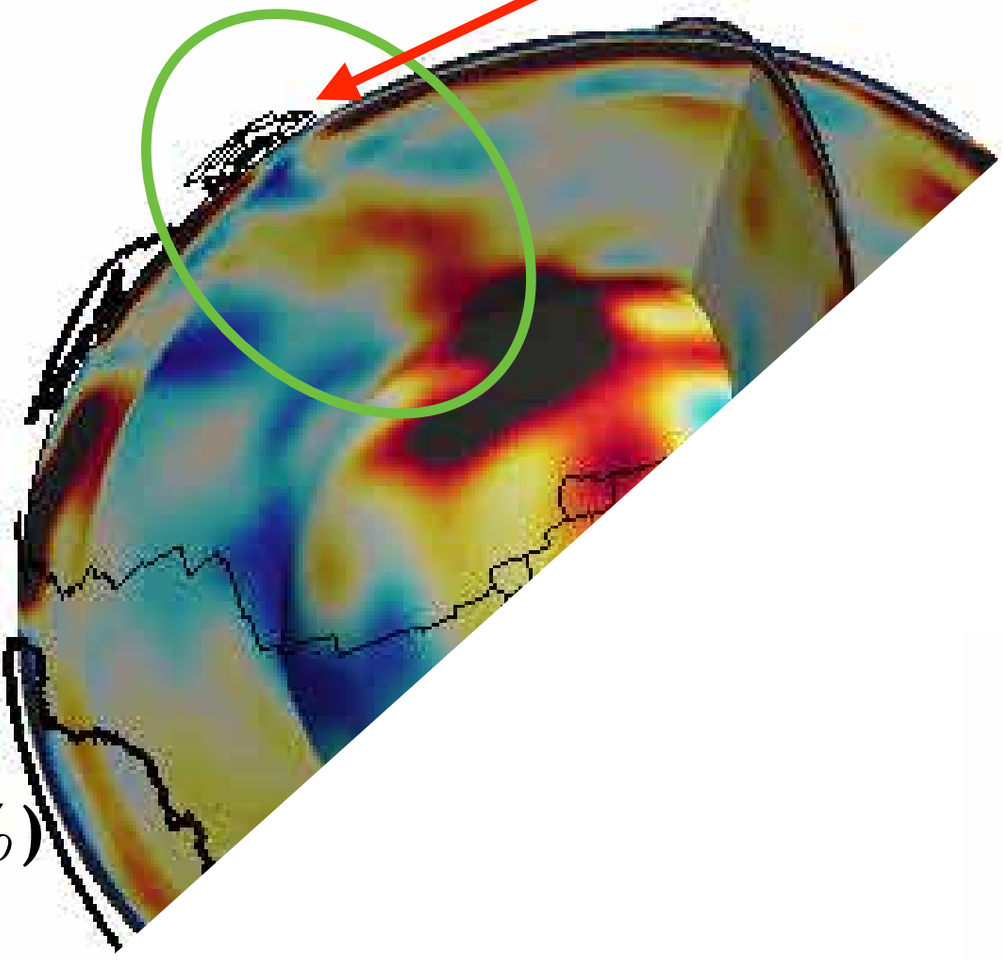

(2%)

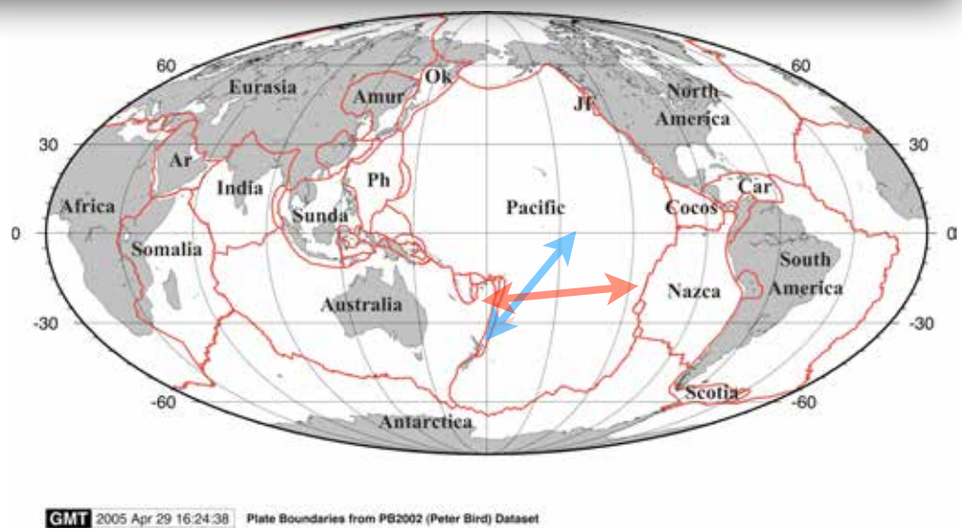

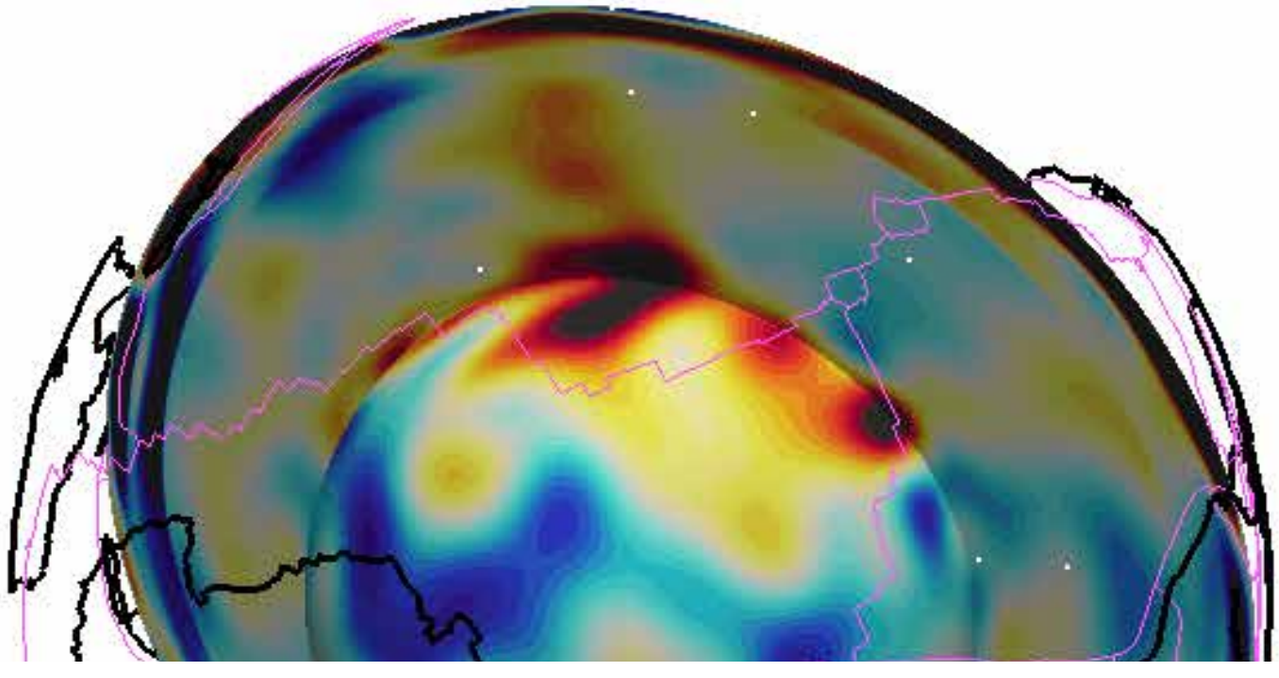

(2%)

dlnVsv

min max

More sections

M15 - 1DREF

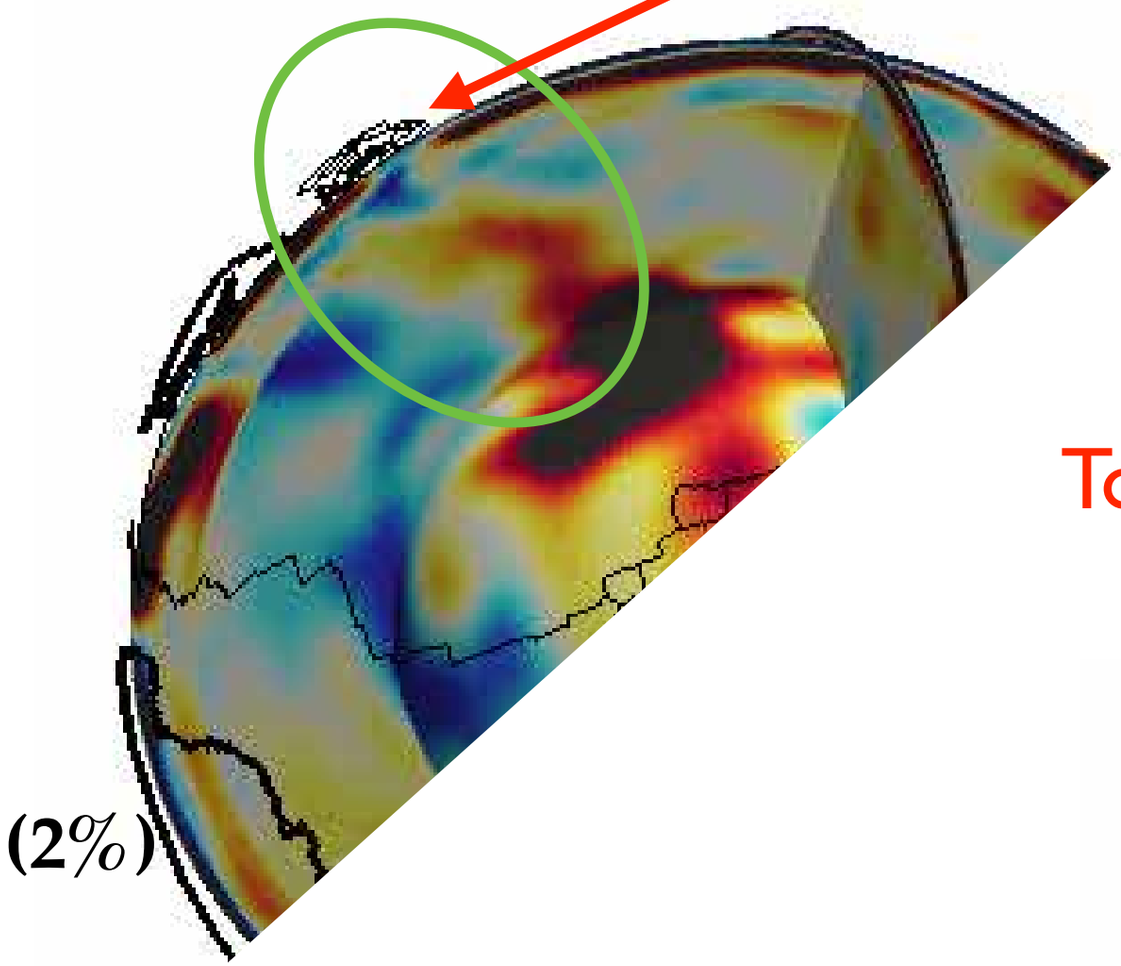

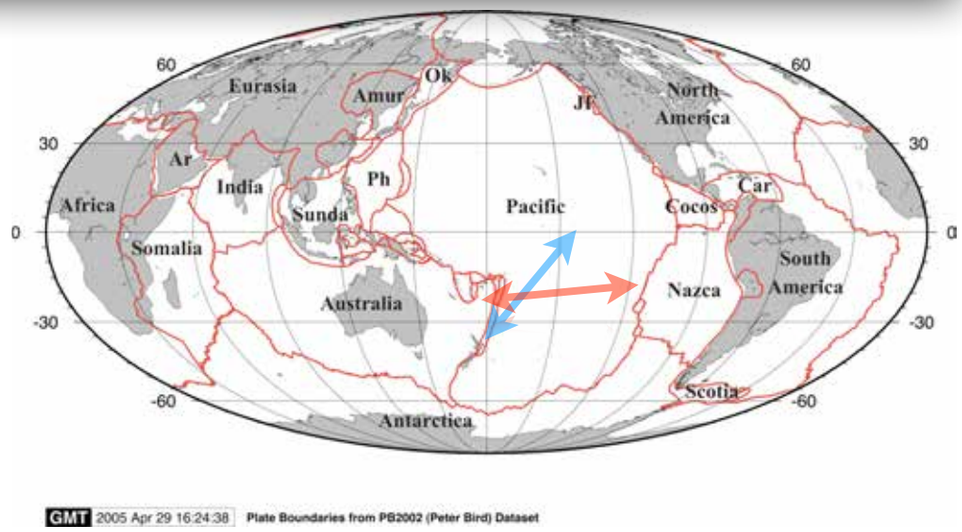

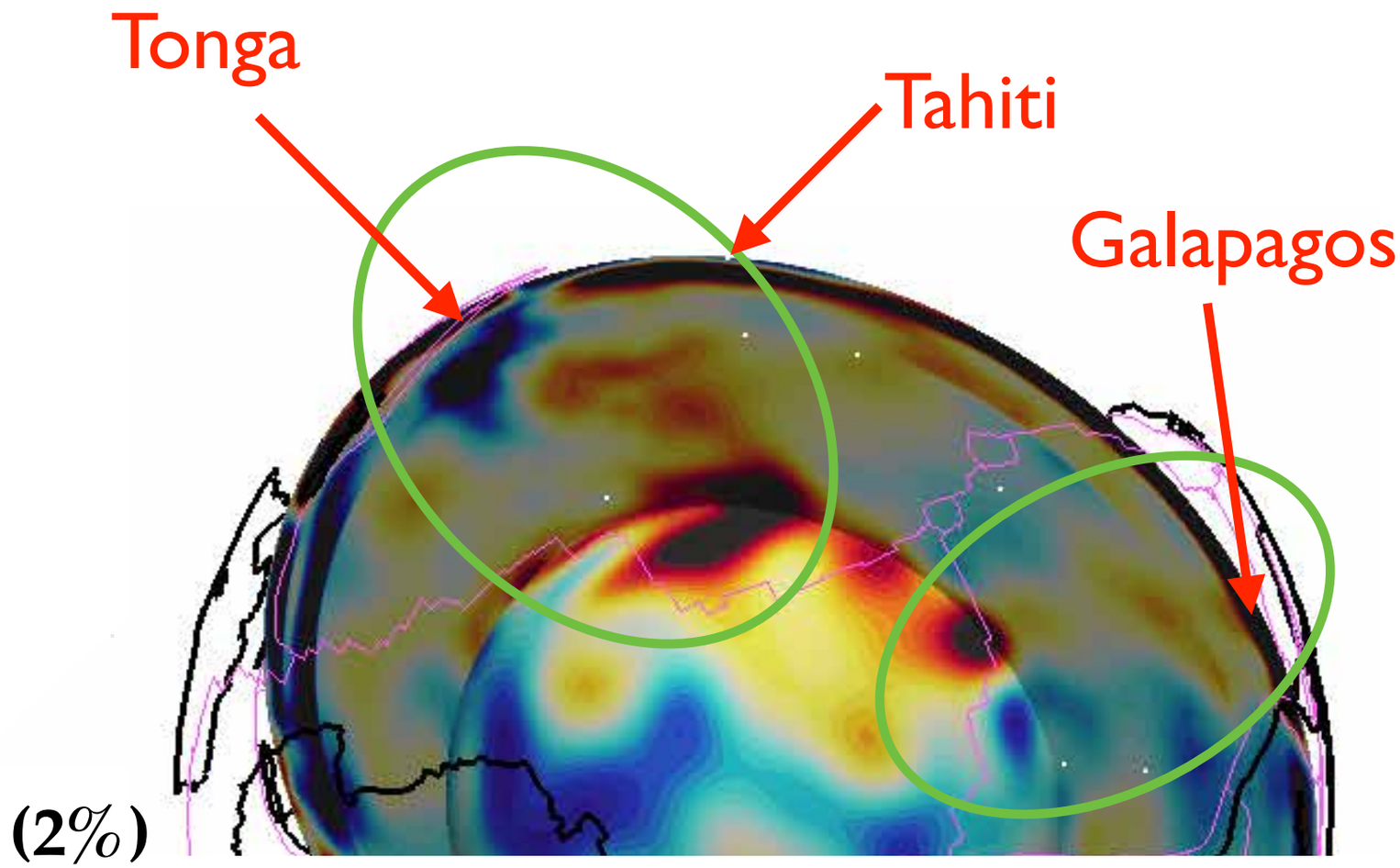

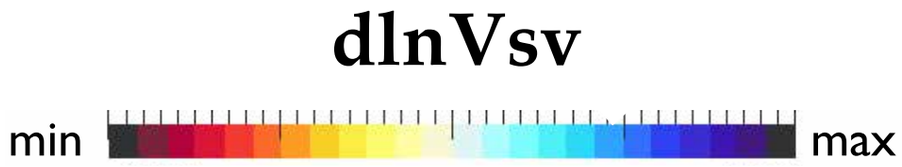

Multi-scale mantle plumes

Stable lower-mantle plumes followed by small upper-mantle plumes ==> primary & secondary plumes

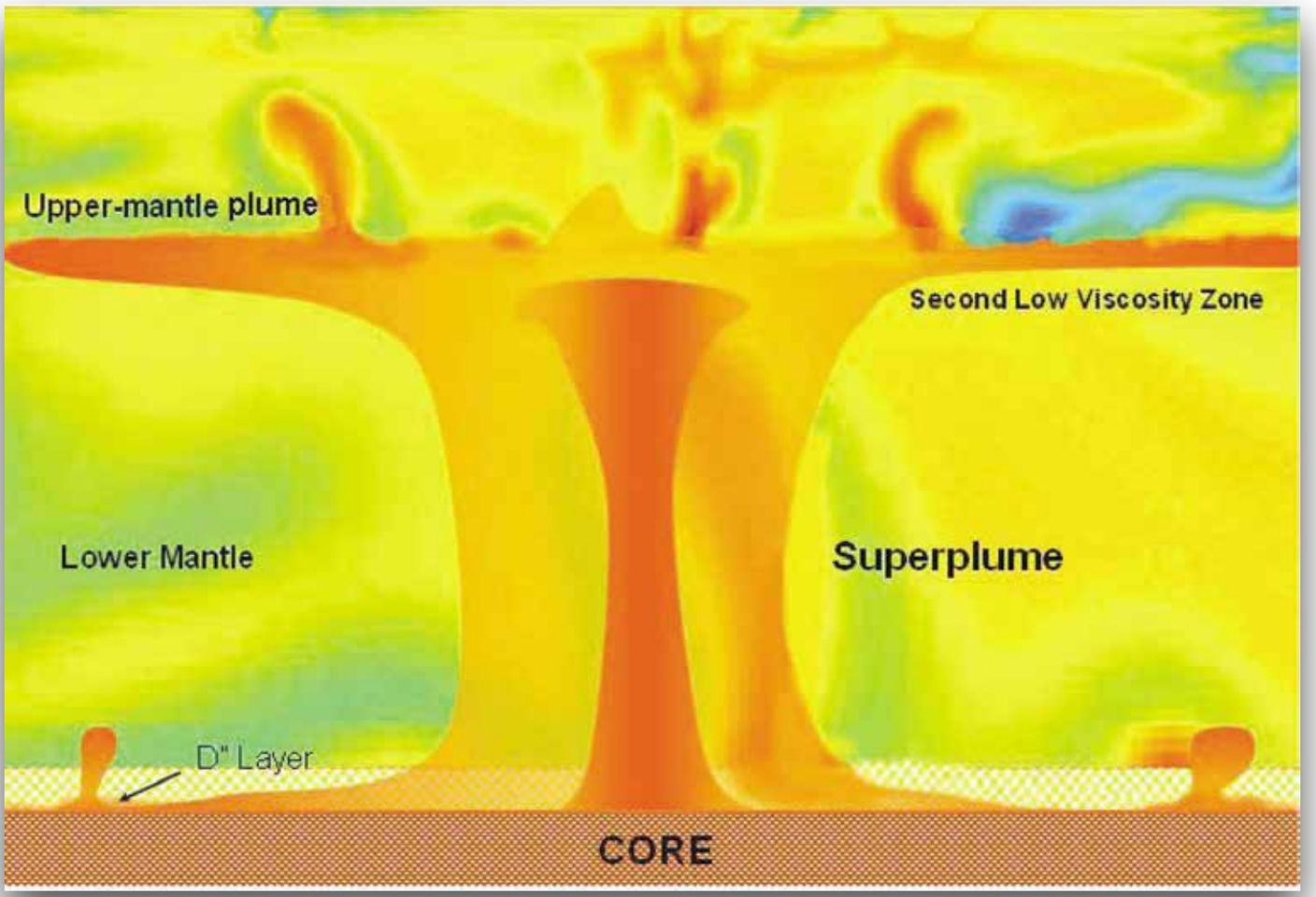

Matyska & Yuen, 2007

- mantle viscosity
- thermal conductivity
- thermal expansivity
- phase transitions
  - spinel to perovskite
  - perovskite to post-perovskite

Courtesy Magali Billen

Tonga / Samoa

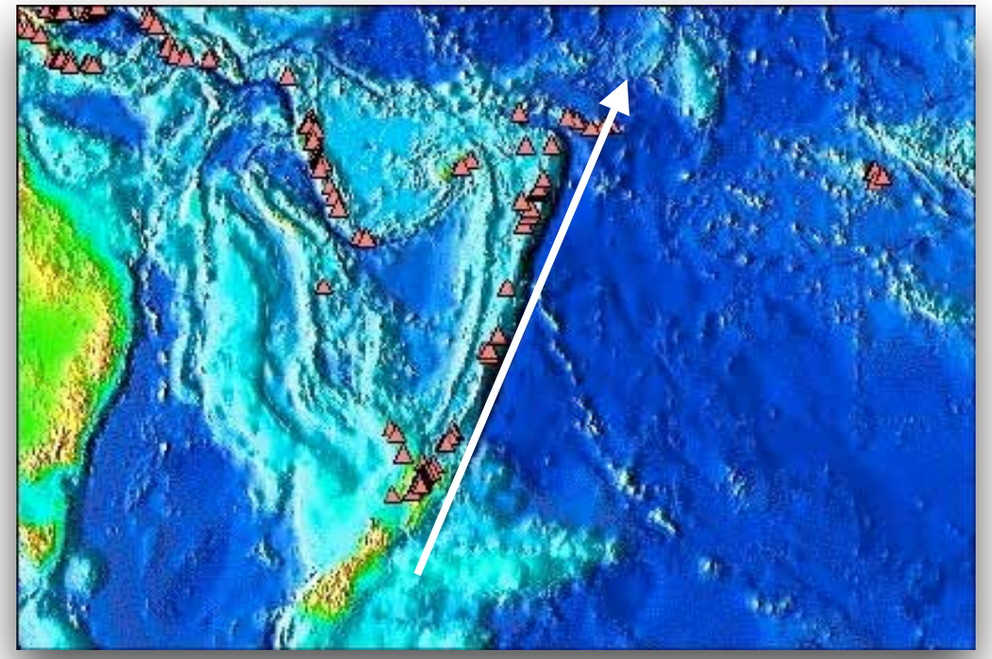

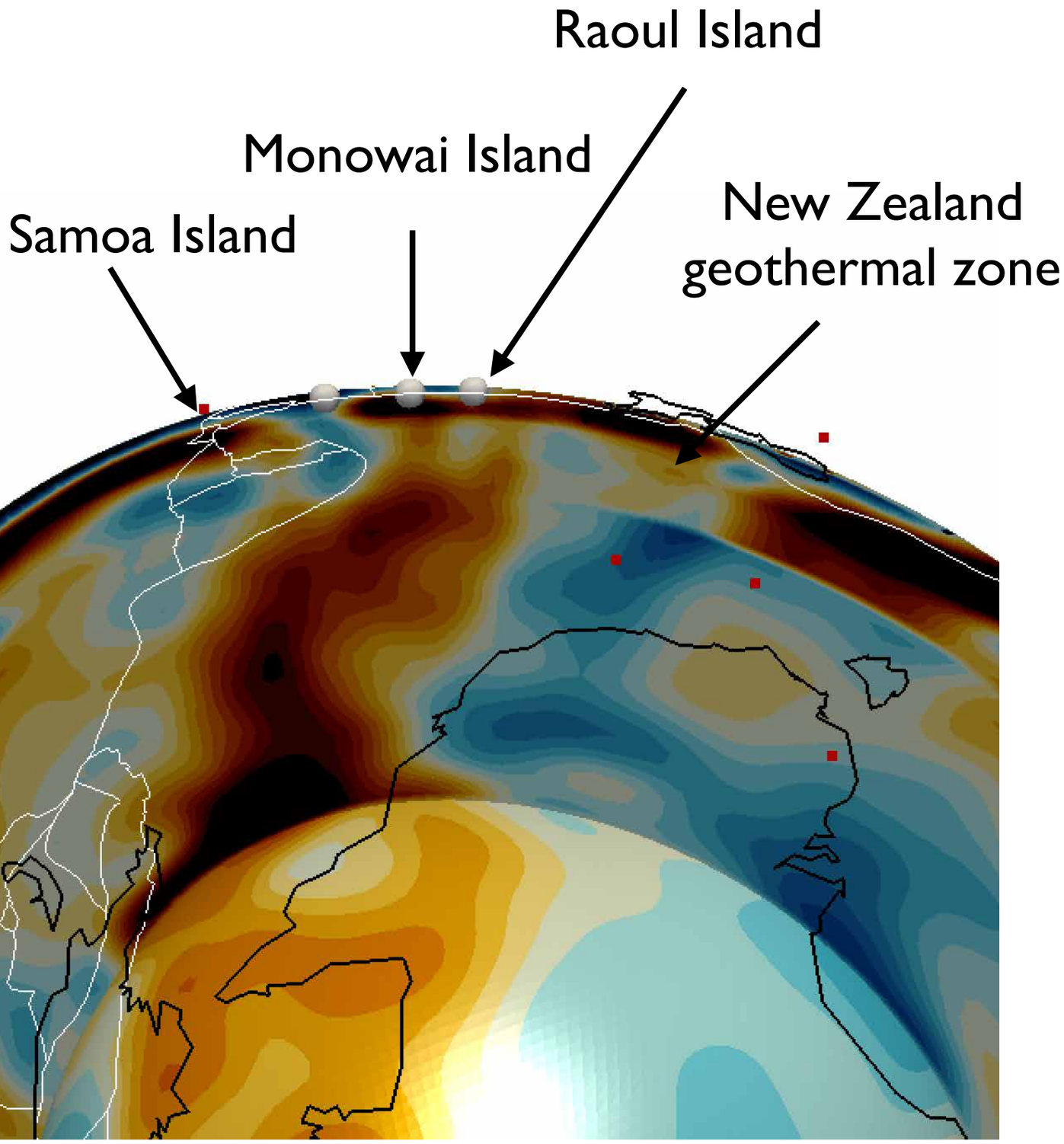
Raoul Island
Monowai Island
Samoa Island
New Zealand
geothermal zone

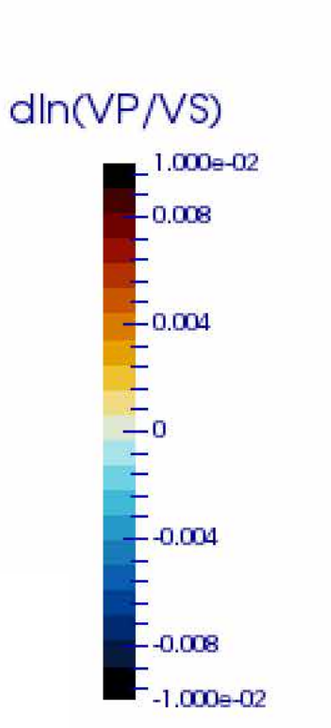
dln(VP/VS)
1.000e-02
0.008
0.004
0
-0.004
-0.008
-1.000e-02

North America - 250 km

S362ANI

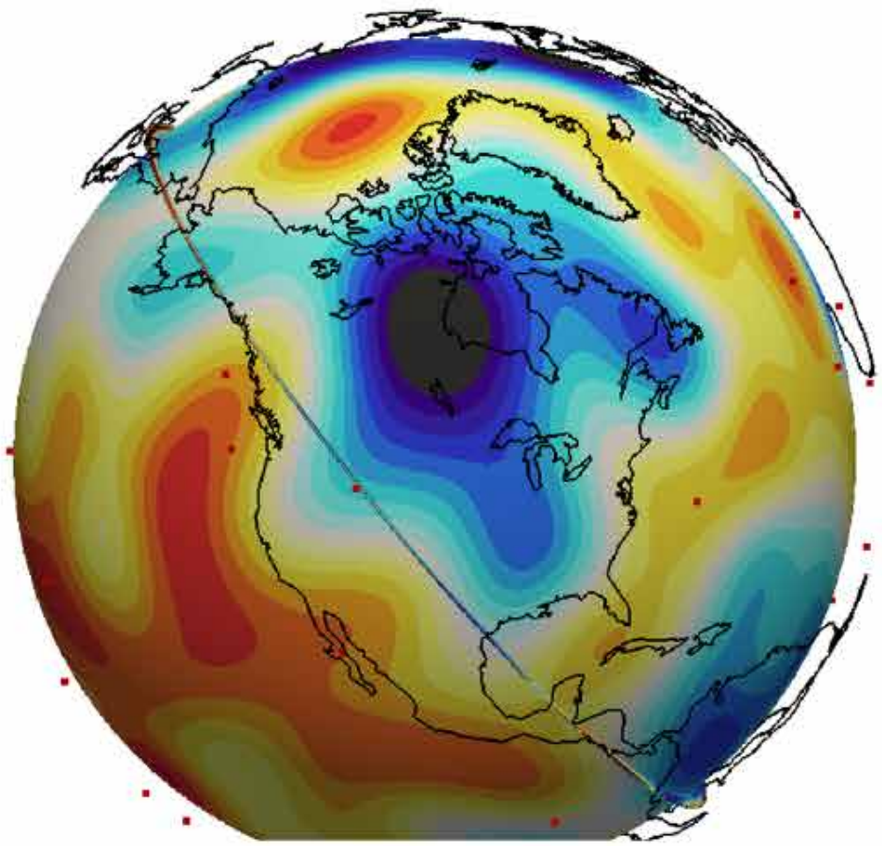

dlnVsv (2%)

min max

GLAD-M15

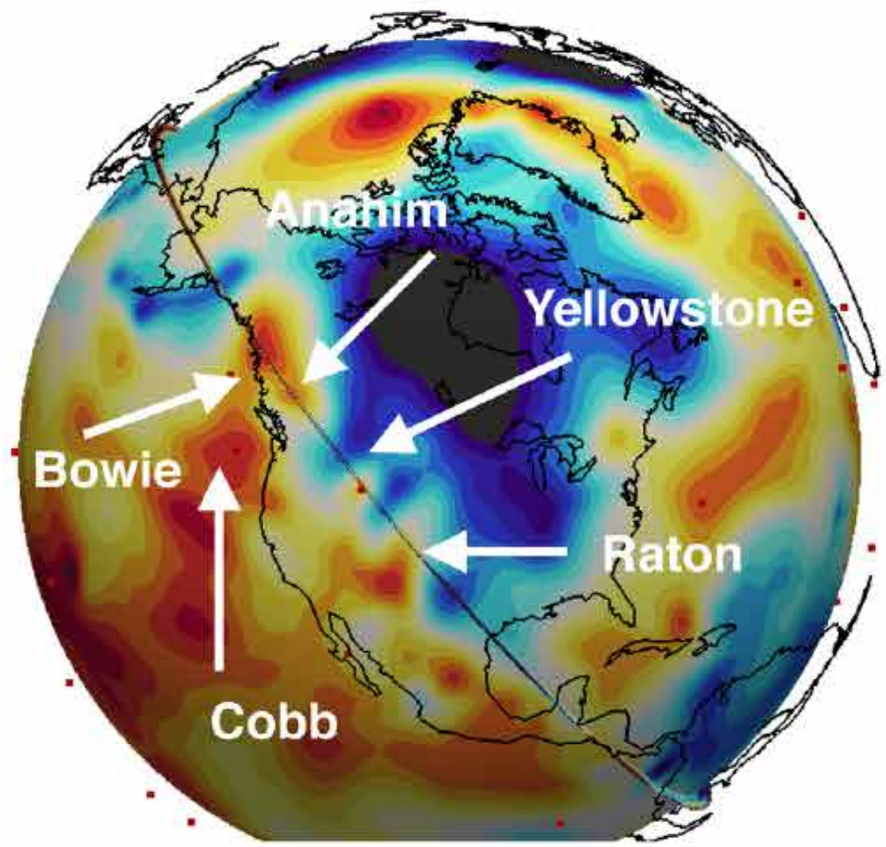

dlnVsv (2%)

min max

More sections..

M00 - 1DREF

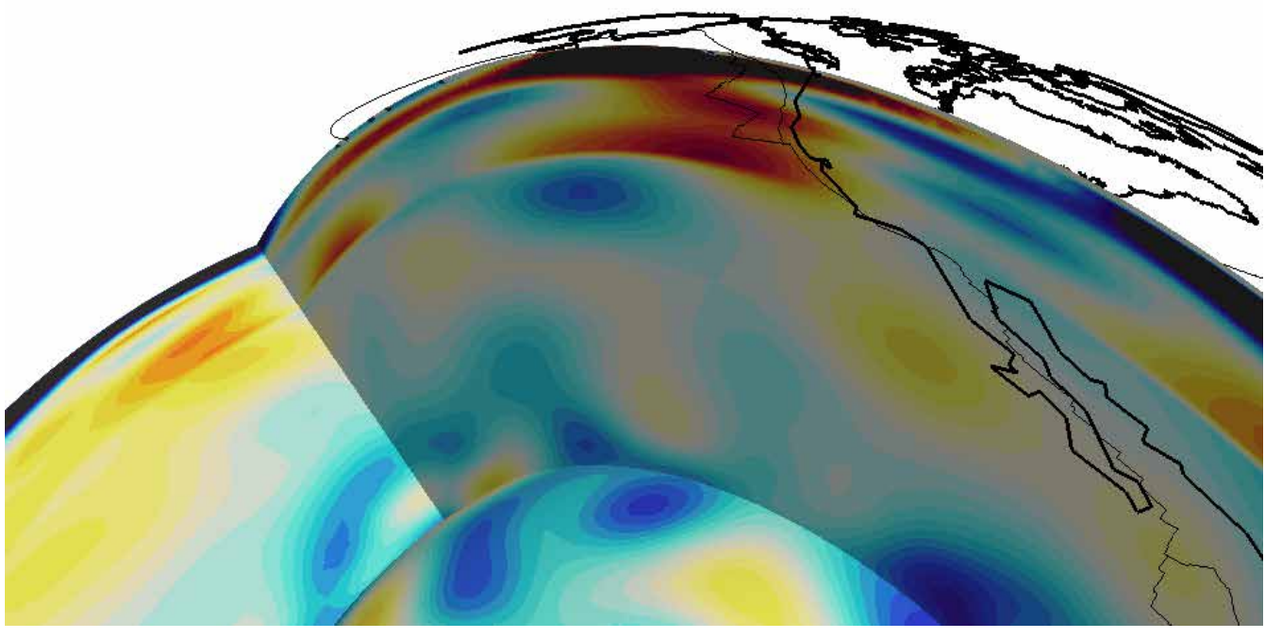

(2%)

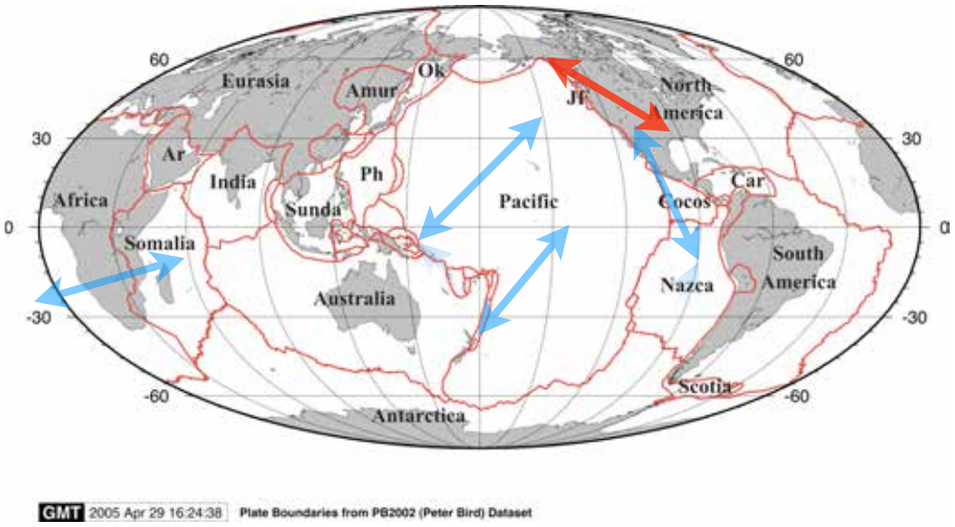

dlnVsv

min max

More sections..

M15 - 1DREF

Bowie

Yellowstone

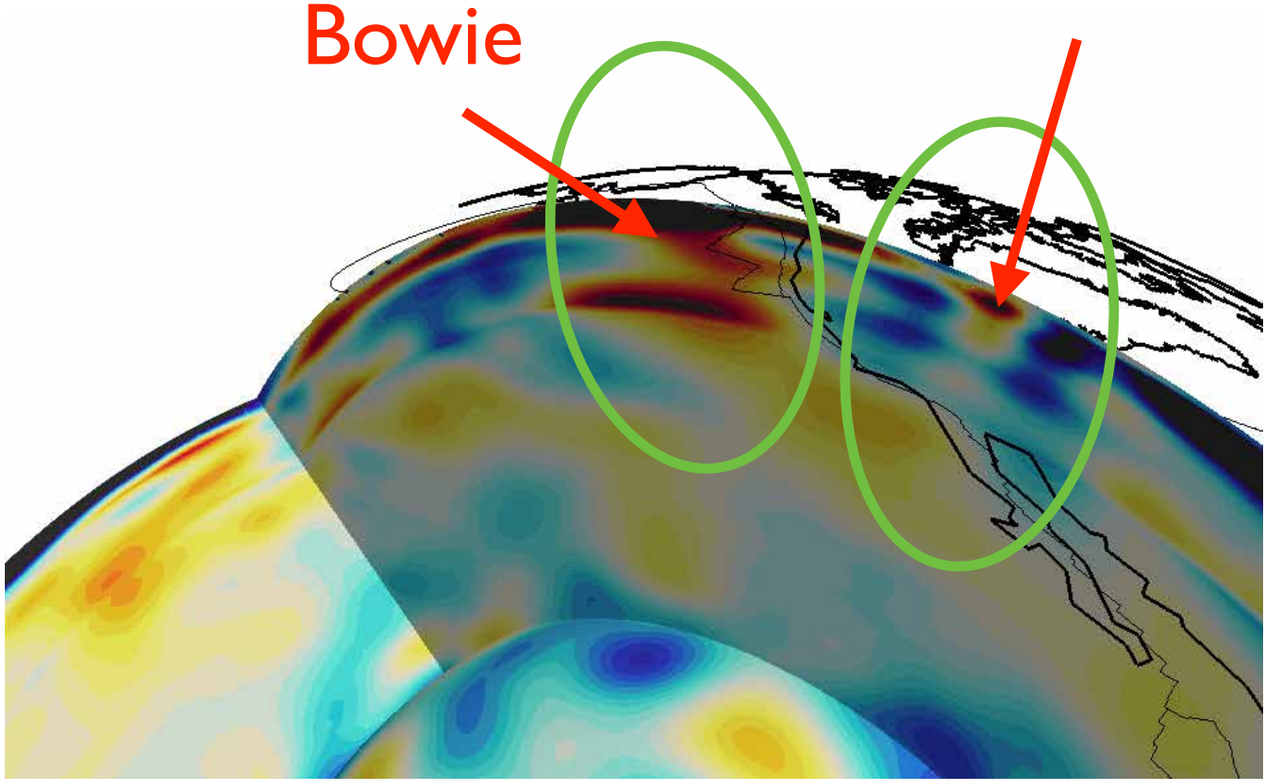

(2%)

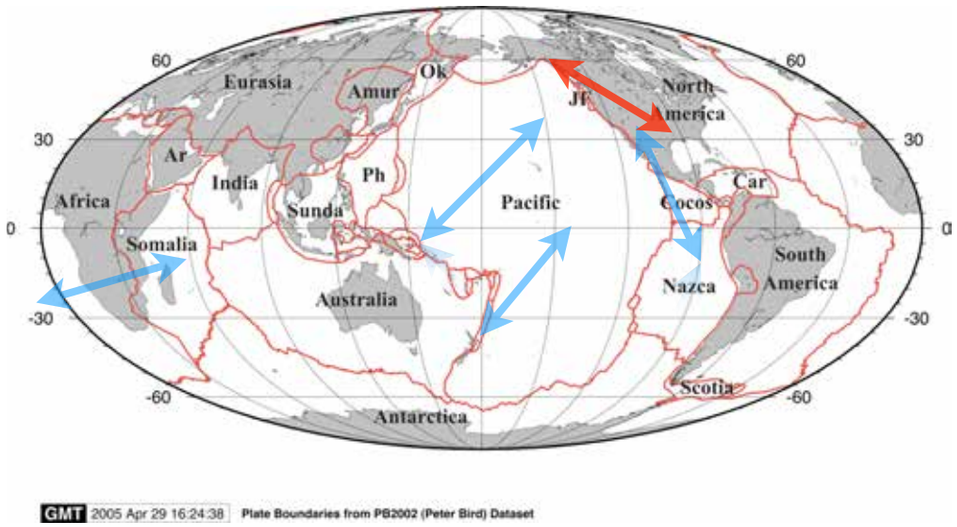

dlnVsv

min max

More sections..

M15 - 1DREF

Bowie

Yellowstone

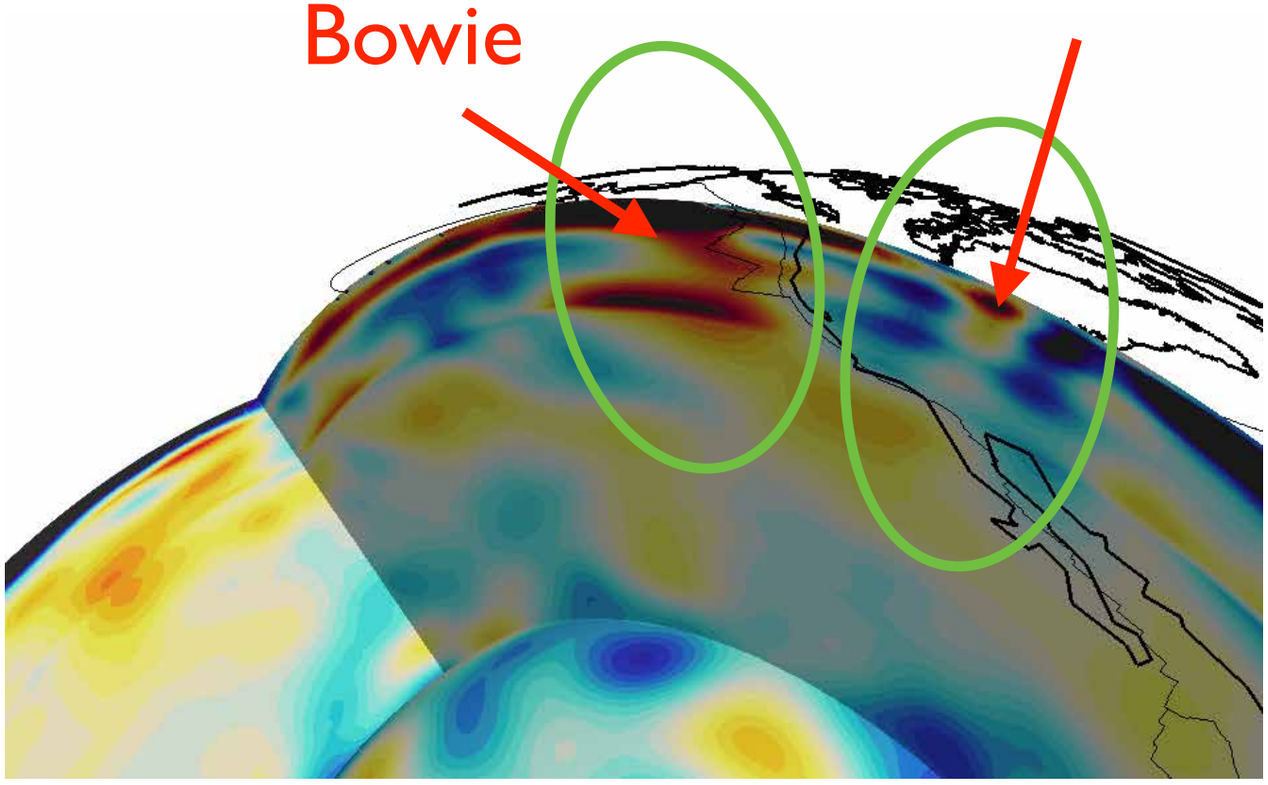

(2%)

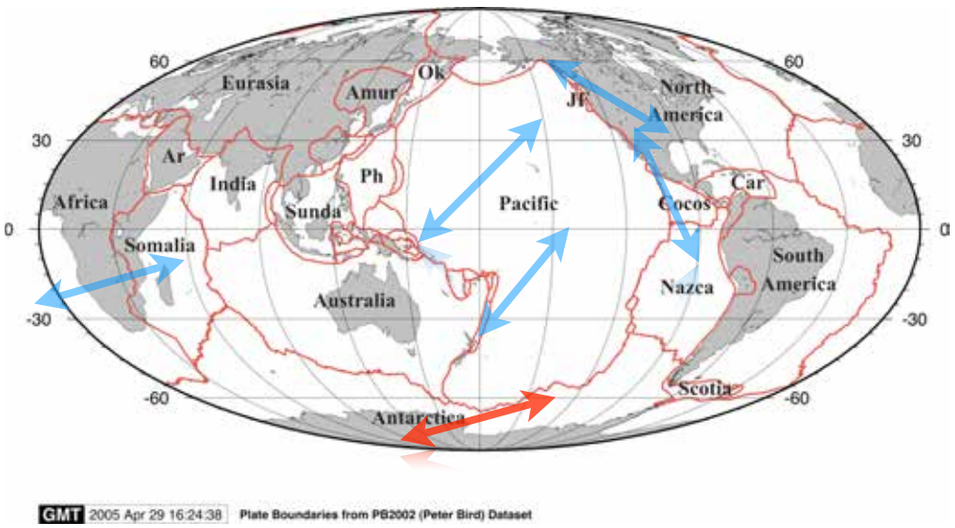

M00 - 1DREF

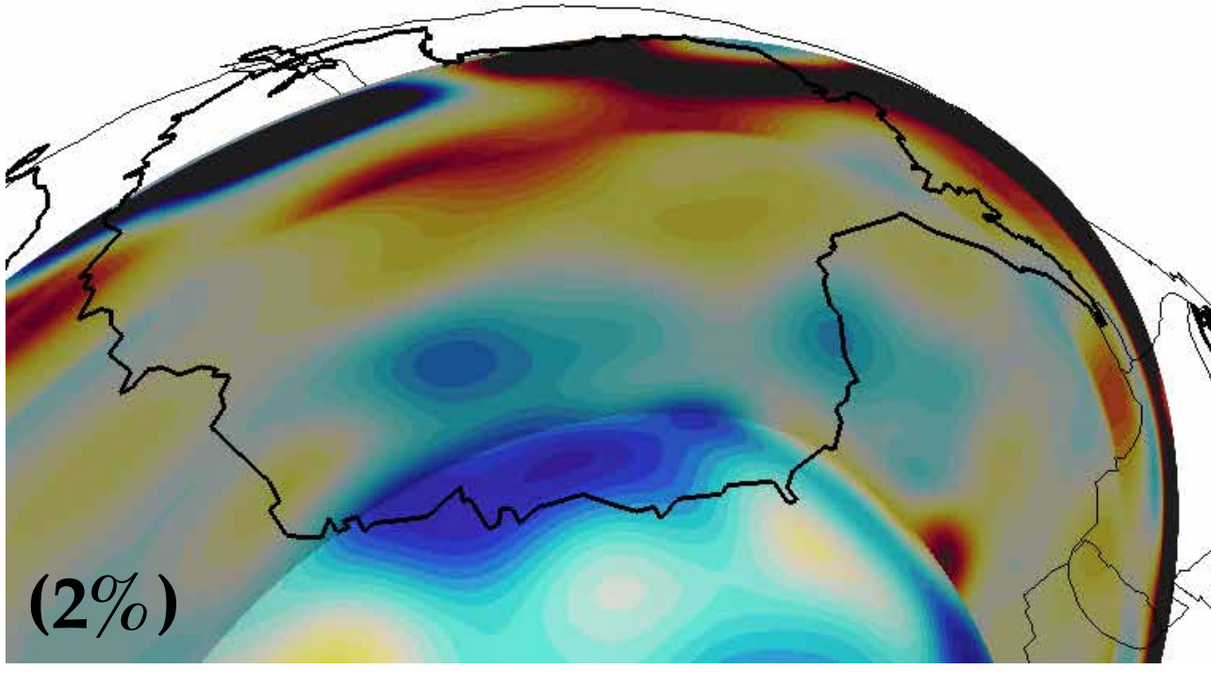

(2%)

dlnVsv

min max

More sections..

M15 - 1DREF

Bowie

Yellowstone

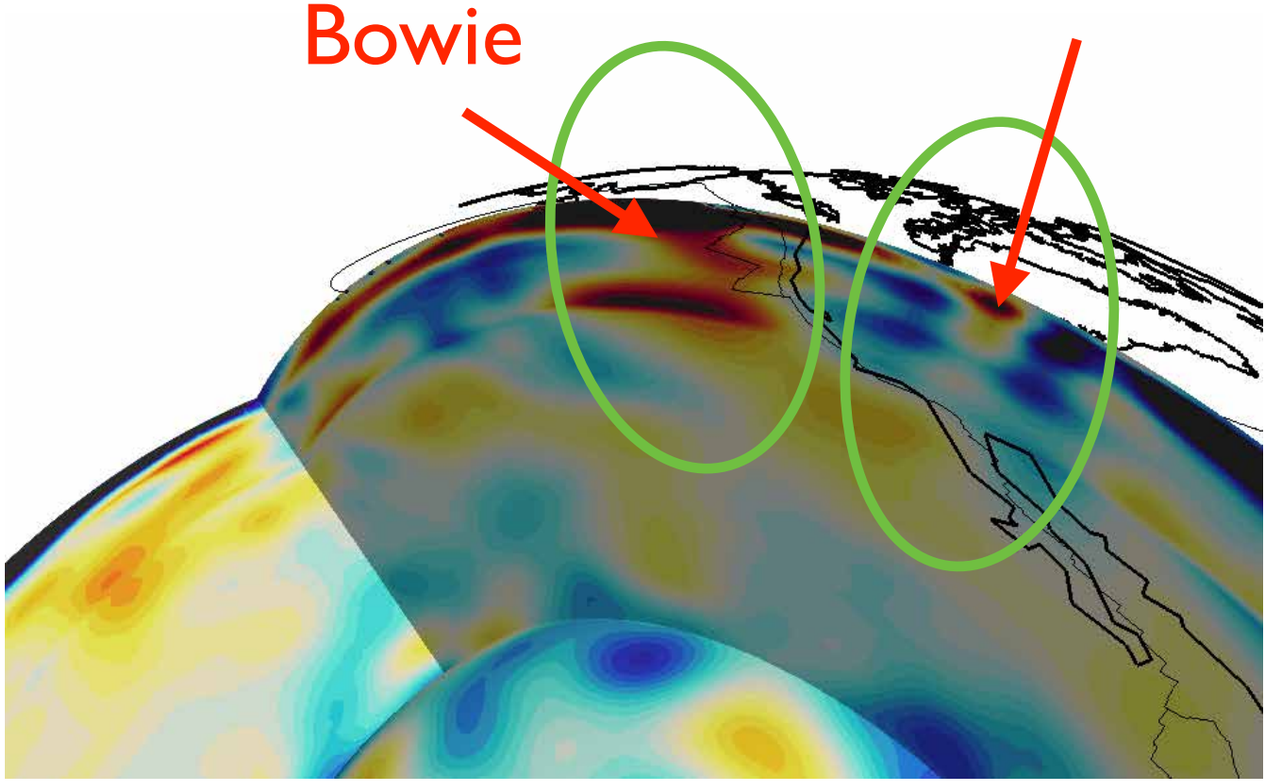

(2%)

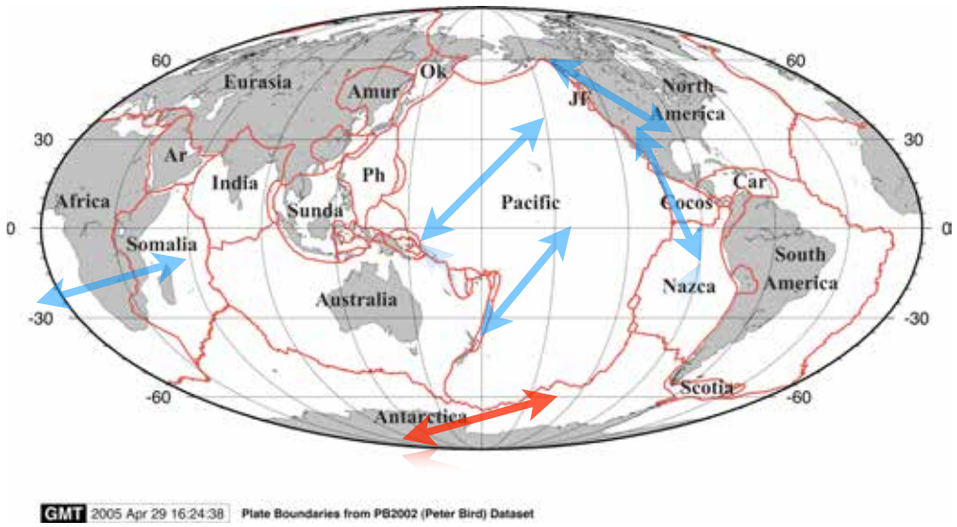

Erebus

M15 - 1DREF

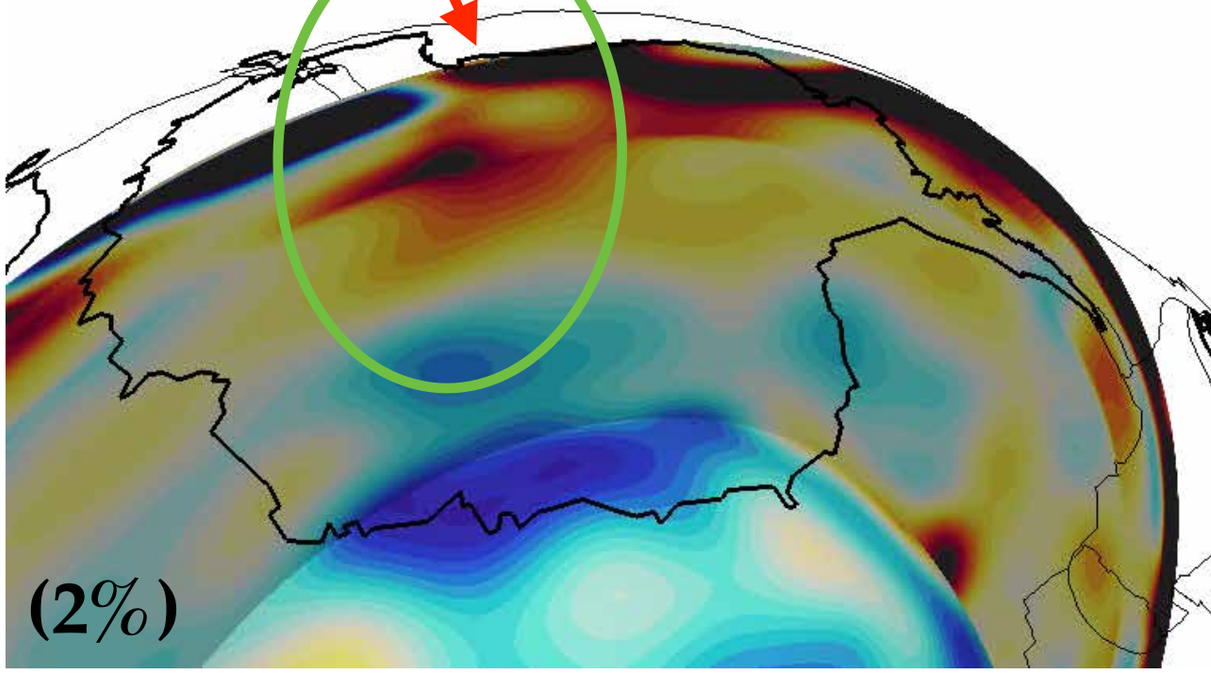

dlnVsv

min — max

Resolution tests

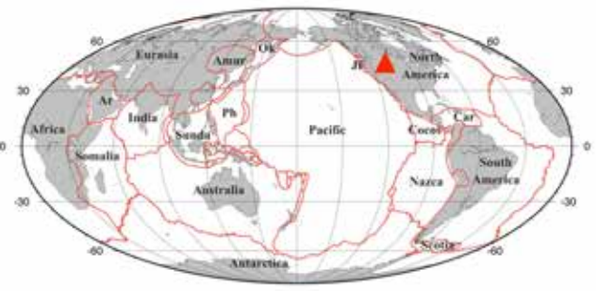

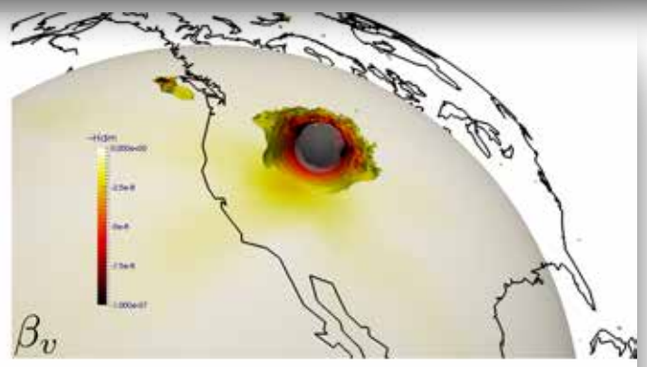

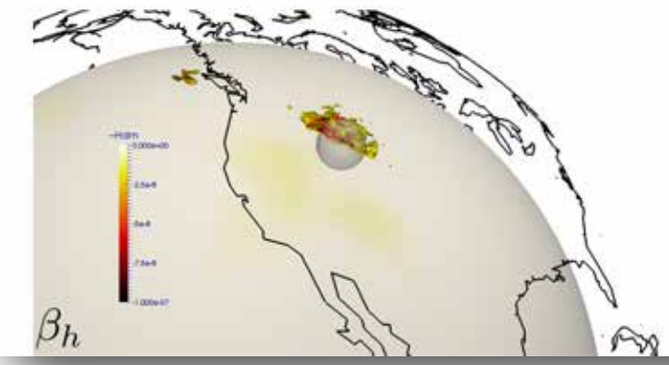

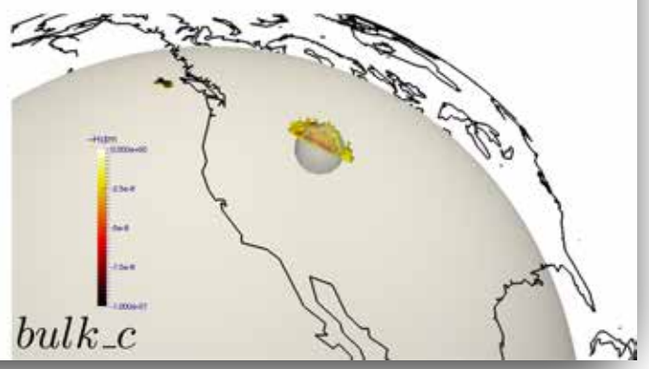

PSF
(Point-Spread Function)
tests
(Fichtner & Trampert 2011, GJI)

$$\mathbf{H}(\mathbf{m})\delta\mathbf{m} \approx \mathbf{g}(\mathbf{m}+\delta\mathbf{m}) - \mathbf{g}(\mathbf{m})$$

Yellowstone

Erebus

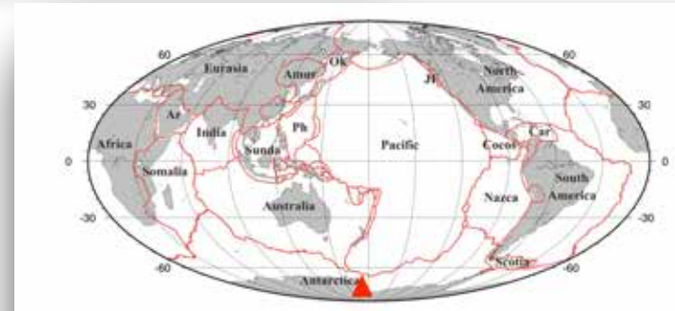

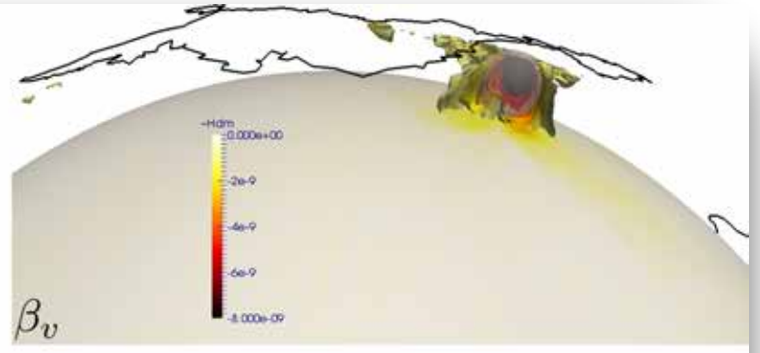

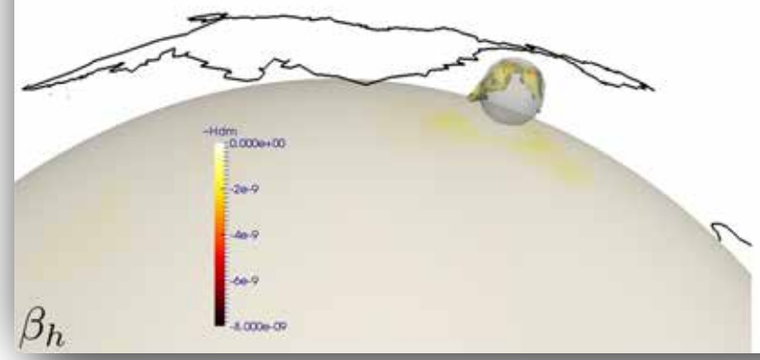

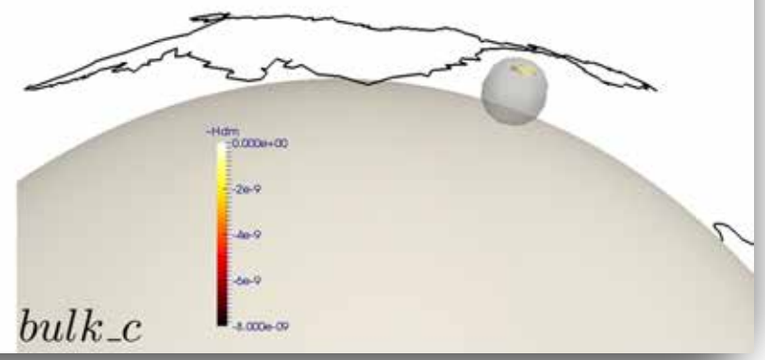

Misfit reduction

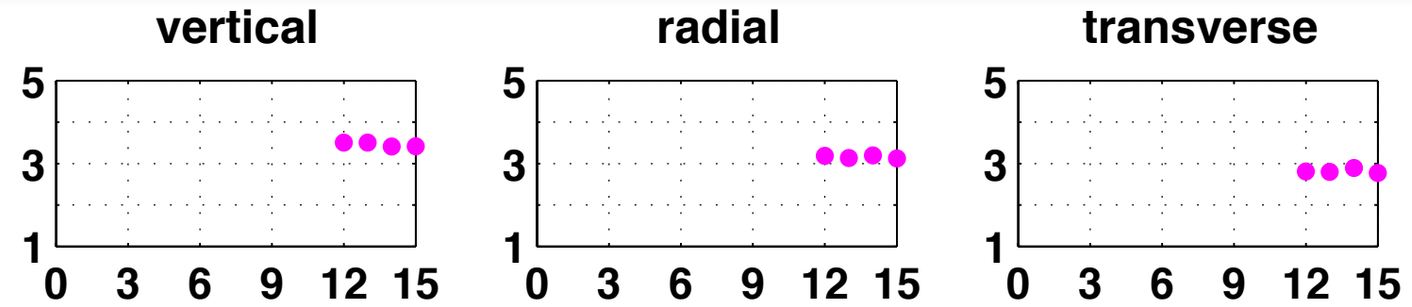

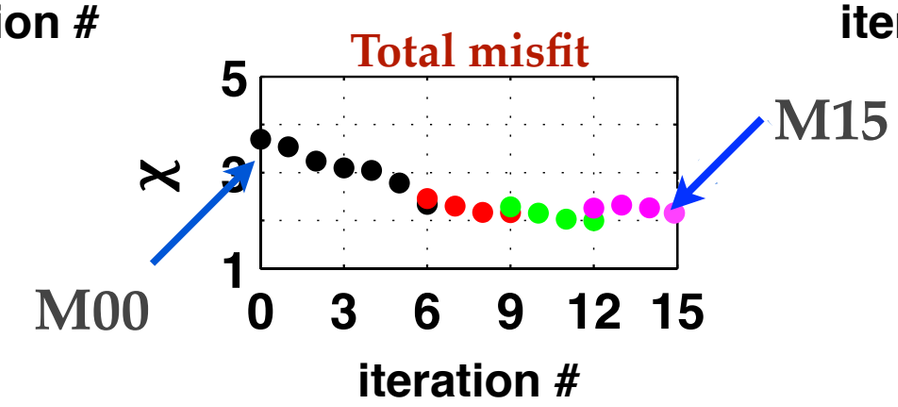

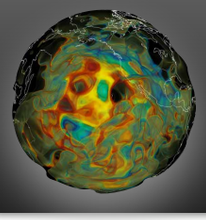

GLAD-M24*

Wenjie Lei, Youyi Ruan

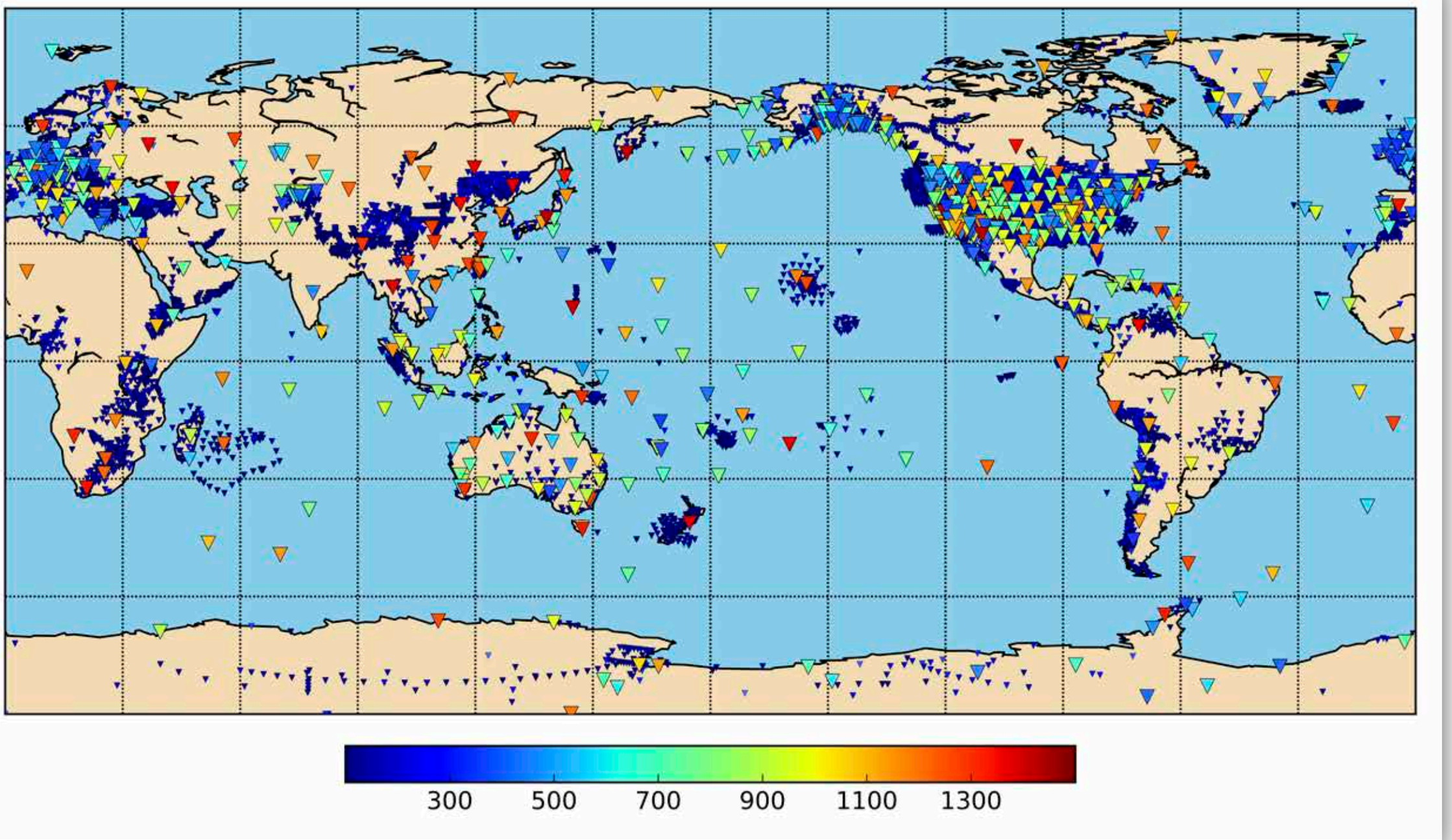

11,800 seismic stations, 1480 earthquakes

Data selection / measurements

window selections:
FLEXWIN
Maggi et al. 2009

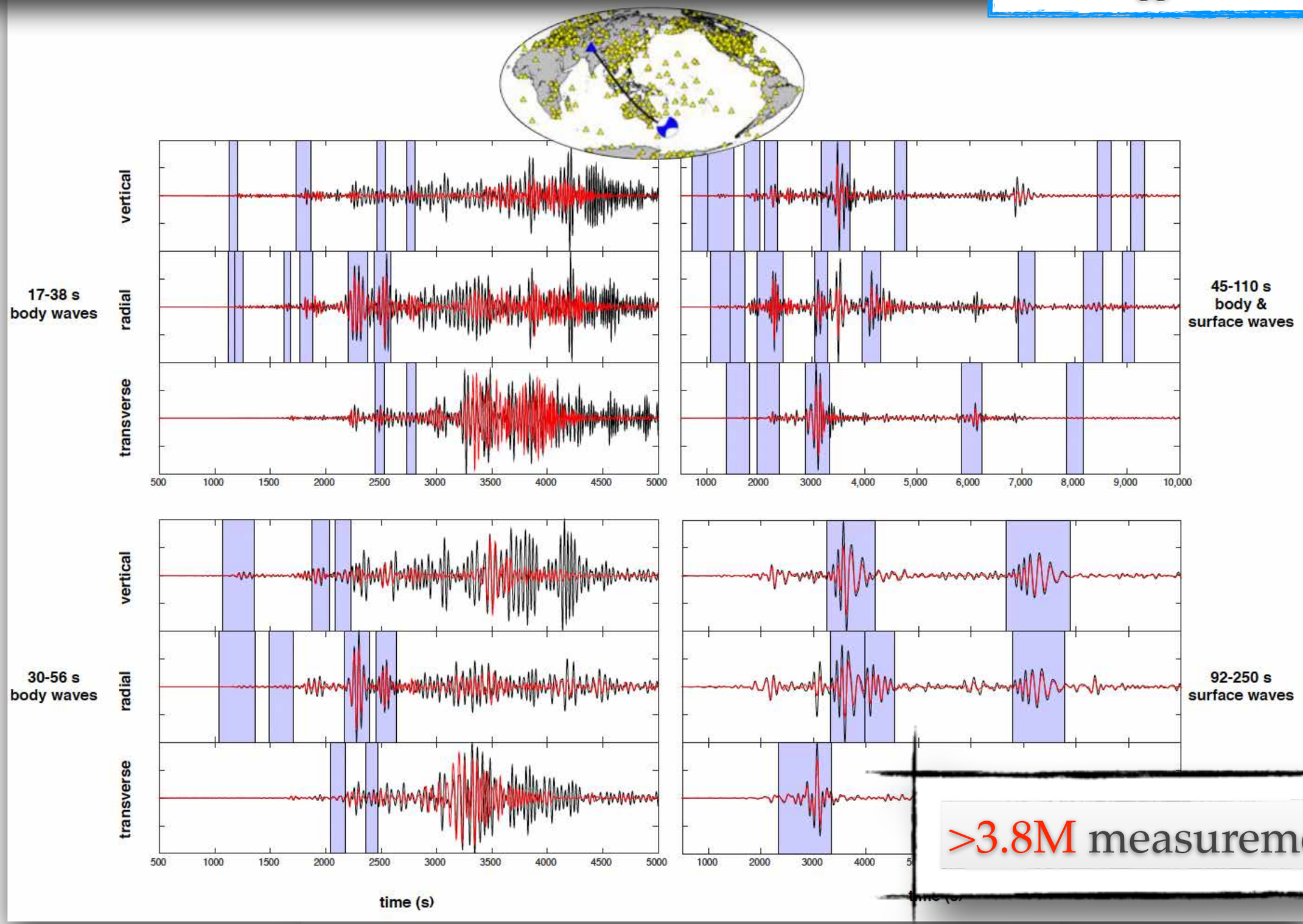

>3.8M measurements

$$\chi_c = \frac{1}{N_c} \sum_{e=1}^{E} \sum_{i=1}^{N_c^s} \int w_i(\omega) \left[\frac{\Delta\tau_i(\omega)}{\sigma_i} \right]^2 \mathrm{d}\omega \Big/ \int w_i(\omega)\, \mathrm{d}\omega$$

Data / measurements

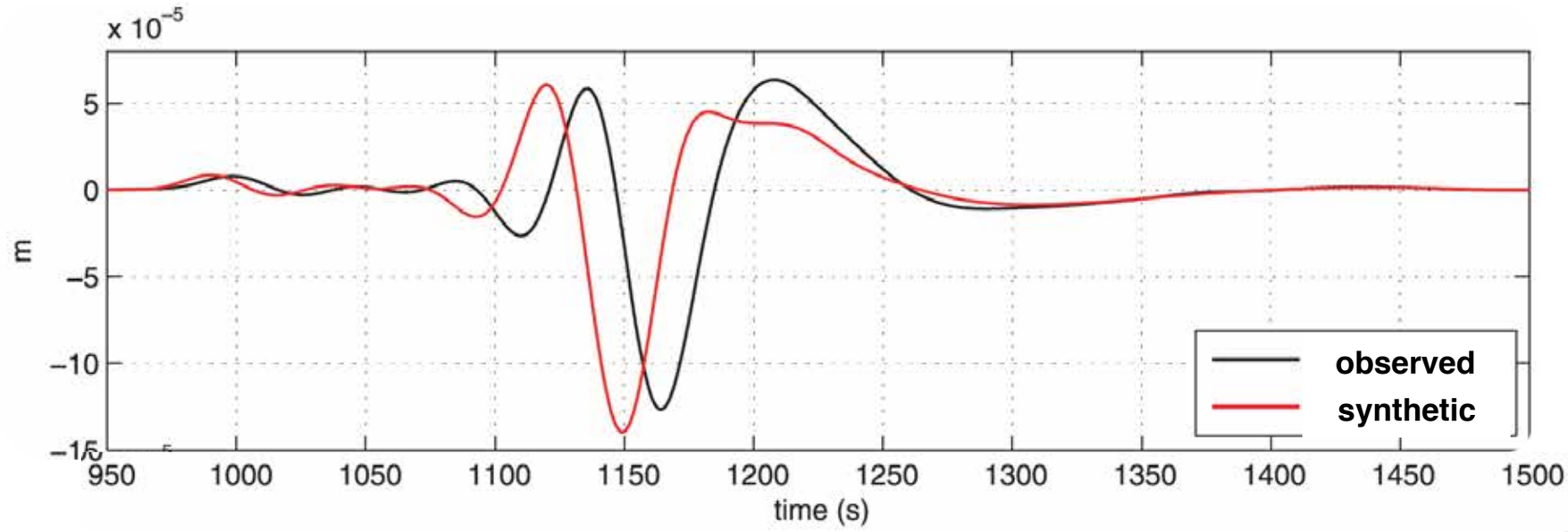

$$\chi = \frac{1}{2} \sum_s \sum_r \int ||d^{obs}(t) - d^{syn}(t,m)||^2 \, \mathrm{d}t$$

Waveform misfit

$$\chi = \frac{1}{2} \sum_s \sum_r [T^{obs} - T^{syn}]^2$$

Traveltime misfit

$$\chi = \frac{1}{2} \sum_s \sum_r \left[\ln \frac{\mathrm{A^{obs}}}{\mathrm{A^{syn}}} \right]^2$$

Amplitude misfit

Define new measurements

Instantaneous-phase misfit

$$\chi_{ip} = \frac{1}{2} \sum_{s,r} \int_0^T ||\phi_d(t) - \phi_s(t, \mathbf{m})||^2 \, \mathrm{d}t$$

E. Bozdag, J. Trampert & J. Tromp, 2011, GJI

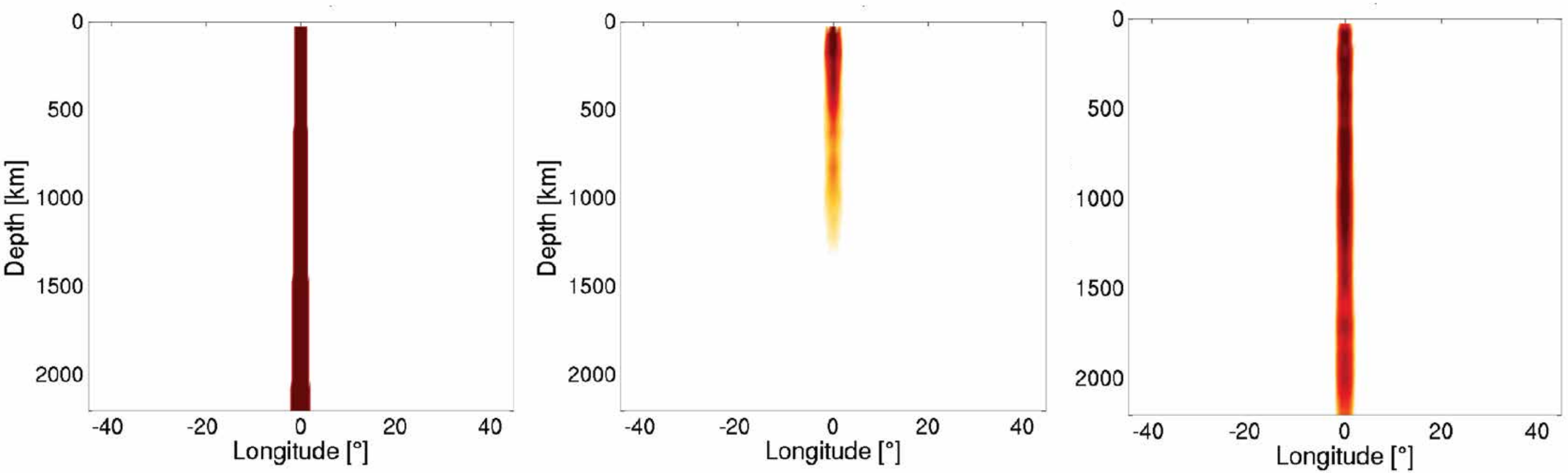

Target model **CC traveltime** **IP**

Rickers, Fichtner & Trampert, 2012, GJI

Define new measurements

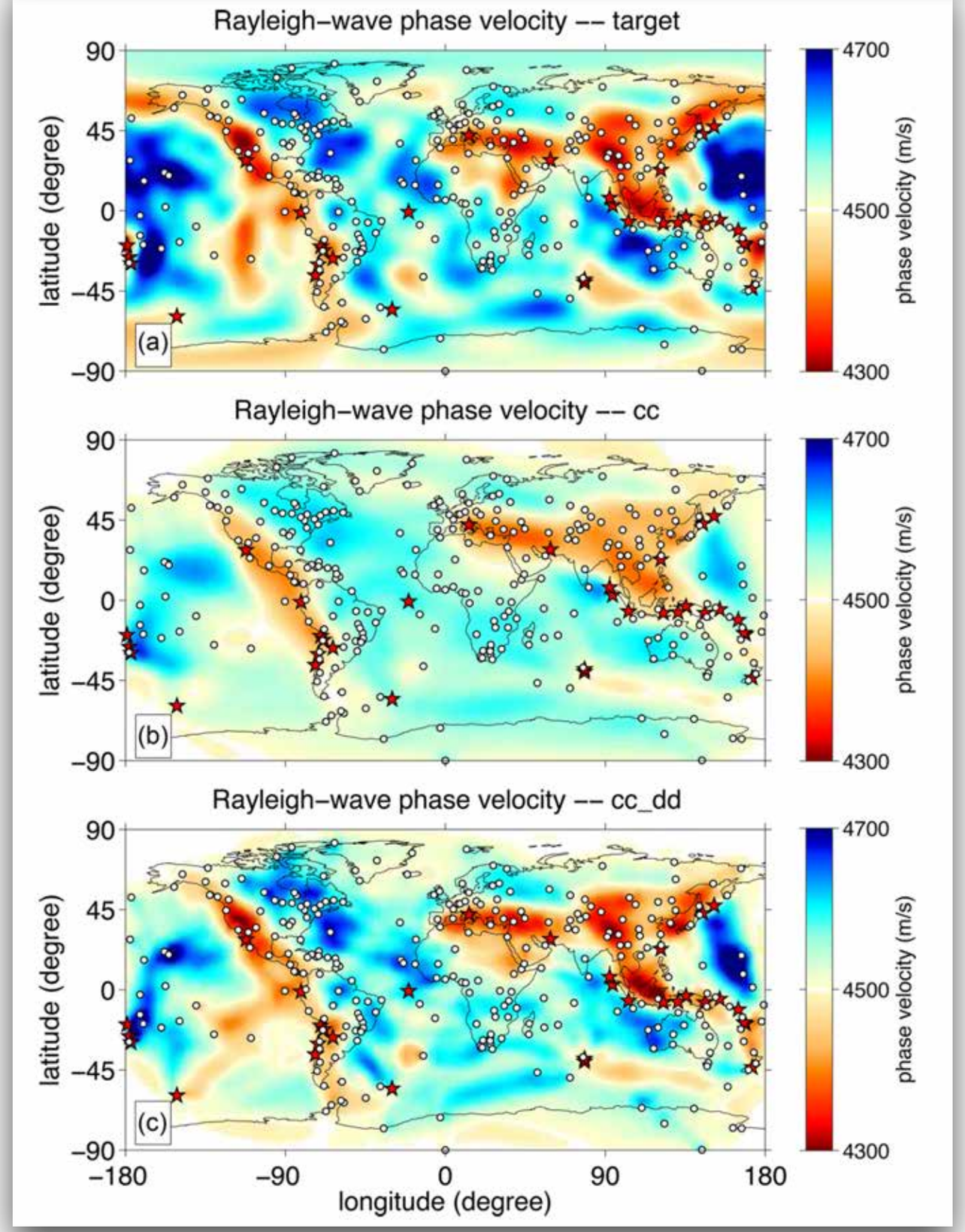

Double-difference misfit

Y. Yuan, F. J. Simons & J. Tromp,
***GJI*, 2016**

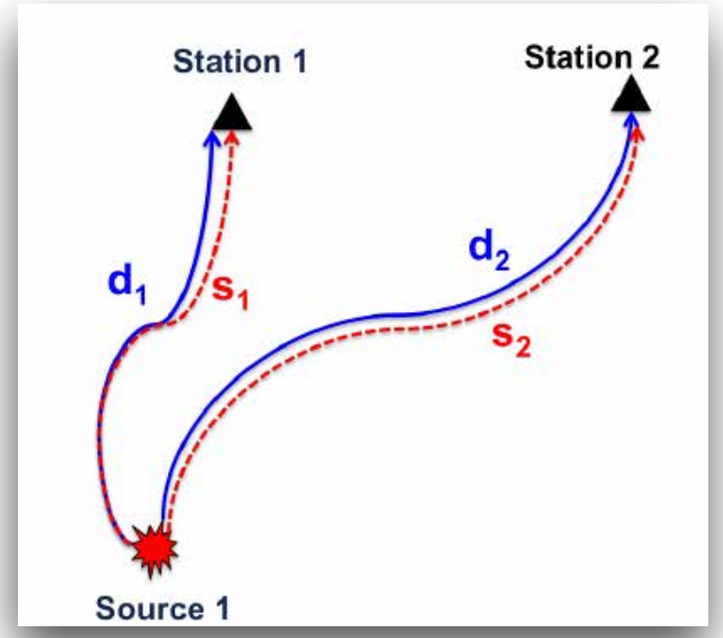

reduce source uncertainties
& bias in sparsly sampled regions

Exponentiated phase -
Hybrid objective functions
(CC+IP, MT+IP, etc..)
Yuan, Bozdağ, Simons, Gao, *AGU*, 2016

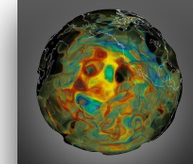

Computational requirements

core hours 180-m seismograms	1 event	1 iteration (255 events)	20 iterations
CPU - ~27 s	~5,400	~1.4M	~28M

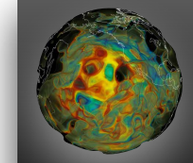

Computational requirements

core hours 180-m seismograms	1 event	1 iteration (255 events)	20 iterations
CPU - ~27 s	~5,400	~1.4M	~28M
CPU - ~17 s	~16,890	~4.3M	~86M

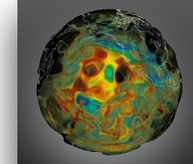

Computational requirements

core hours 180-m seismograms	1 event	1 iteration (255 events)	20 iterations
CPU - ~27 s	~5,400	~1.4M	~28M
CPU - ~17 s	~16,890	~4.3M	~86M

- Code-method development/optimisation
- Current/future computational resources

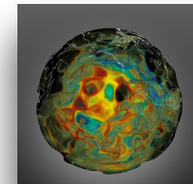

GPU computing

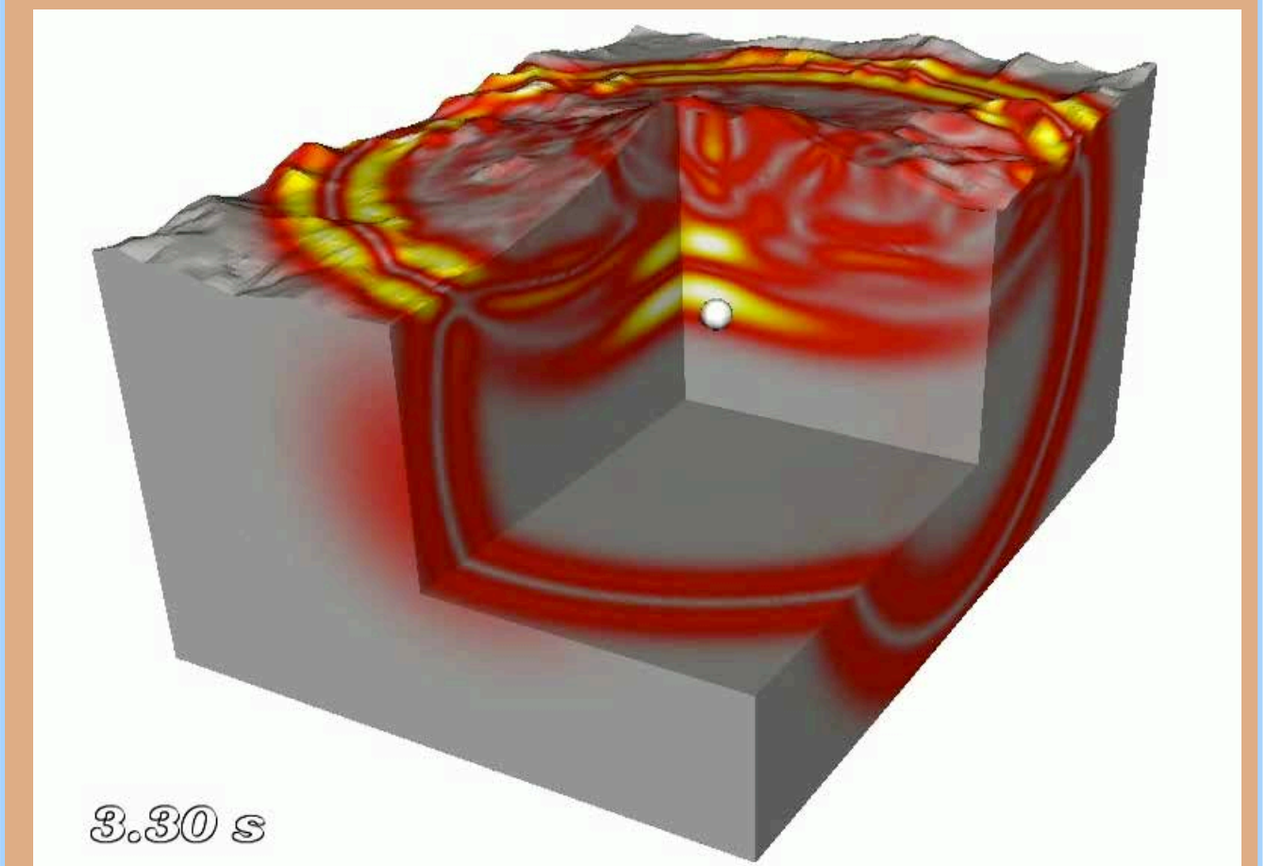

GPU

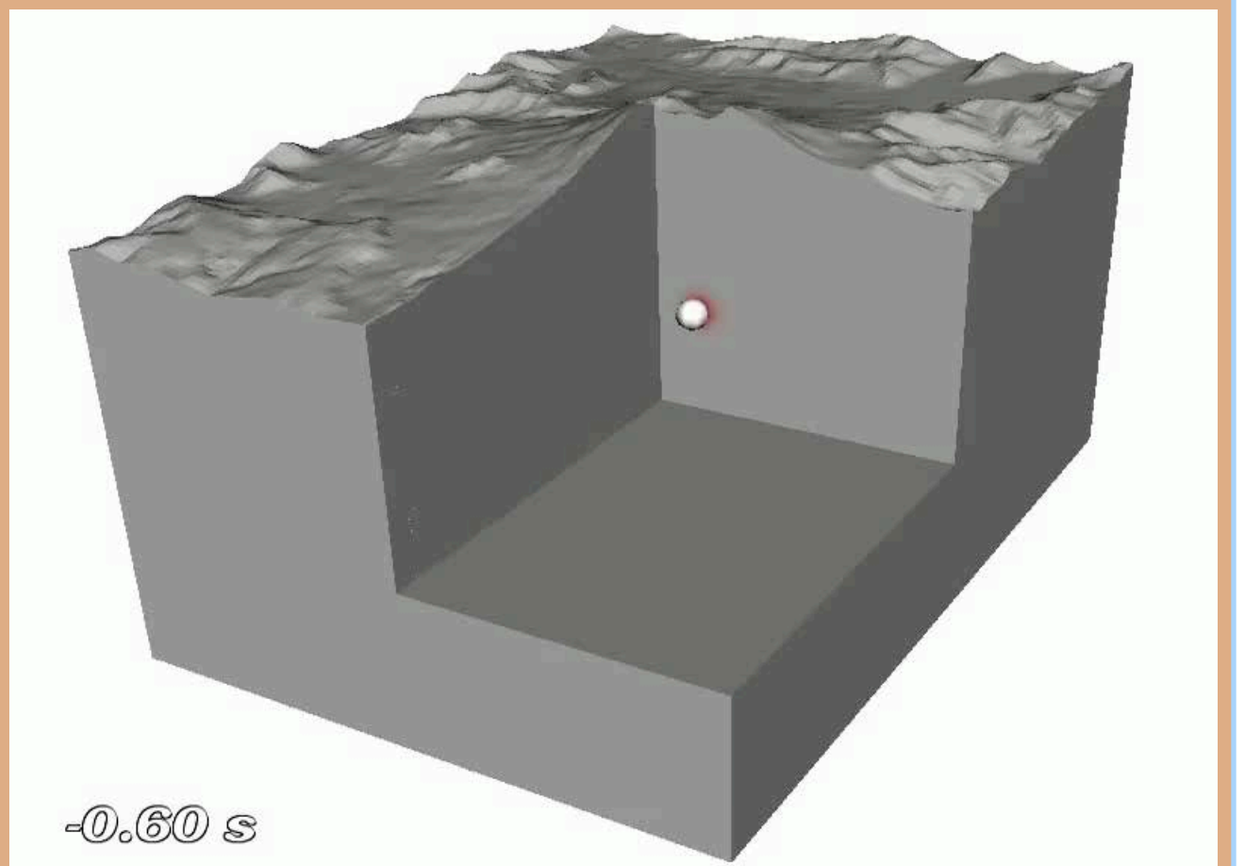

CPU

Daniel Peter

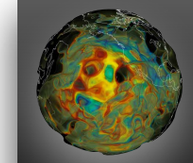

Computational requirements

core hours 180-m seismograms	1 event	1 iteration (255 events)	20 iterations
CPU - ~27 s	~5,400	~1.4M	~28M
CPU - ~17 s	~16,890	~4.3M	~86M
GPU - ~17 s	~600	~153,000	~3.1M

Computational requirements

core hours 180-m seismograms	1 event	1 iteration (255 events)	20 iterations
CPU - ~27 s	~5,400	~1.4M	~28M
CPU - ~17 s	~16,890	~4.3M	~86M
GPU - ~17 s	~600	~153,000	~3.1M

ORNL's Cray XK7 TITAN system
16,384 GPUs

ORNL's next-generation supercomputer SUMMIT, x5 faster, 4086 nodes
The goal is ~9 s, ultimately 1 s (*exascale era*).

Ray (kernel) density

$$P(\mathbf{x}) = \sum_s \int \partial_t^2 \mathbf{s}^\dagger(\mathbf{x}, -t) \cdot \partial_t^2 \mathbf{s}(\mathbf{x}, t)\ \mathrm{d}t$$ **(diagonal terms of Hessian)**

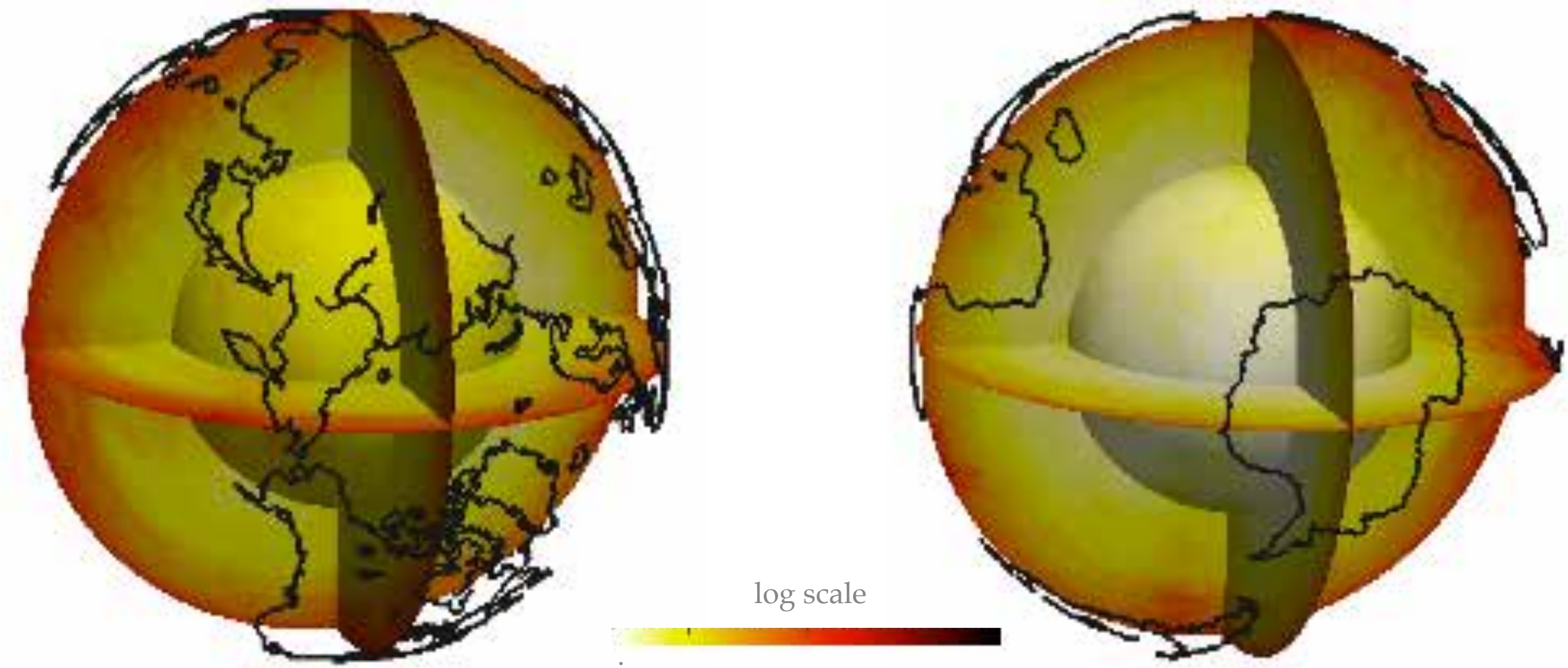

Northern hemisphere **Southern hemisphere**

Bozdag et al. 2016

Increase resolution of simulations

add *high-frequency body waves*

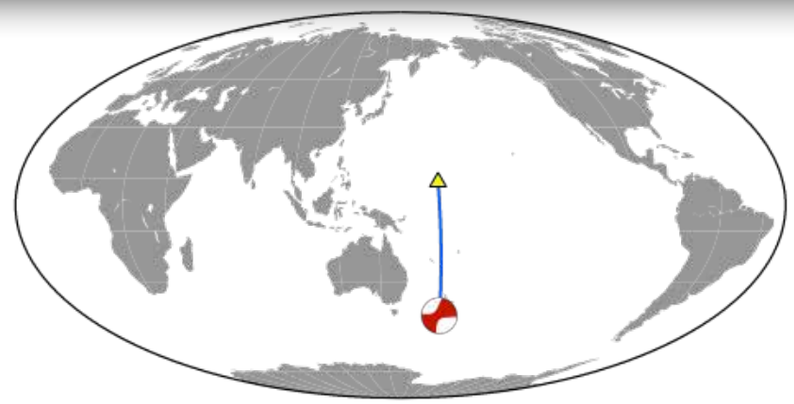

Station: KWAJ
Δ= 52°

27 - 60 s

17 - 60 s

9 - 60 s

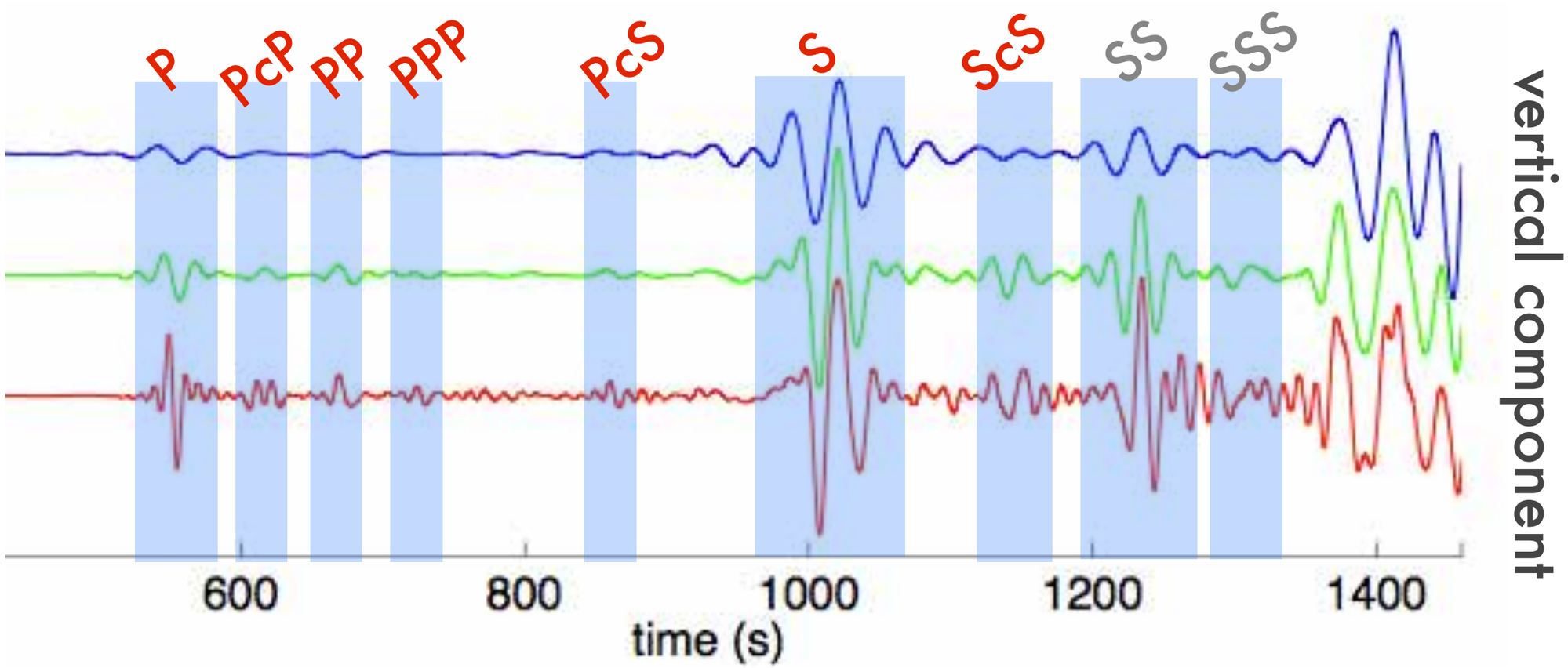

> 6000 global CMT events since 1999 (5.5 ≤ Mw ≤ 7.0)

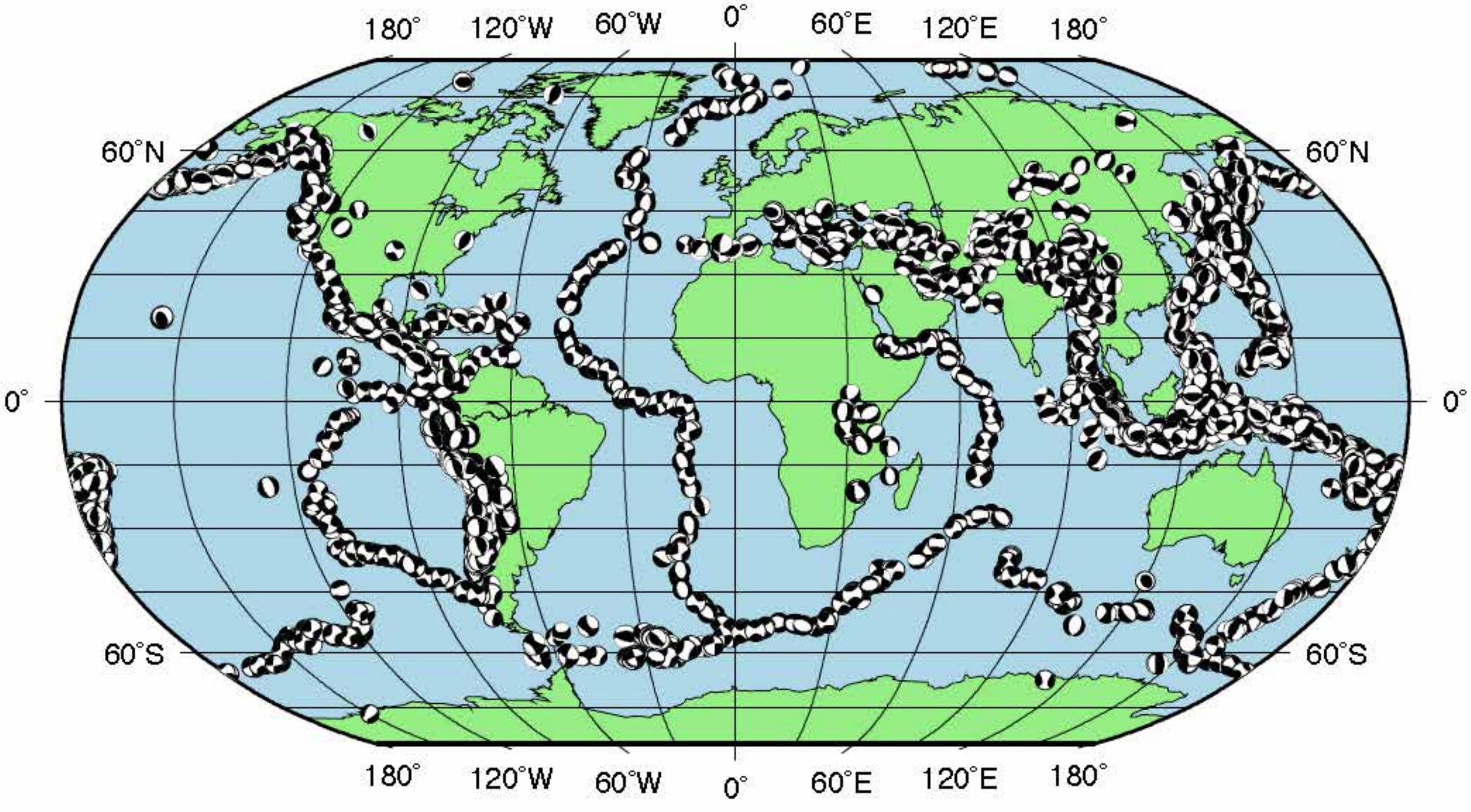

> 6000 global CMT events since 1999 (5.5 ≤ Mw ≤ 7.0)

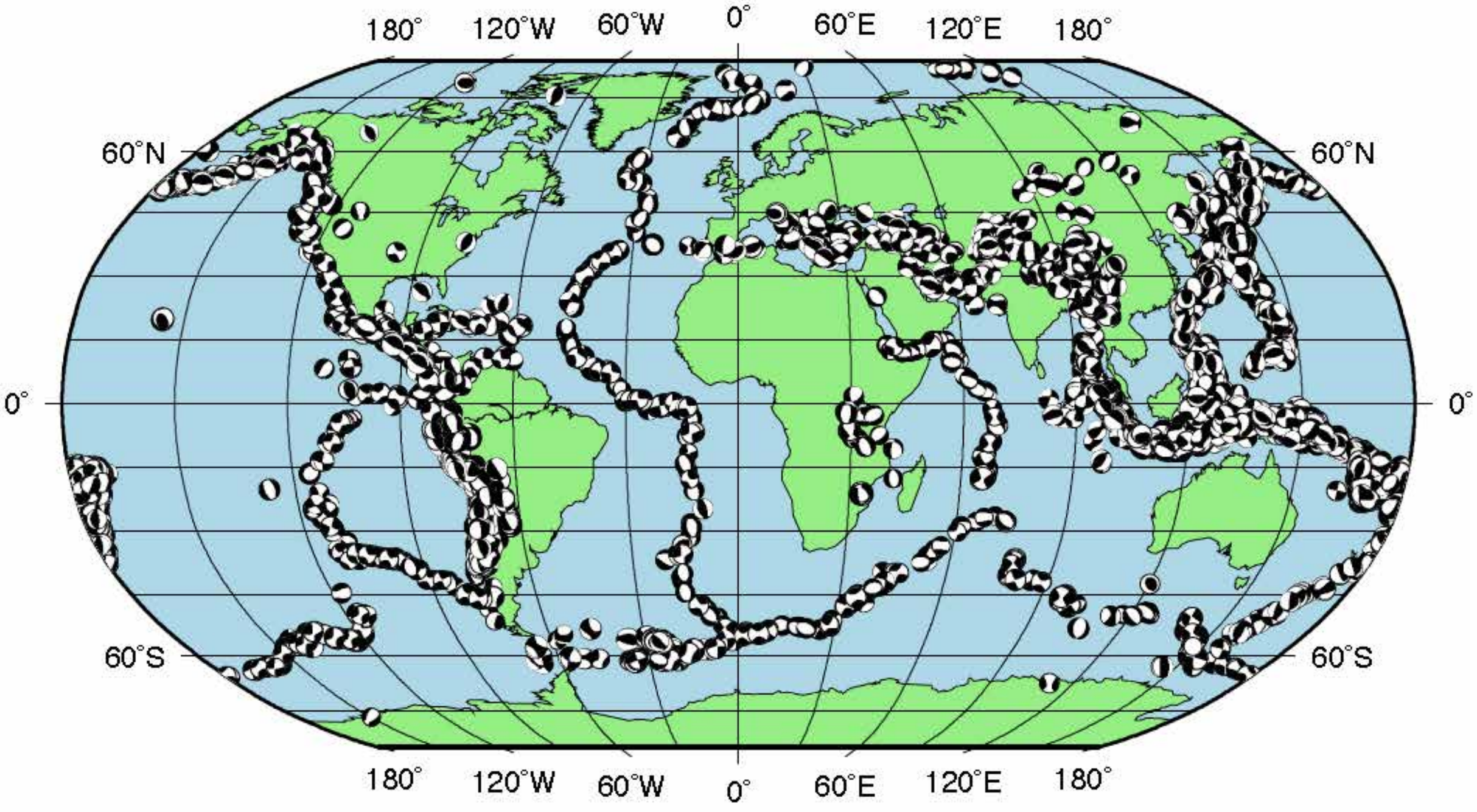

Use all available data!!

Adjoint tomography workflow

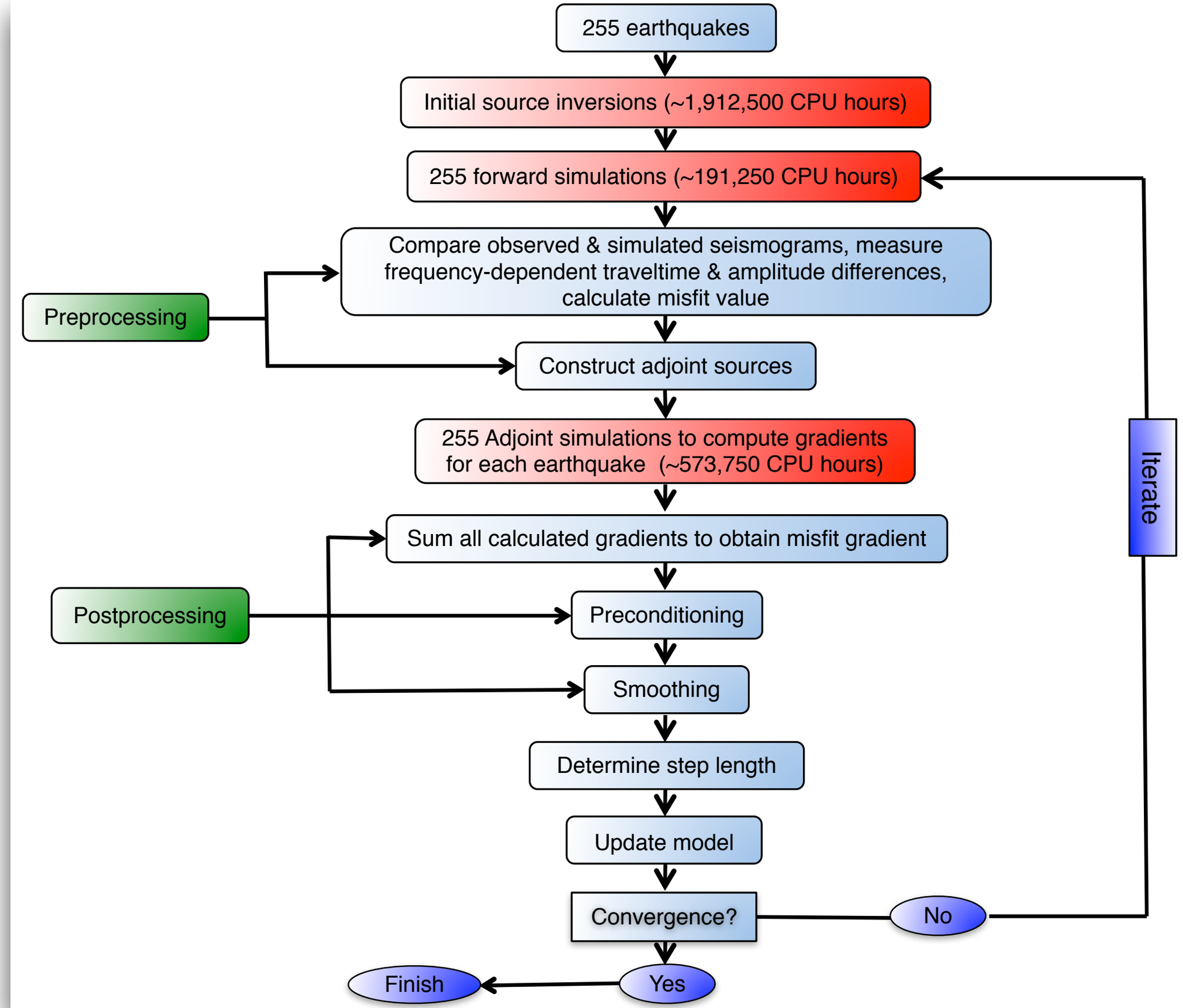

Adjoint tomography workflow

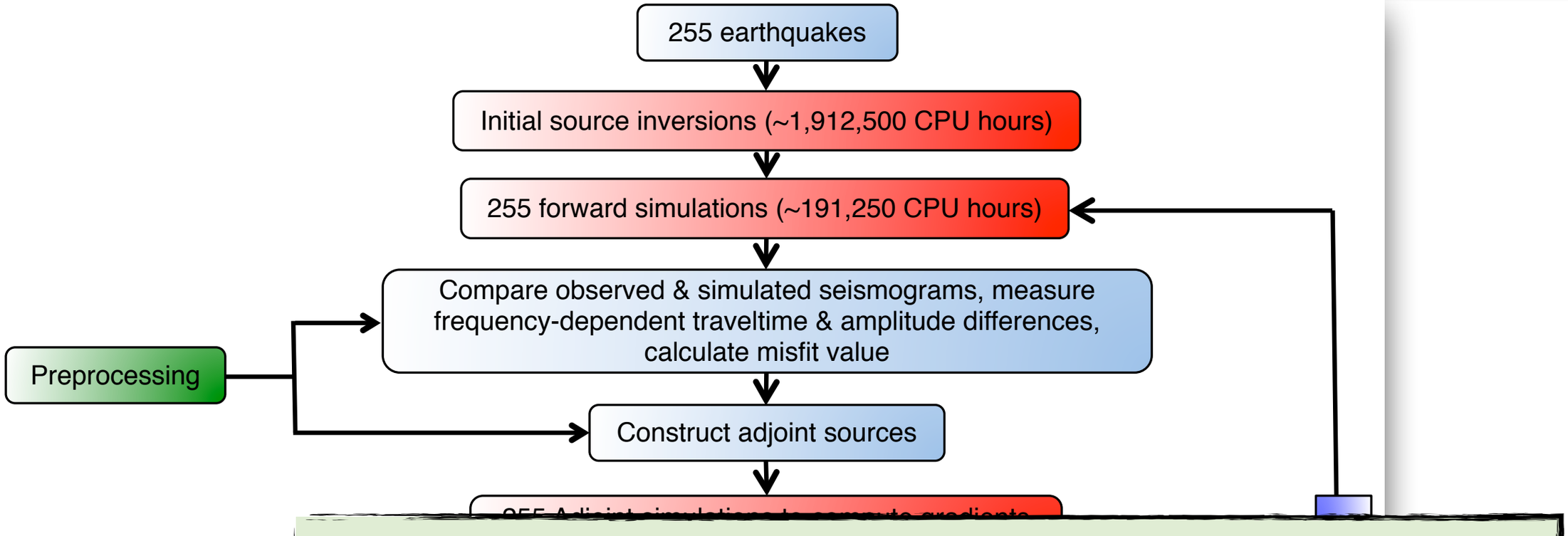

Bottlenecks:

I/O problems

* mesher and solver outputs: mesh/kernel/model files, seismograms (SAC, ASCII, etc.), adjoint sources, ...
* Pre-processing of SAC seismograms (can easily be *millions* of files), etc..

Data quality check for big data

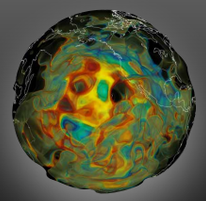

Data format

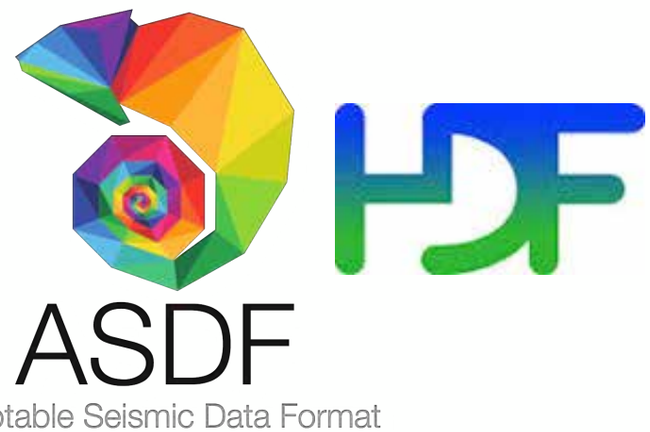

- **two ASDF files (observed & synthetics) per event**
  - **embarrassingly parallel pre-processing**

- **SPECFEM3D outputs: meshes / kernels / models, etc.**
  - **parallel post-processing**

ASDF (Adaptive Seismic Data Format)

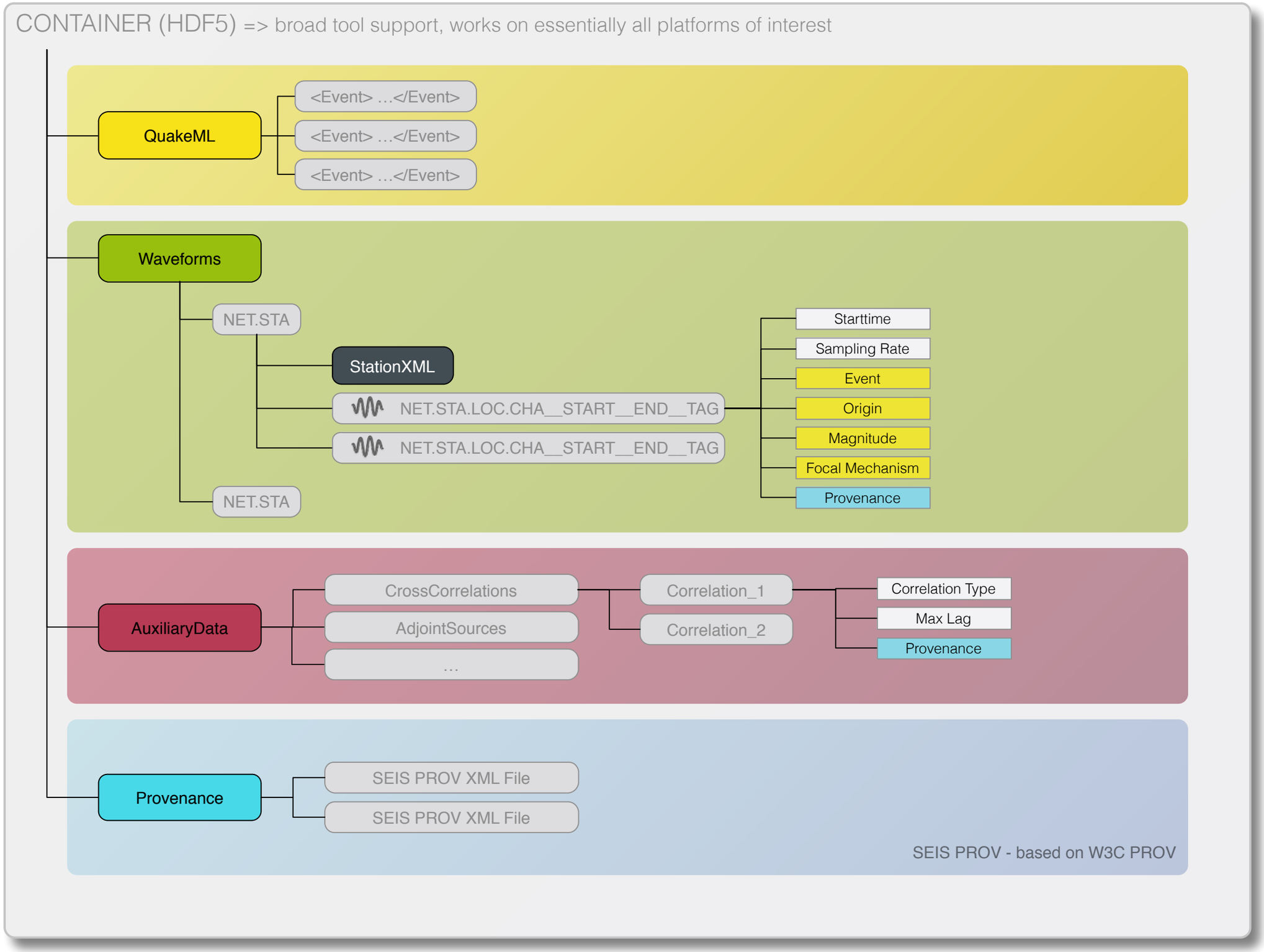

Lion Krischer, James Smith et al. 2016, GJI

Adjoint tomography workflow

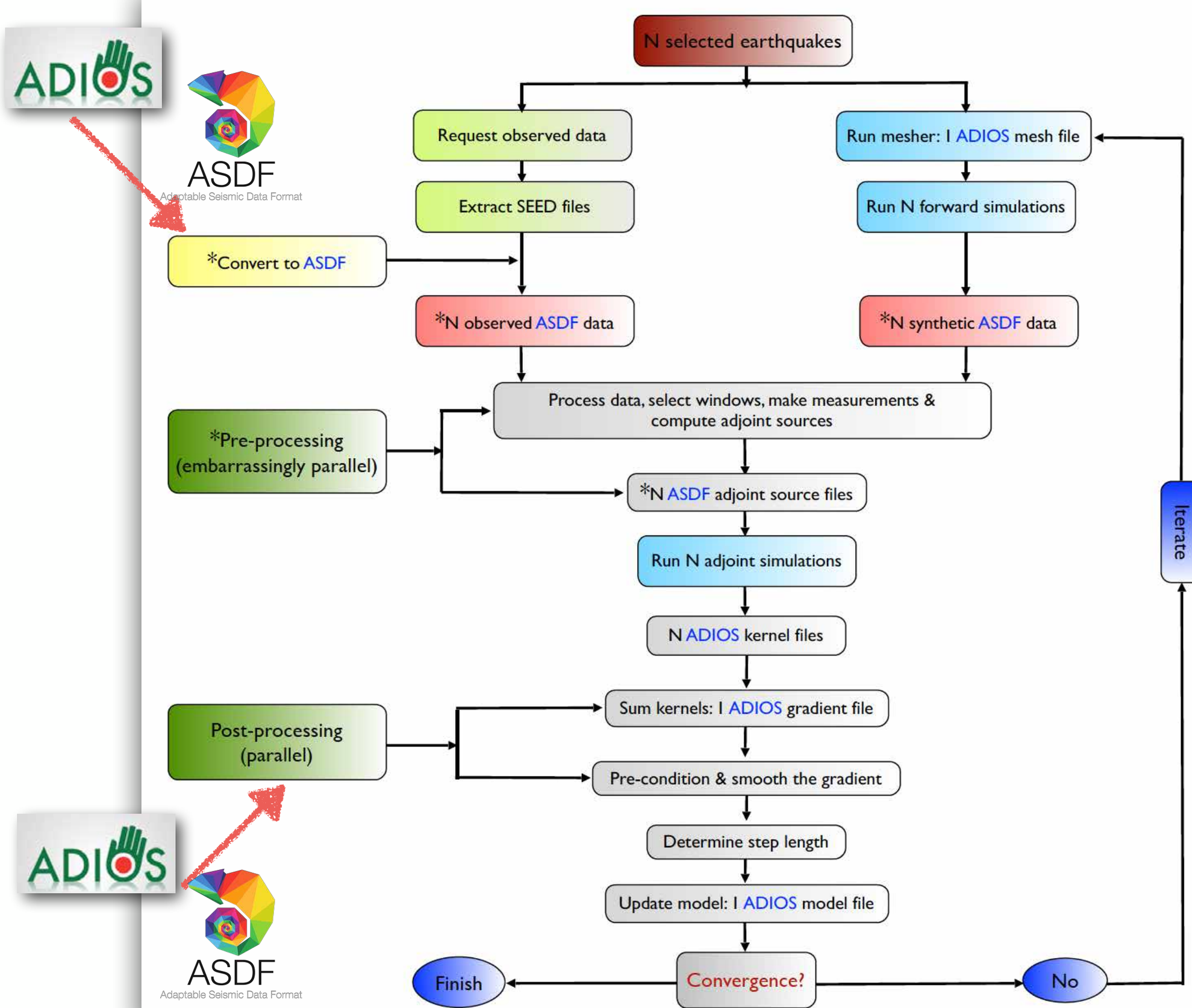

Adjoint tomography workflow

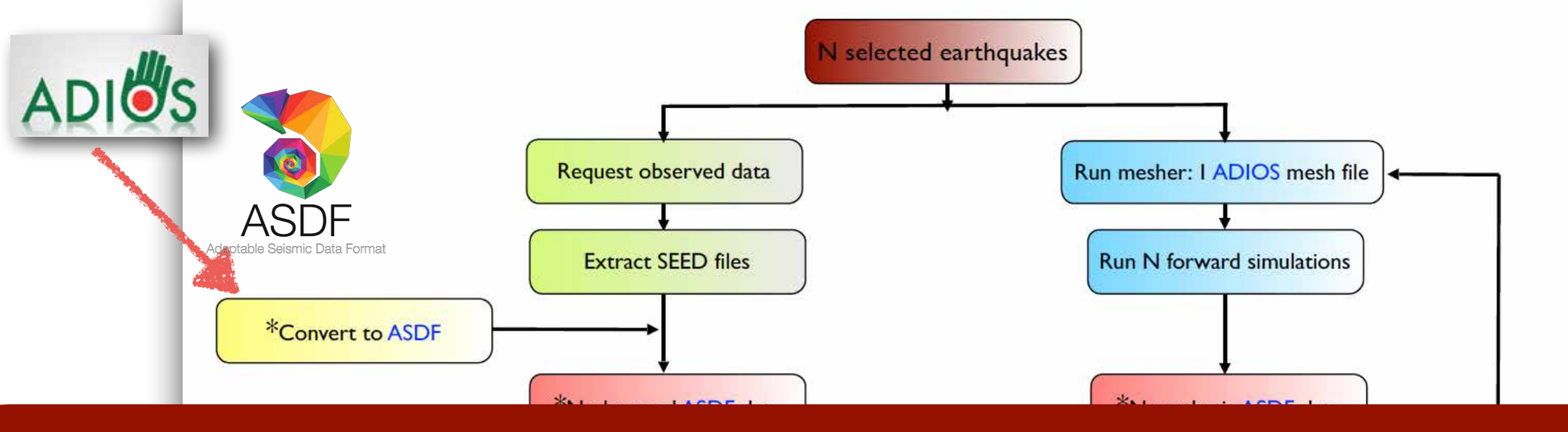

automatize the entire workflow:
Radical EnTK workflow management environment
Matthieu Lefebvre (Princeton) - Rutgers
Balasubramanian et al. 2018

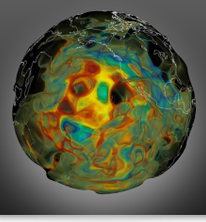

Conclusions / future directions

- **Next-generation models: Better parameterization**
  - **Second-generation model: Azimuthal anisotropy**
  - **Third-generation model: Anelasticity**
  - **Internal topographies, crust, finite-source effects, etc…**

- **Increase the resolution of simulations, ultimately down to 1 Hz ==> whole-Earth inversions**

- **Approaching continental-scale resolution in global tomography in regions with good data coverage**

- **Define better measurements / extract optimum information from each seismogram while keeping a balanced gradient**

- **Resolution/uncertainty analysis ~ Model interpretation**

Visualizing Earth's mantle

GLAD-M15

David Pugmire, ORNL

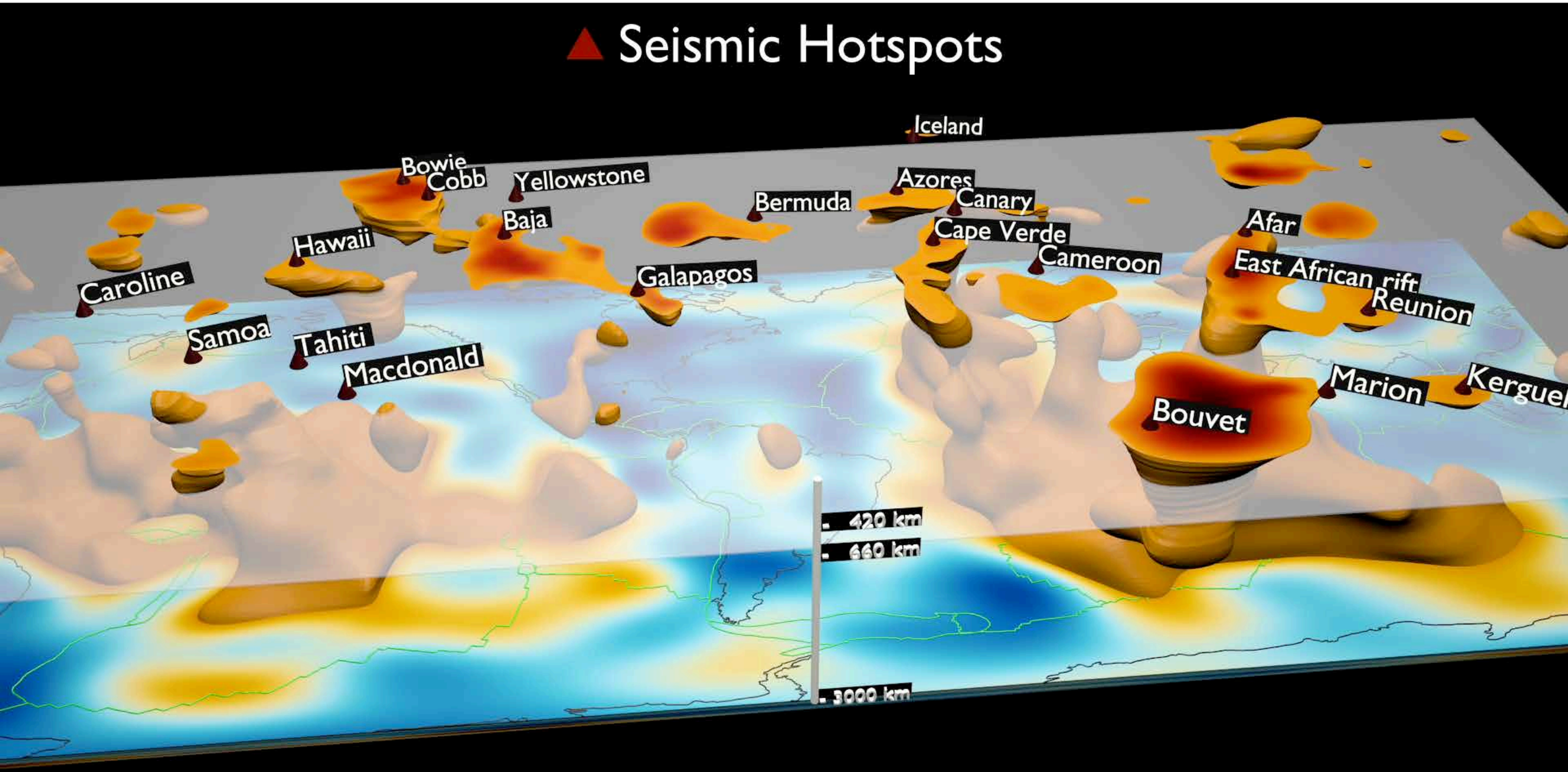

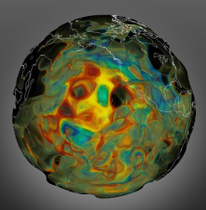

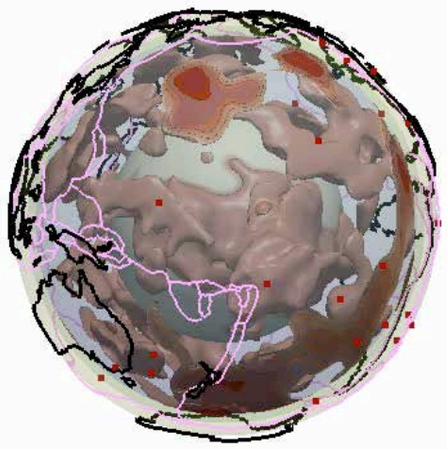

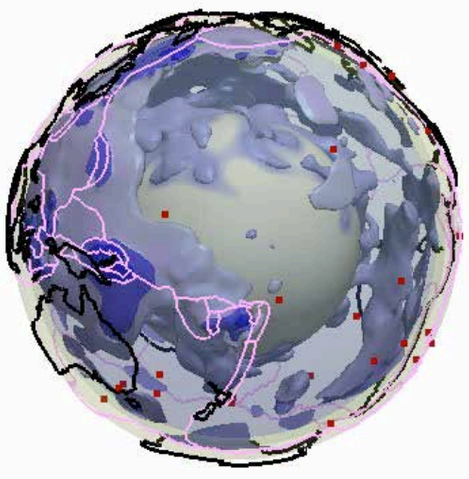

This research (GLAD-M15, GLAD-M24*) used resources of the Oak Ridge Leadership Computing Facility which is a DOE Office of Science User Facility supported under contract DE-AC05-00OR22725.

Special thanks to Princeton Institute for Computational Science and Engineering (PICSciE).